TÉCNICO LISBOA

Aerodynamic Interactions Between Tandem Configuration Rotors

Henrique Antunes Portela Santos

Thesis to obtain the Master of Science Degree in

Mechanical Engineering

Supervisors: Prof. Filipe Szolnoky Ramos Pinto Cunha
Prof. José Raul Carreira Azinheira

Examination Committee

Chairperson: Prof. Carlos Frederico Neves Bettencourt da Silva
Supervisor: Prof. Filipe Szolnoky Ramos Pinto Cunha
Member of the Committee: Prof. Luís Rego da Cunha de Eça

December 2021

Acknowledgments

I must start by thanking my supervisors, Filipe Cunha and José Azinheira, whose advice, support and experience that was indispensable throughout this work. Most of all, thank you for the time spent, for the concern and help. A thank you is also in order to professor André Marta, for lending the necessary equipment and the safety advice provided.

I'm also grateful to my supervisors, my mother and Maria for the assistance in making this much more understandable and readable than the first few drafts ever were.

To Maria, my friends and my family, without whose support this task would have been insurmountable. Thank you.

Finally, I must thank the reader for the attention spared in reading this.

Resumo

Procura-se comparar o desempenho de rotores em configurações tandem (com sobreposição parcial) com configurações planares. Este estudo tem como objectivo identificar os parâmetros críticos para o desempenho deste tipo de configuração. Pretende-se ainda que este trabalho seja mais uma fonte de dados para a implementação de sistemas de propulsão tandem em drones, dada a rápida expansão desta indústria.

Como base teórica, apresenta-se a Teoria do Momento Linear, que permite obter valores de referência para o desempenho dos rotores isolados. A teoria pode ainda ser adaptada para obter intervalos de resultados esperados para os rotores em tandem.

O banco de ensaios desenvolvido por Amado para configurações coaxiais, foi modificado para permitir o estudo de configurações tandem. O procedimento de calibração para as forças e binários necessários foi realizado e verificado com resultados fornecidos pelo fabricante das hélices. Identificaram-se 5 parâmetros para o estudo: direção de rotação, passo e diâmetro de ambos os rotores. Avaliaram-se também a importância do distanciamento entre os eixos dos rotores e entre os planos dos rotores.

Observou-se que o desempenho do rotor inferior sofre um impacto negativo elevado quando este tem um sentido de rotação oposta à do rotor superior ou quando a distância interaxial é reduzida. O mesmo se verifica quando o diâmetro do rotor inferior é reduzido, ou quando o passo do mesmo é aumentado. Uma sensibilidade moderada foi verificada quanto ao passo do rotor superior. Quando a distância entre planos dos rotores ou o diâmetro superior são variados, observou-se muito pouca variação no desempenho.

Palavras-chave: Drones, Configurações tandem, Análise Experimental, Sistema de Propulsão Aérea, Teoria do Momento Linear

Abstract

The main objective of this thesis is to explore the performance of tandem configuration drones (with partial overlap) and compare to planar configurations, identifying critical parameters for these configurations. Additionally, this work is intended as a source of data for the development of alternative configurations for drones.

A summary of Momentum Theory, as a first-approximation reference for isolated rotors, is presented. An adaptation of this theory for tandem-rotor configurations is also explained, as it allows for the computation of the expected experimental results.

A testing bench, originally developed by Amado for coaxial configurations, was modified to allow for the study of rotors in tandem. A calibration procedure was carried out and resulting coefficients verified with results supplied by the propellers' manufacturer. The parameters studied were pitch and diameter for both rotors, rotation direction as well as interrotor and interaxial distances.

The performance of the downstream rotor and the overall performance were very sensitive to rotation direction (where opposite rotation was observed to be less performant). Interaxial distance was also found to be of high importance. Moderate impact was observed when a smaller downstream diameter was used, or when the pitch of the downstream rotor is greater. A moderate sensitivity to upstream pitch was verified. A low sensitivity to interrotor distance and upstream diameter is also of note.

Keywords: Drones, Tandem-rotor Configurations, Experimental Analysis, Aerial Propulsion Systems, Momentum Theory Analysis

Contents

List of Tables

List of Figures

Nomenclature

Greek symbols

δ	Overlap distance ratio.
κ	Induced power correction factor.
κ_{ov}	Overlap coefficient of two rotors in tandem.
Ω	Rotor angular velocity $[\mathrm{RPM}]$.
ρ	Air density.
σ	Rotor solidity.

Roman symbols

A	Area of rotor.
A_{ov}	Overlap area.
$\mathbf{C}^{\mathbf{1}}_{\mathsf{neg}}$	Calibration matrix of IT 1 for the negative torque direction.
$\mathbf{C}^{\mathbf{1}}_{\mathsf{pos}}$	Calibration matrix of IT 1 for the positive torque direction.
$\mathbf{C}^{\mathbf{2}}_{\mathsf{neg}}$	Calibration matrix of IT 2 for the negative torque direction.
$\mathbf{C}^{\mathbf{2}}_{\mathsf{pos}}$	Calibration matrix of IT 2 for the positive torque direction.
c	Propeller blade chord.
C_D	Drag Coefficient.
C_L	Lift Coefficient.
C_M	Coefficient of moment.
C_P	Power Coefficient.
C_{d_0}	Zero-lift drag coefficient.
C_{P_0}	Coefficient of profile power.
$C_{P_{\mathrm{ind}}}$	Coefficient of induced power.

$\mathbf{D}$	Sensitivity coefficients matrix, used in calibration.
D	Diameter of rotor.
D	Rotor diameter.
d	Interaxial distance.
DL	Disk Loading
FM	Figure of Merit
$\vec{F}$	Total force exerted on fluid for a CV.
H	Rotor-plane distance.
$\mathbf{I}_{[N]}$	Identity matrix, $N \times N$.
K_{v}	Electric motor velocity constant $[\mathrm{RPM/V}]$.
$\dot{m}$	Mass flow rate over time.
Re	Reynolds number.
N_b	Number of rotor blades.
p	Rotor pitch.
P_0	Profile power.
P_{d}	Mechanical power for the the downstream rotor.
P_{ind}	Induced power.
P_{mech}	Mechanical power.
P_{total}	Total mechanical power of tandem system.
P_{u}	Mechanical power for the upstream rotor.
$\mathbf{R}$	Output of bridges recorded during calibration.
Ma	Mach number.
r	Bridge outputs for load estimation.
F_{X}	Axial force produced by rotor (thrust).
F_{Y}	Horizontal force produced by rotor.
T	Thrust produced by rotor (MTA).
T_{X}	Torque produced by rotor.
$\mathbf{u}$	Velocity vector.

u, v, w Velocity Cartesian components.

v_i Induced velocity at the rotor plane.

$\mathbf{V}^{\mathbf{1}}_{\text{neg}}$ Error computation matrix of IT 1 for the negative torque direction.

$\mathbf{V}^{\mathbf{1}}_{\text{pos}}$ Error computation matrix of IT 1 for the positive torque direction.

$\mathbf{V}^{\mathbf{2}}_{\text{neg}}$ Error computation matrix of IT 2 for the negative torque direction.

$\mathbf{V}^{\mathbf{2}}_{\text{pos}}$ Error computation matrix of IT 2 for the positive torque direction.

$\mathbf{V}_{\text{R}}$ Covariance matrix for the outputs of the bridges, used in calibration.

$\mathbf{V}_{\text{w}}$ Statistical estimation of accidental errors introduced during calibration.

$\overrightarrow{V_{\text{d}}}$ Downstream rotor linear velocity vector.

$\overrightarrow{V_{\text{rel}}}$ Relative velocity vector.

$\overrightarrow{V_{\text{uw}}}$ Incoming wake velocity vector.

$\vec{V}$ Velocity of fluid.

$\mathbf{W}$ Weighting matrix used during calibration process.

W Total fluid energy on some CV.

w Velocity of the slipstream in the far wake.

$\mathbf{Y}$ Static load matrix applied during calibration.

$\hat{y}$ Loads estimation using the calibration matrix.

y_0 Expected or true load.

Subscripts

∞ Far-wake condition.

i Computational index.

ov Related to overlap.

d Index referring to downstream.

ind Induced.

u Index referring to upstream.

uw Index referring to the wake of the upstream rotor.

Superscripts

T Transpose.

Glossary

BLDC	Brushless Direct Current (Motors)
CCW	Counter-clockwise rotation direction
CFD	Computational Fluid Dynamics
CV	Control Volume
CW	Clockwise rotation direction
ER	Equal Rotation, rotation direction of upstream and downstream rotors is the same
FM	Figure of Merit
IT1	Instrumented Tube 1
IT2	Instrumented Tube 2
MRE	Mean Relative Error
MTA	Momentum Theory Analysis
OR	Opposite Rotation, rotation direction of upstream and downstream rotors is opposite
RPM	Rotations per Minute
UAV	Unmanned Aerial Vehicle
WLS	Weighted Least-Squares

Chapter 1

Introduction

1.1 Motivation and Context

Drones, or UAVs, have become extremely relevant in countless areas of application. These include the timely delivery of goods, applications in surveillance and aerial imaging, weather forecasting, topographic surveys and even on the assessment of structural integrity, where the use of human labour would prove to be either unsafe or too costly.

In more recent applications, a deeper body of research for coaxial twin-rotor configurations has been developed. Introducing alternative rotor configurations, that can provide more lift at a smaller footprint has become more and more interesting. Indeed, computational models, to-scale and full-scale designs for coaxial rotor configurations have been studied and even implemented. This body of research for coaxial configurations was reviewed by Coleman [1] in a 1997 survey for the NASA Ames Research Centre.

For drones in particular, where more propellers are used with relatively smaller diameters, the research is still largely under way. In fact, very few empirical studies for tandem-rotor configurations have been developed for either full scale transport helicopters or drones.

1.2 Topic Overview

Multi-rotor aerial vehicles provide several advantages over the traditional helicopter design, where a single rotor provides lift. These vehicles are often more efficient in their usage of power, since all rotors provide lift force. The command of such vehicles is also of simpler implementation for automation than that of traditional, single-rotor aircraft: movement and rotation can be controlled by adjusting the speed of the rotors. Another key advantage is reliability, since they can, with a sufficiently robust control system, operate (or at least safely land) even when there is a rotor failure.

The overall trend in UAV design has been towards the improvement of reliability, efficiency and payload carrying capability. The ability to carry a larger payload on a smaller footprint aircraft is undoubtedly desirable. This option has been explored for military transport helicopters, such as the Boeing Chinook

CH-47. A similar configuration can be implemented in small scale aerial transport, to achieve a larger payload for the same footprint area.

Using tandem rotors for full-scale or small scale transport is not without its disadvantages. Firstly, the downstream rotor faces interference, and thus reduced performance. This implies that for the same payload (and thrust), more power is required. The interference between the rotors also implies more noise. If the interference is of unequal magnitude across time, there can be induced vibrations in the aircraft.

1.3 Research on Tandem Rotor Configurations

The majority of studies use two parameters to define rotor overlap geometrically: d and H. The former, hereafter referred to as interaxial distance, is the distance between the (parallel) axes of rotation of the rotors. The latter, called interrotor or interplanar distance, is the distance between the rotor planes. These variables are often adimensionalised by means of rotor diameter D.

Before the year 2000, research into alternative rotor configurations was very scarce. In 1954, Dingeldein [2] studied a planar (where all rotors are in the same plane) configuration with $1.03\ d/D$ spacing. The work concluded remarking that, while theoretical predictions would imply that hovering efficiency would be similar or slightly lower, it was, in fact, greatly improved due to a reduction in induced power (relative to a coaxial configuration). Huston [3] expanded on this work by evaluating both overlapping and non-overlapping configurations ($d/D = 1.03$ and 1.23), in hover as well as forward flight.

The results mentioned above and others were compiled in a 1984 book by Stepniewski and Keys [4], providing an in-depth review of helicopter design as well as an analysis of previous research results and respective theoretical predictions.

In 1996, a paper by Bagai and Leishman [5] showed a novel free-wake model that could accurately predict the behavior of coaxial configurations, as well as 3-rotor tandem. In 2002, Leishman et al. [6] then developed a set of free-vortex methods for rotor wake modeling, with good empirical agreement.

After the year 2000, research into drones has been rapidly evolving, both regarding numerical simulations and empirical research. Making a drone with a smaller overall footprint as well as reducing noise and other undesirable characteristics have become increasingly attractive in most areas of application. Theys et al. [7] found that pusher configurations for overlapping propeller configurations are more desirable, since they provided a slight efficiency increase. The maximum efficiency of the configuration was found to be for the smallest H/D possible and 1.10 to $1.15\ d/D$. This is, of course, in disagreement with the theoretical prediction that the greater the overlap, the larger the power requirements over isolated rotors.

More recently, Ramasamy [8] analysed the effects of blade twist, interrotor distance and interaxial distance, power and thrust distribution on overall hover efficiency, and other relevant coefficients such as the Figure of Merit. A surprising observation was that the downstream rotor operated at higher efficiencies if the interrotor distance was beyond a certain threshold, which depended on the blade planform. The author also found that, as predicted by momentum theory, with decreasing interaxial

distance the performance of tandem-rotors decreased as well.

Lastly, an empirical study by Brazinskas et al. [9] found fairly consistent results if the rotors were subject to the torque balance requirement (not always applicable) to drones in hover. The authors tested a single 2-blade (16$\times$5.4) rotor model, subject to various tandem conditions. Overall and downstream-rotor efficiency increased as overlap distance d increased. Peak efficiency was measured at $d/D = 0.97$, but was measured as 3% less efficient when compared to two isolated rotors.

1.4 Objectives

This work aims to identify and characterize the relevant parameters for the performance of tandem rotor systems. As such, the following objectives must be completed:

- Define which parameters are important for tandem configurations, which require more study and which are not critical;
- Design and perform modifications to a testing bench originally designed by Amado [10], to allow for the testing of tandem rotors;
- Create and execute a testing plan in order to isolate and analyse the selected variables;
- Study the influence of interaxial and interrotor distance on the downstream rotor;
- Compare the performance of the downstream rotor with its isolated counterpart.

Chapter 2

Theoretical Background

In helicopter and UAV design, the most applied method for first-order engineering approximations is the Momentum Theory Analysis (MTA). It is thus presented here, as explained by Leishman [11].

2.1 Momentum Theory Analysis for an Isolated Hovering Rotor

The conservation laws that are relevant to any fluid dynamics problem are the conservation of fluid mass across some control volume (equation (2.1)), balance of fluid momentum (eq. (2.2)) and balance of fluid energy (eq. (2.3)). Here, $\vec{V}$ is the velocity of the fluid, $\vec{S}$ is the normal to the boundary of the CV and W is the total energy of the fluid in the CV. $\vec{F}$ is the force that the fluid is subjected to.

$$\iint_S \rho\vec{V} \cdot d\vec{S} = 0 \tag{2.1}$$

$$\vec{F} = \iint_S p d\vec{S} + \iint_S \vec{V}(\rho\vec{V} \cdot d\vec{S}) \tag{2.2}$$

$$W = \iint_S \frac{1}{2}|\vec{V}|^2(\rho\vec{V} \cdot d\vec{S}) \tag{2.3}$$

The fluid flow through the rotor-disk (see fig. 2.1(a)) is assumed to be one-dimensional, quasi-steady, incompressible and inviscid. As such, it can be divided into two parts: one where velocities are more substantial (slipstream or wake), and another where the flow is mostly quiescent. As the flow develops in the wake, there is an increase in flow velocity and the wake diameter shrinks. For an ideal, non-viscous fluid flow, the necessary increase in kinetic energy of the rotor slipstream is referred to as *induced power*; it is the only unavoidable loss in a hovering rotor within an ideal fluid. Additional non-ideal effects and losses such as drag can be accounted for with non-ideal factors, which are included at the very end of the analysis. Another source of losses not accounted for in MTA is the continuous vortex shedding at the tip of the rotor blades, which are convected downstream. An experimental measurement of velocity fields around a hovering rotor is shown in fig. 2.1(b), as well as vortex shedding around the wake.

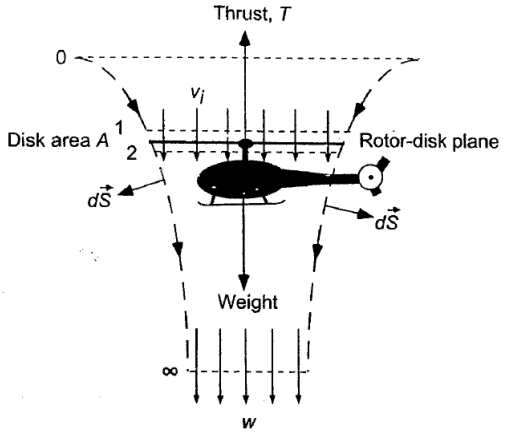

(a) Flow model across a rotor disk, with notations for momentum theory analysis. Sections 1 and 2 are planes just above and below the rotor-disk. 0 and ∞ represent the sections far from the rotor, upstream and in the 'far' wake, respectively.

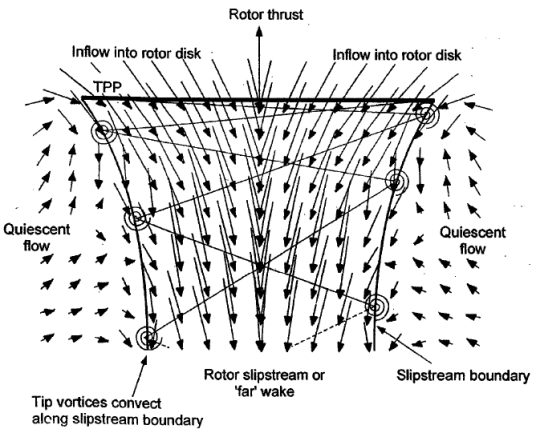

(b) Experimental measurements by Leishman (1995), near a two-bladed rotor. Note the contraction of the wake as distance from the rotor increases.

Figure 2.1: Flow model and experimental results from Leishman [11]

Figure 2.1(a) shows a hovering rotor and the relevant planes for this analysis. Assuming that the flow velocity through the rotor disk is v_i then equation (2.1) can be simplified to:

$$\dot{m} = \rho A_\infty w = \rho A_2 v_i = \rho A v_i \tag{2.4}$$

The conservation of fluid momentum (eq. (2.2)) implies that the rotor thrust is equal and opposite to the force imparted on the fluid (that is, $\vec{T} = -\vec{F}$). Thus, the momentum conservation equation becomes

$$T = \iint_\infty \rho(\vec{V} \cdot d\vec{S})\vec{V} - \iint_0 \rho(\vec{V} \cdot d\vec{S})\vec{V} \tag{2.5}$$

and can be further simplified to equation (2.6), by noting that the flow far upstream of the rotor must be quiescent (implying that the second term on the right-hand side is equal to 0).

$$T = \iint_\infty \rho(\vec{V} \cdot d\vec{S})\vec{V} = \dot{m}w \tag{2.6}$$

The principle of conservation of energy allows for further simplifications. Starting with equation (2.3) and noting that the work done per unit time is the power consumed by the rotor (that is $W = Tv_i$):

$$Tv_i = \underbrace{\iint_\infty \frac{1}{2}(\rho\vec{V} \cdot d\vec{S})\vec{V}^2}_{=\frac{1}{2}\dot{m}w^2} - \underbrace{\iint_0 \frac{1}{2}(\rho\vec{V} \cdot d\vec{S})\vec{V}^2}_{=0} = \frac{1}{2}\dot{m}w^2 \tag{2.7}$$

From equations (2.6) and (2.7), it should be clear that

$$v_i = \frac{1}{2}w \iff w = 2v_i \tag{2.8}$$

Because in the *vena contracta* the velocity must increase, the slipstream area (and especially at ∞)

must decrease, to maintain continuity. Equivalently, $\rho A v_i = \rho A_\infty w = 2\rho A_\infty v_i$, from which it follows that $\frac{A_\infty}{A} = \frac{1}{2} \implies r_\infty = \frac{R}{\sqrt{2}}$.The *wake contraction ratio* for an ideal setting is, thus, $\frac{1}{\sqrt{2}} \approx 0.707$. Non ideal effects due to fluid viscosity, nonuniform flow and a swirl component (induced by the rotating blades) imply that this ratio is usually slightly greater (Leishman [11] suggests a value of 0.78).

The power required to hover follows from equation (2.6), which can now be developed using eqs. (2.8) and (2.4), as well as $P_i = T v_i$:

$$T = \dot{m} w = 2(\rho A v_i) v_i = 2\rho A {v_i}^2 \implies v_i = \sqrt{\frac{T}{2\rho A}} \tag{2.9}$$

$$P_i = T\sqrt{\frac{T}{2\rho A}} = \frac{T^{3/2}}{\sqrt{2\rho A}} \tag{2.10}$$

$$P_i = (2\dot{m} v_i) v_i = 2\rho A {v_i}^3 \tag{2.11}$$

Equation (2.11) has important implications regarding helicopter design: for a given thrust, a lower induced velocity but higher mass flow (and thus, higher area) minimizes the induced power required. This suggests an explanation for the gradual increase in rotor area in helicopter design, so as to reduce power requirements as much as possible.

Defining Ω as the angular velocity of a rotor and R as its radius, the thrust (C_T), rotor shaft torque (C_Q) and ideal power (C_P) coefficients can be obtained[1]:

$$C_T = \frac{T}{\frac{1}{2}\rho A(\Omega R)^2} \qquad C_Q = \frac{Q}{\frac{1}{2}\rho A(\Omega R)^2 R} \qquad C_{P_{\text{ideal}}} = \frac{P_{\text{ideal}}}{\frac{1}{2}\rho A(\Omega R)^3} = \frac{C_T^{3/2}}{\sqrt{2}} \tag{2.12}$$

To allow for nonideal effects, the *induced power correction factor* κ is introduced, which must be experimentally obtained:

$$C_{P_{\text{ind}}} = \frac{\kappa C_T^{3/2}}{\sqrt{2}} = \kappa C_P \tag{2.13}$$

For a reasonable estimation of the power consumed by a rotor, the profile power P_0 must also be computed. By definition, it is the integration of the sectional drag force D along the length of the blades, multiplied by Ω. Drag is a function of the Mach number Ma, the Reynolds number Re, as well as the physical properties of the rotor blades themselves (e.g. pitch, diameter). Because this computation is fairly effortful, P_0 is often approximated by means of the no-lift drag coefficient, C_{d_0}. This coefficient, assumed constant and independent of Ma and Re for the zero-lift angle of attack, allows for the approximation of P_0 with eq. (2.14), where c is the blade chord and N_b is the number of blades.

$$P_0 = \frac{1}{8}\rho N_b \Omega^3 c C_{d_0} R^4 \tag{2.14}$$

Converting to a power coefficient and simplifying:

[1] $\frac{1}{2}\rho A v^2$ represents the dynamic pressure, which is used for adimensional coefficients in most of the world. In the US, the factor $\frac{1}{2}$ is often omitted, yielding coefficients that are a factor of 2 smaller. Since these coefficients are presented by Leishman [11] using US conventions, these are also used here.

$$C_{P_0} = \frac{P_0}{\rho A(\Omega R)^3} = \frac{1}{8}\underbrace{\left(\frac{N_b c}{\pi R}\right)}_{=\sigma} C_{d_0} = \frac{1}{8}\sigma C_{d_0} \tag{2.15}$$

Where σ is known as the rotor solidity, as it is only a function of geometric attributes of the rotor itself. Finally, the rotor power requirements can now be computed, as well as the respective coefficient C_P:

$$C_P = C_{P_{\text{ind}}} + C_{P_0} = \frac{\kappa C_T^{3/2}}{\sqrt{2}} + \frac{\sigma C_{d_0}}{8} \tag{2.16}$$

For rotors with the same Disk Loading ($DL = T/A$), the Figure of Merit (FM) is suggested as the adimensional efficiency measure. For a hovering rotor, it is defined as

$$FM = \frac{\text{Ideal Power}}{\text{Actual Power}} = \frac{P_{\text{ideal}}}{P_{\text{ind}} + P_0} \tag{2.17}$$

2.2 Momentum Theory Analysis for Rotors in Tandem

The standard momentum theory analysis can be adapted for tandem rotor systems, the main object of study of this work. The adaptation presented here is as outlined by Leishman [11]. In tandem configurations the rotors interfere with one another reducing the produced thrust by some amount. Figure 2.2 shows a schematic view of these rotor configurations, with some additional dimensions.

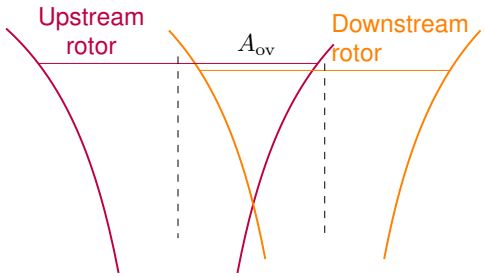

(a) Side view of two rotors in tandem, in very close proximity to one another, with overlap area indicated.

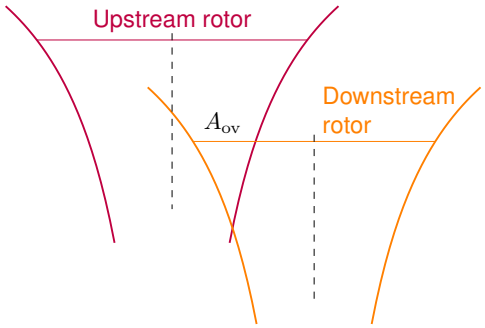

(b) Side view of 2 rotors in tandem, where the downstream rotor is in the wake of the upstream one.

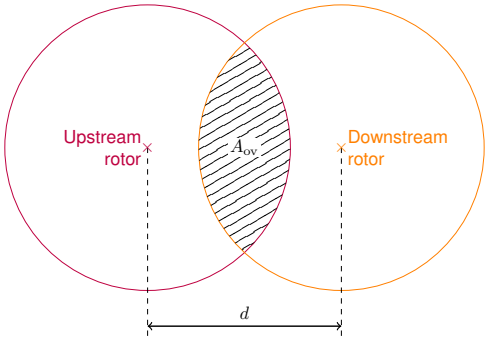

(c) Top view of 2 rotors in tandem, in very close proximity. Both rotors have the same diameter, D

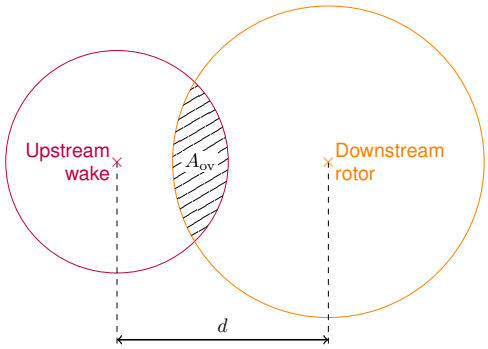

(d) Top view of 2 rotors in tandem, where one rotor is in the wake of the other.

Figure 2.2: Naming conventions in horizontal and vertical views for MT analysis (wake shape is not physically accurate)

2.2.1 MTA for Tandem Configurations in Close Proximity

For rotors in very close vertical proximity (see figures 2.2(a) and 2.2(d)), the area of overlap (and thus interference) can be easily computed. Upstream and downstream rotors are interchangeable, since interplanar distance $H = 0$. Defining m' as the ratio between the overlap area and the total area, and δ as the ratio d/D:

$$m' = \frac{A_{\text{ov}}}{A} = \frac{2}{\pi}\left[\theta - \delta \sin\theta\right], \text{where } \theta = \cos^{-1}\delta \tag{2.18}$$

If T_1 and T_2 are the thrusts of each of the rotors (which may be unequal), $m'(T_1 + T_2)$ is the thrust on the overlapping region. The induced powers of each undisturbed region (P_1 and P_2) as well as the overlapped region (P_{ov}) are:

$$P_1 = \frac{(1-m')\,T_1^{3/2}}{\sqrt{2\rho A}} \qquad P_2 = \frac{(1-m')\,T_2^{3/2}}{\sqrt{2\rho A}} \qquad P_{\text{ov}} = \frac{m'\,(T_1+T_2)^{3/2}}{\sqrt{2\rho A}} \tag{2.19}$$

The overlap induced power factor is defined as the ratio between the total induced power required to hover and that of two isolated rotors, or $\kappa_{\text{ov}} = (P_{\text{ind}})_{\text{ov}} / P_{\text{ind}}$.

$$\kappa_{\text{ov}} = \frac{(1-m')\,T_1^{3/2} + (1-m')\,T_2^{3/2} + m'\,(T_1+T_2)^{3/2}}{T_1^{3/2} + T_2^{3/2}} \tag{2.20}$$

Taking T as the total thrust produced and A as the area of one of the rotors, the total induced power can be expressed as:

$$P_{\text{ind}} = \kappa_{\text{ov}} \kappa T \sqrt{\frac{T}{4\rho A}} \tag{2.21}$$

Two more equations can be applied for specific cases. Firstly, if each rotor produces an equal amount of thrust ($T_1 = T_2$), then:

$$\kappa_{\text{ov}} = 1 + \left(\sqrt{2} - 1\right) m' \approx 1 + 0.4142\, m' \tag{2.22}$$

Finally, Harris [12] suggests a prediction for κ_{ov} based solely on δ. This result has been shown to underpredict the overlap coefficient, but is based on experimental results.

$$\kappa_{\text{ov}} \approx \left[\sqrt{2} - \frac{\sqrt{2}}{2}\delta + \left(1 - \frac{\sqrt{2}}{2}\right)\delta^2\right] \tag{2.23}$$

The assumption that does not apply to drones within this analysis is that the rotors carry an equal fraction of the thrust. In any type of aircraft, thrust balance is a requirement for hover, though in drones it is achieved across multiple rotors, and not just two. It can, however, be shown that even if this assumption is not accurate, the results for κ_{ov} are not significantly affected by this, insofar as the torques remain balanced.

2.2.2 Theoretical Analysis for a Rotor in the Wake of Another

The other case that can be analysed is when one of the rotors is in the fully developed wake of another, such as in fig. 2.2(b). In such cases, the overlap area factor m' is either computed numerically or through a slightly more complex closed-form equation (see subsection 2.2.2). Subscripts d and u refer to downstream and upstream rotors, respectively. Individual rotor thrusts can be determined through eq. (2.6) to be:

$$T_{\mathrm{u}} = (\rho A v_{\mathrm{u}})(2v_{\mathrm{u}}) \qquad T_{\mathrm{d}} = (\dot{m}w)_{\mathrm{d}} - (\dot{m}w)_{\mathrm{u}} \tag{2.24}$$

Mass flow across each rotor is then determined with

$$\dot{m}_{\mathrm{u}} = m'\rho A(2v_{\mathrm{u}}) \qquad \dot{m}_{\mathrm{d}} = (1-m')\rho A v_{\mathrm{d}} + m'\rho A(v_{\mathrm{d}} + 2v_{\mathrm{u}}) \tag{2.25}$$

If both rotors are responsible for the same thrust, an approximation which is not completely valid but which yields reasonable results:

$$[(1-m')\rho A v_{\mathrm{d}} + m'\rho A(v_{\mathrm{d}} + 2v_{\mathrm{u}})]\, w_{\mathrm{d}} - [m'\rho A(2v_{\mathrm{u}})](2v_{\mathrm{u}}) = (\rho A v_{\mathrm{u}})(2v_{\mathrm{u}}) \tag{2.26}$$

Which can be simplified to

$$\frac{v_{\mathrm{u}}^2(4m'+2)}{w_{\mathrm{d}}} = (v_{\mathrm{d}} + 2m'v_{\mathrm{u}}) \tag{2.27}$$

Conservation of energy (Eq. (2.7)) applied to the lower rotor yields

$$\begin{aligned} P_{\mathrm{d}} = T[(1-m')v_{\mathrm{d}} + m'(v_{\mathrm{d}} + 2v_{\mathrm{u}})] &= \left(\frac{1}{2}\dot{m}w^2\right)_{\mathrm{d}} - \left(\frac{1}{2}\dot{m}w^2\right)_{\mathrm{u}} \\ \implies T(v_{\mathrm{d}} + 2m'v_{\mathrm{u}}) &= \frac{1}{2}\rho A(v_{\mathrm{d}} + 2m'v_{\mathrm{u}})w_{\mathrm{d}}^2 - 4\rho A m' v_{\mathrm{u}}^3 \end{aligned} \tag{2.28}$$

Which can then be simplified by noting that $T/(\rho A) = 2v_{\mathrm{u}}^2$ (eq. (2.24)):

$$2v_{\mathrm{u}}^2(v_{\mathrm{d}} + 2m'v_{\mathrm{u}}) = \left(\frac{w_{\mathrm{d}}^2}{2}\right)\underbrace{\left(\frac{v_{\mathrm{u}}^2(4m'+2)}{w_{\mathrm{d}}}\right)}_{\text{from (2.27)}} - 4m'v_{\mathrm{u}}^3 \tag{2.29}$$

Expanding, equation (2.29) can be simplified to give the slipstream velocity at the downstream rotor w_{d} as:

$$w_{\mathrm{d}} = \frac{8m'v_{\mathrm{u}} + 2v_{\mathrm{d}}}{2m'+1} \tag{2.30}$$

Which can then be substituted back into eq. (2.27), yielding

$$v_{\mathrm{u}}^2(4m'+2) = \left(\frac{8m'v_{\mathrm{u}} + 2v_{\mathrm{d}}}{2m'+1}\right)(v_{\mathrm{d}} + 2m'v_{\mathrm{u}}) \tag{2.31}$$

which, finally, this can be expanded and simplified into a quadratic equation for v_{d} in terms of v_{u}:

$$\left(\frac{16m'^2}{2m'+1} - 4m' - 2\right) v_{\mathrm{u}}^2 + \left(\frac{12m'}{2m'+1}\right) v_{\mathrm{u}} v_{\mathrm{d}} + \left(\frac{2}{2m'+1}\right) v_{\mathrm{d}}^2 = 0 \tag{2.32}$$

As the value of m' can be determined, equation (2.32) can be solved to give v_{d} as a function of v_{u} (see subsection 2.2.2 for the full solution). Defining $v_{\mathrm{d}} = G(m')v_{\mathrm{u}}$, the total power P_{total} is:

$$P_{\mathrm{total}} = \underbrace{T_{\mathrm{u}} v_{\mathrm{u}}}_{=P_{\mathrm{u}}} + \underbrace{T_{\mathrm{d}} \left(v_{\mathrm{d}} + 2m' v_{\mathrm{u}}\right)}_{=P_{\mathrm{d}}} \tag{2.33}$$

By applying eq. (2.24), P_{total} becomes:

$$P_{\mathrm{total}} = T \left(G(m') + 1 + 2m'\right) v_{\mathrm{u}} \tag{2.34}$$

Which is simplified by (2.9), yielding:

$$P_{\mathrm{total}} = \frac{\left(G(m') + 1 + 2m'\right) T^{3/2}}{\sqrt{2\rho A}} \tag{2.35}$$

Equation (2.35) can be used to determine κ_{ov}:

$$\kappa_{\mathrm{ov}} = \frac{P_{\mathrm{total}}}{2P_{\mathrm{iso}}} = \frac{\left(G(m') + 1 + 2m'\right)}{2} \tag{2.36}$$

Modifications for Tandem Rotors with Large Spacing

The overlap area of two *circles* of different diameters can be computed in similar fashion to what is done for equal-diameter circles. Fig. 2.3 shows the relevant names for this computation.

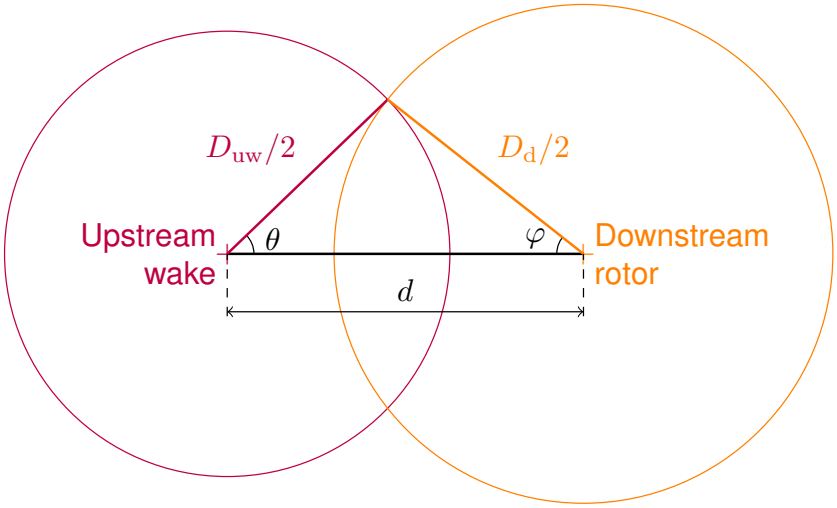

Figure 2.3: Overlap area designations.

Angles θ and φ can be determined using the law of cosines,

$$\begin{cases} \cos\theta = \frac{D_{\mathrm{uw}}^2 - D_{\mathrm{d}}^2 + 4d^2}{4dD_{\mathrm{uw}}} \\ \cos\varphi = \frac{D_{\mathrm{d}}^2 - D_{\mathrm{uw}}^2 + 4d^2}{4dD_{\mathrm{d}}} \end{cases} \tag{2.37}$$

meaning that the overlap area is

$$A_{\mathrm{ov}} = \frac{1}{2}\left[D_{\mathrm{uw}}^2\theta + D_{\mathrm{d}}^2\varphi - d \cdot D_{\mathrm{uw}} \sin\theta\right] \tag{2.38}$$

This, in turn, implies that the overlap coefficient m' can be computed precisely, given both diameters and interrotor distance:

$$m' = \frac{2}{\pi}\left[\left(\frac{D_{\mathrm{uw}}}{D}\right)^2\theta + \left(\frac{D_{\mathrm{d}}}{D}\right)^2\varphi - \frac{d}{D}\frac{D_{\mathrm{uw}}}{D}\sin\theta\right] \tag{2.39}$$

Of course, this is only useful for the base assumption that power is proportional to m', which does not apply in a clear way for cases where the rotors are of different sizes. Therefore, this computation is only useful for those cases where both rotors are of the same size.

Another important addition is that equation (2.32) can be solved by hand, providing a mathematical expression for $G(m')$:

$$G(m') = \sqrt{5m'^2 + 4m' + 1} - 3m' \tag{2.40}$$

2.2.3 Comparison of Theoretical Results

The overlap coefficients κ_{ov} can now be compared to one another, as can be seen in fig. 2.4. The experimental correlation from Harris [12] is also presented. For all three examples shown, $D = D_{\mathrm{d}}$. It is now evident that the Harris correlation underestimates κ_{ov} (especially since it should prove to be higher than theoretical estimations provide), but that neither of these three alternatives for computation is too dissimilar to one another. No variations in diameter are presented, since the MTA assumes that power is proportional to m'.

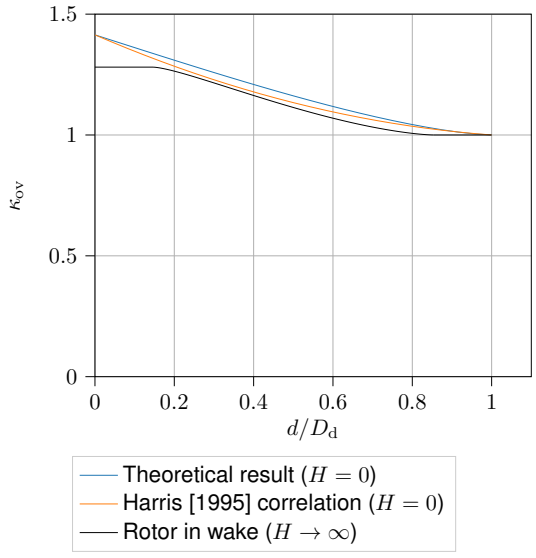

Figure 2.4: Graphical comparison of κ_{ov}, in three different cases.

2.3 Limitations of MTA

The assumptions of Momentum Theory Analysis are applicable in a fairly wide range of circumstances. However, the same cannot be said for its equivalent within tandem rotor systems. The cases presented in the previous section (interrotor distance close to 0 or large enough for a fully developed wake) may not be applicable for a drone in hover. However, the approximations obtained provide useful edge cases for comparison and evaluation of general performance, where these values would otherwise be lacking.

Because this theory was developed and is applied with regard to helicopters, it does not have inclusions for rotors of different diameters. In tandem-rotor helicopters, it is more common for rotors to be of the same diameter; this allows for much simpler momentum balancing of the aircraft, since both rotors can be physically coupled to one another at the same rotation speed. This, however, is not the case for drones, where most applications use several rotors in pairs of opposing rotation to achieve this. This is also relevant for drones since the angular velocity of the rotors can be adjusted independently.

For a rotor in the wake of another, no closed-form solution to the overlap coefficient m' is presented, though it does exist. As these cases are more relevant to the present work than they would be for helicopters, they will be be explored in more detail here. Thus, firstly a closed-form expression for calculating the power overlap factor is of some importance for this problem.

Chapter 3

Experimental Setup and Methodology

3.1 Experimental Test Bench

3.1.1 Original Test Bench

The experimental set-up was adapted from Amado [10] to allow for movement in both horizontal axes. The original test bench is shown in fig. 3.1 and was only capable of movement in the coaxial direction. It has provisions for two BLDC electric motors, Current, Voltage and RPM sensors. It has two Instrumented Tubes (IT), referred to as IT1 and IT2. IT1 is equipped with 3 extensometer bridges, for force measurement (F_{X} and F_{Y}) and torque (T_{X}) measurement. IT2 only measures torque.

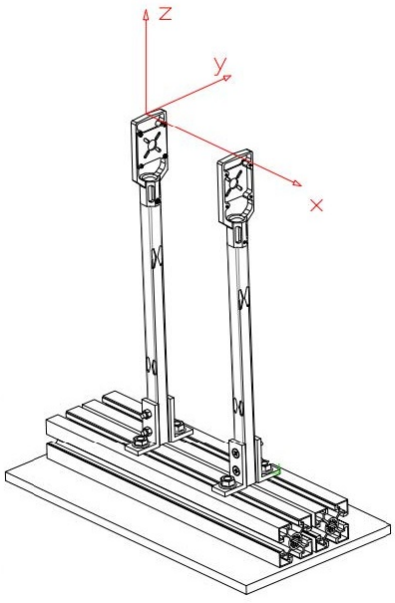

Figure 3.1: Perspective view of the original test bench, as designed by Amado [10]. Axis layout was maintained throughout this work

3.1.2 Modified Test Bench

The original test bench was modified with a set of profiles, to decouple interaxial and interrotor distance. For axial movement, another set of short profiles were added. For movement on the remaining horizontal axis a set of longer profiles was also added on the lower plane. Figure 3.1 shows the final movement range after these additions. A third tube with no extensometers was projected to be added, and some parts were acquired. However, due to issues with the supply of necessary parts, the third tube was never implemented or used. This can, in future, be expanded upon for further studies on tandem configuration propulsion systems.

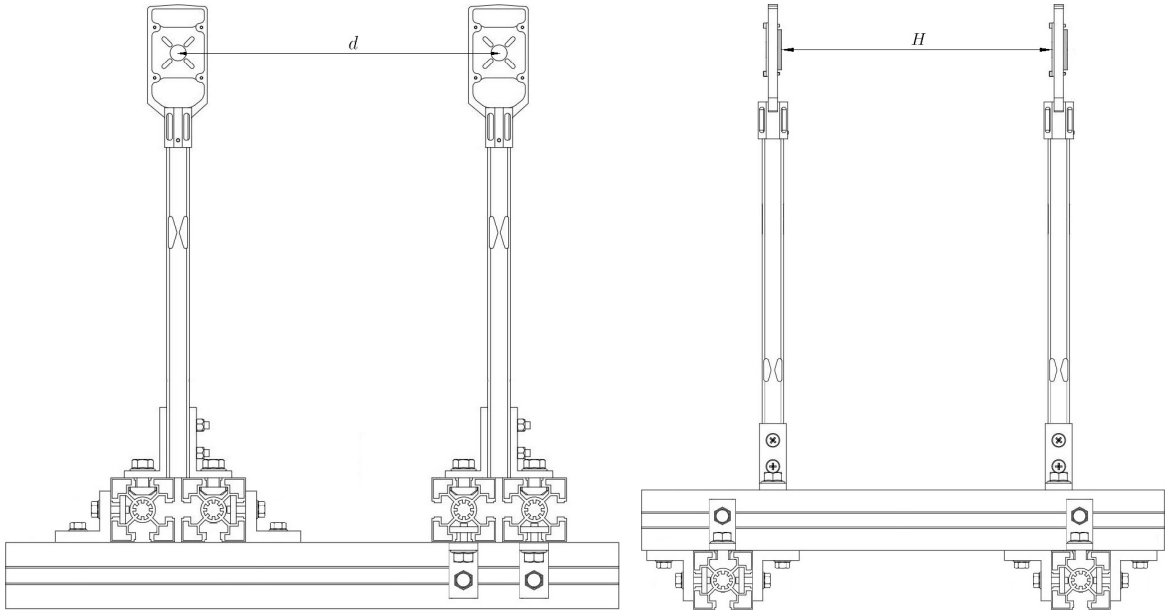

(a) Projected front view of the setup; Left-to-right movement is assured by the bottom rails (inter-axial distance, d)

(b) Projected right-side view of the test bench; Left-to-right movement is done on the top rails (coaxial distance, H).

Figure 3.2: Schematic representation of the modified testing bench, from two projection planes. Image adapted from Amado [10].

Figure 3.3 shows the design in operation. Markings on the left profiles were made to aid in repeatability of the distances used in the experimental procedure. In operation, the downstream rotor was kept fixed (on the right side in fig. 3.3). In place of the baseplate, the lower profiles were clamped to prevent any creeping over multiple tests.

3.1.3 Calibration Procedure

A static calibration was done according to what was originally designed by Amado [10], with the same mathematical structure, using a weighted variant of the Least-Squares method (described in 3.1.4). Offset correction was done by removing the zero-load component in each loading set: When in its working position, the offsets were recorded once more, and are corrected before any computation is done.

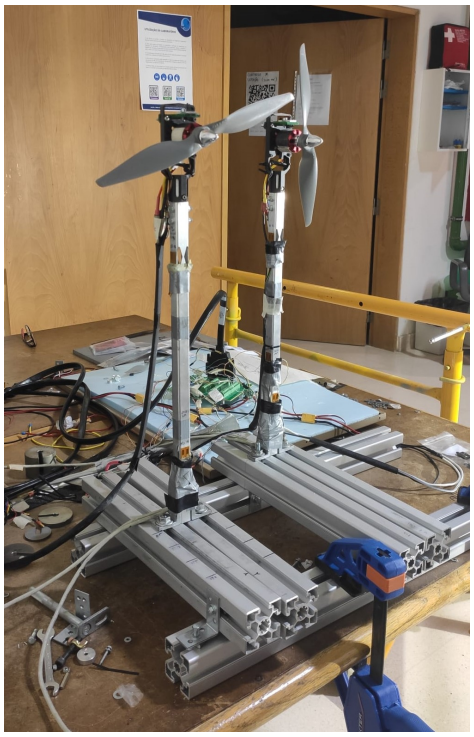

Figure 3.3: A photograph of the experimental setup at its final configuration.

Since linearity in output has already been verified by Amado [10] to be good and the maximum forces experienced by the instrumented tubes will be under $10\ \mathrm{N}$, lower force thresholds of $25\ \mathrm{N}$ were used instead of $30\ \mathrm{N}$. Increments of $1\ \mathrm{N}$ were applied up to $10\ \mathrm{N}$, and of $5\ \mathrm{N}$ thereafter. To improve reliability of this data, a load-unload plan was developed, both to model hysteresis and as an additional set of points for correct calibration. The loading plan is detailed in table 3.1, in the positive direction. Indexes are pertinent to the file-indexing system implemented, so that the load is more easily matched with the responses recorded. Input forces are similar for the reverse direction, but were applied by rotating the calibration setup 180 degrees. The gravitational constant used to compute weights was $g = 9.81\ \mathrm{m/s^2}$.

Torque calibration was done with a similar load-unload plan as was done regarding force. The full range of torques was applied (up to a nominal $1\ \mathrm{Nm}$), both positive and negative. To change the sign of the applied torque, the IT was left in the solid set-up and only the direction of forces was inverted, maintaining vertical alignment.

Calibration results are presented in figure 3.4 for force and figures 3.5(a) and 3.5(b) for torque, in IT1 and IT2 respectively.

3.1.4 Weighted Least-Squares Method

A weighted Least-Squares (WLS) approach was also implemented here. A python script, using the *numpy*, *pandas* and *scipy* libraries, was developed to compute these matrices. The set of static loads applied was recorded as an $N \times k$ matrix ($\mathbf{Y}$), and the bridge responses as an $N \times k$ matrix ($\mathbf{R}$), where

Table 3.1: Loading plan for X and Y forces for IT1, and X for IT2

Index	Applied Weight [N]	Index	Applied Weight [N]	Index	Applied Weight [N]
0	0.000	9	8.907	18	7.916
1	0.965	10	9.895	19	6.923
2	1.963	11	14.928	20	5.931
3	2.957	12	19.960	21	4.939
4	3.950	13	24.993	22	3.950
5	4.939	14	19.960	23	2.957
6	5.931	15	14.928	24	1.963
7	6.923	16	9.895	25	0.965
8	7.916	17	8.907	26	0.000

Table 3.2: Loading plan for torque along X, for both IT1 and IT2

Index	Applied Torque [Nm]	Index	Applied Torque [Nm]	Index	Applied Torque [Nm]
0	0.000	5	0.494	10	0.196
1	0.097	6	0.997	11	0.097
2	0.196	7	0.494	12	0.000
3	0.295	8	0.395		
4	0.395	9	0.295		

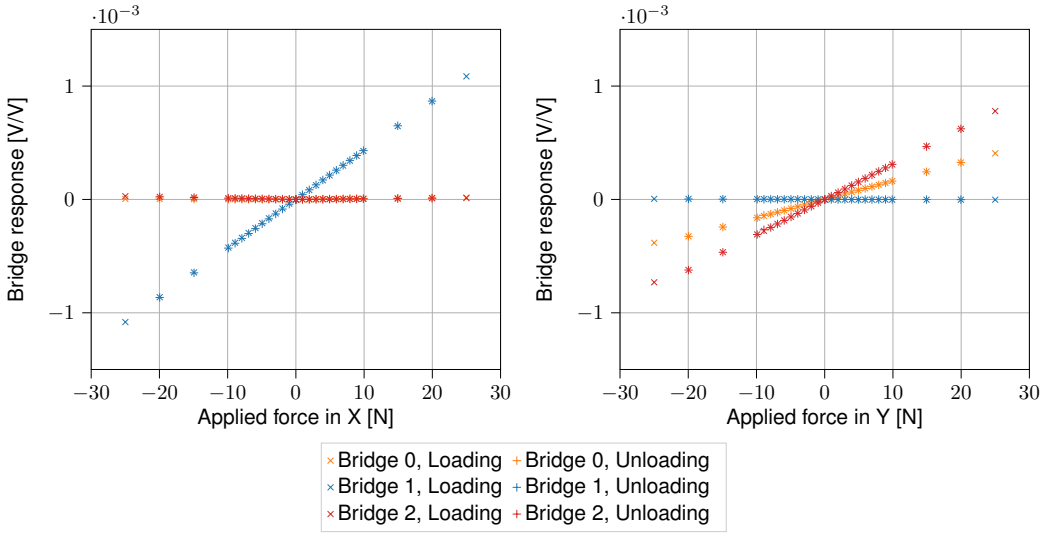

Figure 3.4: Calibration data for force along X and Y in IT1.

$k = 3$ for IT1 and $k = 1$ for IT2.

A first estimation of the calibration matrix $\mathbf{C}$ is obtained, which is then used to compute a first approximation of the weights matrix $\mathbf{W}$ based on error estimation. This matrix is then used to estimate $\mathbf{C}$ once again. Then, the final estimation of $\mathbf{W}$ is computed, using the sensitivity coefficients from $\mathbf{C}$ as well as a covariance matrix. As a first estimation, $\mathbf{C}$ is computed as if $\epsilon = 0$ in 3.1:

$$\mathbf{Y} = \mathbf{RC} + \epsilon \rightarrow \mathbf{C} = (\mathbf{R}^T\mathbf{R})^{-1}\mathbf{R}^T\mathbf{Y} \tag{3.1}$$

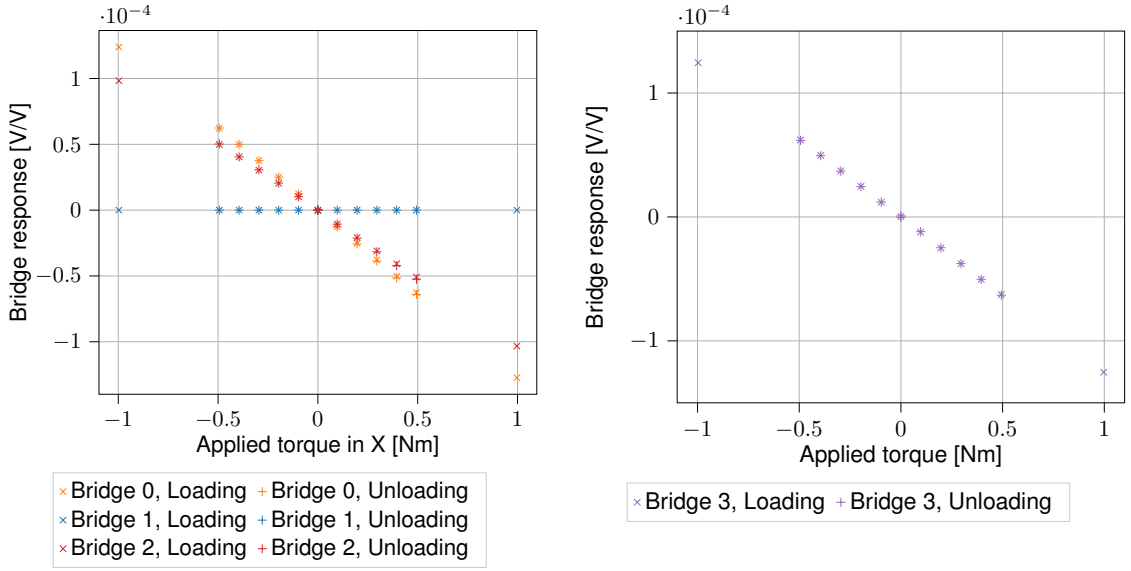

(a) IT1 torque calibration results.

(b) IT2 torque calibration results.

Figure 3.5: Torque calibration data for both ITs.

An estimate of $\mathbf{W}$, the weight matrix, can then be obtained with an auxiliary matrix:

$$\mathbf{W} = {\mathbf{V_w}}^{-1} \tag{3.2}$$

The matrix $\mathbf{V_w}$ encompasses a statistical estimation of the uncertainties introduced due to cable misalignment, vibrations and perturbations from other sources as well as the uncertainties in the masses measured (u_L). Here, N is the number of loads applied, m is the number of degrees of freedom (and is equal to k), $y_{\hat{k},i}$ is the estimated load using $\mathbf{C}$ and $y_{k,i}$ is the true value of the load applied.

$$\sigma_i^2 = \frac{1}{N-m} \sum_{k=1}^{N} (y_{k,i} - y_{\hat{k},i})^2 \tag{3.3}$$

As for the uncertainties related to the masses and the scale used (u_L, where L corresponds to the load), these are shown in tables 3.3 and 3.4:

Table 3.3: Uncertainties in force due to the scale used.

Index	Uncertainty $u_F \times 10^3$ [N]	Index	Uncertainty $u_F \times 10^3$ [N]	Index	Uncertainty $u_F \times 10^3$ [N]
0	0.00	9	8.83	18	7.85
1	0.98	10	9.81	19	6.87
2	1.96	11	10.79	20	5.89
3	2.94	12	11.77	21	4.91
4	3.92	13	12.75	22	3.92
5	4.91	14	11.77	23	2.94
6	5.89	15	10.79	24	1.96
7	6.87	16	9.81	25	0.98
8	7.85	17	8.83	26	0.00

The total uncertainty can then be estimated, and thus the $N \times N$ diagonal matrix $\mathbf{V_w}$:

Table 3.4: Uncertainties in torque due to the scale used.

Index	Uncertainty $u_T \times 10^3$ [Nm]	Index	Uncertainty $u_T \times 10^3$ [Nm]	Index	Uncertainty $u_T \times 10^3$ [Nm]
0	0.00	5	9.81	10	3.92
1	1.96	6	11.77	11	1.96
2	3.92	7	9.81	12	0.00
3	5.89	8	7.85		
4	7.85	9	5.89		

$$(\sigma_{\text{tot}}^2)_{i,j} = \sigma_i^2 + u_{ij}^2 \tag{3.4}$$

$$\begin{bmatrix} (\sigma_{\text{tot}})_{1,1} & & & & & & & & & \\ & \ddots & & & & & & & & \\ & & (\sigma_{\text{tot}})_{1,N_1} & & & & & & & \\ & & & (\sigma_{\text{tot}})_{2,1} & & & & & & \\ & & & & \ddots & & & & & \\ & & & & & (\sigma_{\text{tot}})_{2,N_2} & & & & \\ & & & & & & (\sigma_{\text{tot}})_{3,1} & & & \\ & & & & & & & \ddots & & \\ & & & & & & & & (\sigma_{\text{tot}})_{3,N_3} \end{bmatrix} \tag{3.5}$$

Where N_i are the number of loading sets for each type of load (F_X, F_Y and T_X, respectively) and $N_1 + N_2 + N_3 = N$. For IT2, this matrix is $N \times N$, since only torque is measured and applied. With $\mathbf{V}_{\text{w}}$, a first estimate of $\mathbf{W}$ can be obtained with eq. (3.2). The calibration matrix $\mathbf{C}$ can then be reevaluated to be:

$$\mathbf{C} = (\mathbf{R}^T \mathbf{W} \mathbf{R})^{-1} \mathbf{R}^T \mathbf{W} \mathbf{Y} \tag{3.6}$$

With a new estimate for $\mathbf{C}$, new estimates for $\mathbf{W}$ can be computed.

$$\mathbf{W}_{\text{i}} = \left(\mathbf{V}_{\text{w}} + \mathbf{D}_{\text{i}} \mathbf{V}_{\text{R}} \mathbf{D}_{\text{i}}{}^T \right)^{-1} \tag{3.7}$$

$\mathbf{V}_{\text{R}}$ is the covariance matrix (or, since only one set of data was acquired, a scalar), which can be obtained using the *numpy.cov* function. Firstly, the matrix $\mathbf{R}$ is converted to a $k.N \times 1$ vector, which is then input to the function.

The final matrix that must be determined is $\mathbf{D}$, which actually comprises k different $N \times k.N$ matrices. $\mathbf{D}_{\text{i}}$ is the sensitivity coefficients matrix. It can be computed through the horizontal concatenation (represented by $\oplus$) of k $N \times N$ matrices:

$$\left.\begin{array}{ll} \mathbf{D}_{\text{i}} = \mathbf{I}_{1,\text{i}} \oplus \mathbf{I}_{2,\text{i}} \oplus \mathbf{I}_{3,\text{i}} & \text{for IT1} \\ \mathbf{D}_{\text{i}} = \mathbf{I}_1 & \text{for IT2} \end{array}\right\} \quad \text{where } \mathbf{I}_{\text{i,j}} = \mathbf{C}_{\text{i,j}} \mathbf{I}_{\text{N}} \tag{3.8}$$

With all matrices determined, the final weights are computed using (3.7). It is then applied to eq. (3.6), with each column $\mathbf{C}_{\text{i}}$ being determined separately for each load type. $\mathbf{C}$ can then be applied to estimate loads $\hat{y}$ through the following equation, where r is a vector containing the output of the bridges (corrected for offset) for a specific IT:

$$\hat{y} = r\mathbf{C} \tag{3.9}$$

3.1.5 Resulting Calibration Coefficients

The resulting calibration coefficients after the WLS method was applied fully are displayed as matrices (equations (3.10) for IT1 and (3.11) for IT2). Note that there are 2 matrices for each IT, depending on the direction of the torque. In either case, the force F_X was applied in the positive direction. Thus, $\mathbf{C}^{\mathbf{i}}_{\text{pos}}$ and $\mathbf{C}^{\mathbf{i}}_{\text{neg}}$ refer only to the direction of T_X.

$$\begin{aligned}
\mathbf{C}^{\mathbf{1}}_{\text{pos}} &= \begin{bmatrix} -5.9481 \times 10^3 & -4.4920 \times 10^4 & -1.3601 \times 10^4 \\ 2.3047 \times 10^4 & 4.9334 \times 10^0 & 1.2046 \times 10^2 \\ 3.1583 \times 10^3 & 5.5488 \times 10^4 & 7.1048 \times 10^3 \end{bmatrix} \\
\mathbf{C}^{\mathbf{1}}_{\text{neg}} &= \begin{bmatrix} 3.5036 \times 10^2 & -4.4624 \times 10^4 & -1.3746 \times 10^4 \\ 2.2989 \times 10^4 & -8.6823 \times 10^0 & 1.2166 \times 10^2 \\ -3.3463 \times 10^1 & 5.6235 \times 10^4 & 7.1874 \times 10^3 \end{bmatrix}
\end{aligned} \tag{3.10}$$

For IT2, the results are two scalars, since only one bridge was used to obtain T_X:

$$\begin{aligned}
\mathbf{C}^{\mathbf{2}}_{\text{pos}} &= \begin{bmatrix} -7.9009 \times 10^3 \end{bmatrix} \\
\mathbf{C}^{\mathbf{2}}_{\text{neg}} &= \begin{bmatrix} -7.9908 \times 10^3 \end{bmatrix}
\end{aligned} \tag{3.11}$$

3.1.6 Uncertainty Computation

The computation of the uncertainty present in the calibration coefficients was done according to specifications in [13]. Uncertainties are computed for both positive and negative values; the methodology presented is, however, only valid for one axis. Matrix $\mathbf{V}_{\text{p}} = \left(\mathbf{R}^T\mathbf{W}\mathbf{R}\right)$, the error matrix, has diagonal elements corresponding to the variances (or squared uncertainties u_{c}^2). The law of propagation of uncertainty is equivalent to the statement that:

$$\mathbf{V}_{\hat{y}_{\text{i}}} = r\mathbf{V}_{p_{\text{i}}}r^T = r\left(\mathbf{R}^T\mathbf{W}_{\text{i}}\mathbf{R}\right)r^T \tag{3.12}$$

The uncertainties for the obtained calibration coefficients are, thus:

$$\mathbf{V}^{\mathbf{1}}_{\text{pos}} = \begin{bmatrix} 3.9926 \times 10^{1} & 1.9275 \times 10^{0} & 2.1285 \times 10^{1} \\ 1.2459 \times 10^{2} & 6.0150 \times 10^{0} & 6.6422 \times 10^{1} \\ 2.6520 \times 10^{1} & 1.2804 \times 10^{0} & 1.4138 \times 10^{1} \end{bmatrix}$$
$$\mathbf{V}^{\mathbf{1}}_{\text{neg}} = \begin{bmatrix} 4.5228 \times 10^{1} & 2.1619 \times 10^{0} & 2.4124 \times 10^{1} \\ 1.3799 \times 10^{2} & 6.5959 \times 10^{0} & 7.3602 \times 10^{1} \\ 3.0510 \times 10^{1} & 1.4584 \times 10^{0} & 1.6274 \times 10^{1} \end{bmatrix} \tag{3.13}$$

for the corresponding coefficient in $\mathbf{C}_{\text{pos}}$ and $\mathbf{C}_{\text{neg}}$ respectively. For IT2, the uncertainties are, as expected, significantly higher, since only one bridge is used for estimation of the relevant parameter.

$$\mathbf{V}^{\mathbf{2}}_{\text{pos}} = \begin{bmatrix} 1.4748 \times 10^{3} \end{bmatrix}$$
$$\mathbf{V}^{\mathbf{2}}_{\text{neg}} = \begin{bmatrix} 1.4646 \times 10^{3} \end{bmatrix} \tag{3.14}$$

Uncertainties for IT1 are expected to be lower in magnitude than those for IT2. However, these results are low in magnitude compared to the calibration coefficients. Though not ideal (especially for torque) these results can be deemed satisfactory.

3.1.7 Calibration Verification

With the calibration coefficients obtained, it is important to verify whether the static coefficients obtained are in agreement with theoretical or otherwise expected results. As such, a set of propellers was tested in isolation and its properties evaluated and compared to manufacturer-provided values [14]. Reference values are not the result of other experimental works, rather they are values provided by APC [14] as computed by CFD models. As such, results may not reflect the real thrust and torque as measured. For either IT, propellers were tested at nominal Ω in increments of $500\ \mathrm{RPM}$. 4 propellers were used for the remainder of this work, from the same family of designs for electrical motors: [10×6E, 9×6E, 9×4.5E, 9×4.5EP][1].

Error bars are presented for a 95% confidence interval (2σ). For IT1, a lift vs mechanical power plot was also computed, whereas for IT2 only P_{mech} vs Ω can be computed, as lift was not a part of the calibration for this IT. For IT1, figures 3.6 and 3.7 include the obtained data. In the following figures, expected values for 9×4.5E and 9×4.5EP overlap, since the propellers have the same aerodynamic characteristics.

Mean relative error (MRE), computed for each test case, are presented in table 3.5. Results were computed using the relative error (RE) equation presented, and then the mean of each set was calculated. In eq. (3.15), y_0 represents the true load, which is the reference provided by the manufacturer [14].

[1] APC Propellers [14] uses the standard nomenclature diameter×pitch. This designation was maintained in this work. The propeller designation is followed by either E or EP, to differentiate CCW and CW rotation directions respectively. For example, a 10×6E propeller has a 10 inch diameter, a pitch of 6 inches and rotates CCW

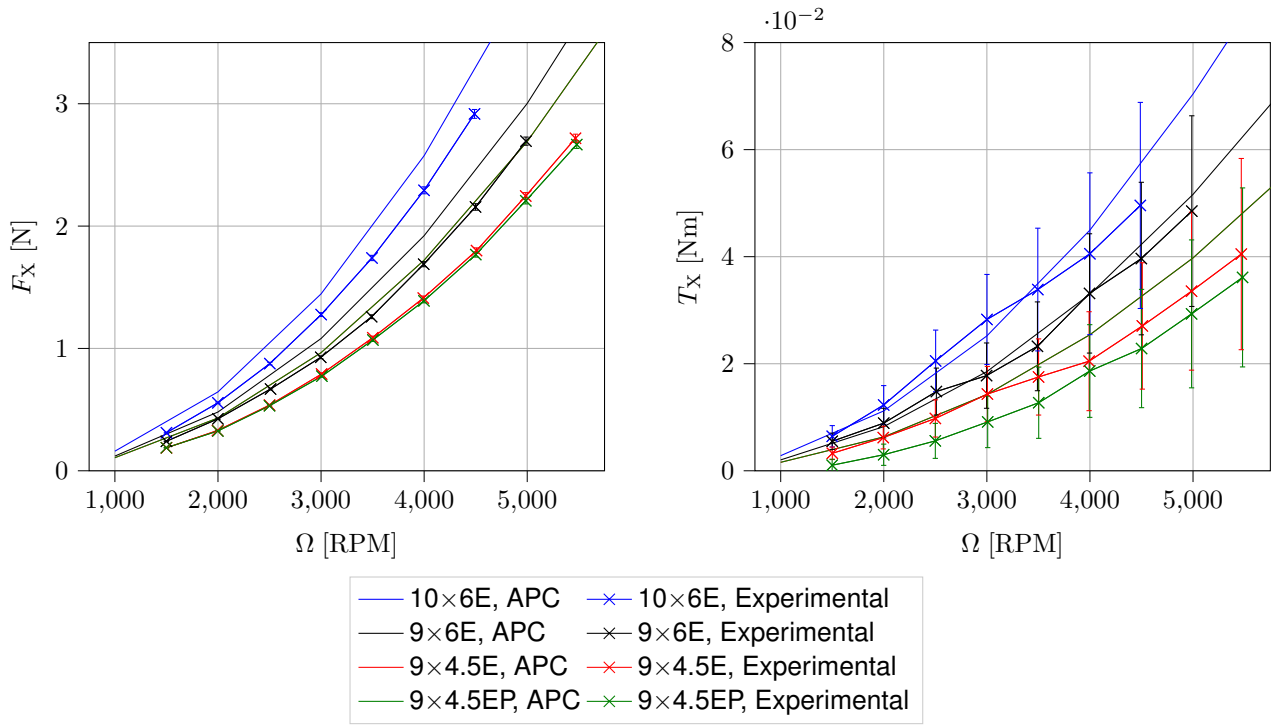

Figure 3.6: Directly computed values for thrust (F_X) and torque (T_X), as functions of Ω, as measured by IT1. Confidence intervals provided are 2σ.

$$\text{RE} = \frac{\hat{y} - y_0}{y_0} \tag{3.15}$$

Table 3.5: Mean relative error for force and torque calibration on IT1

Propeller	MRE F_X	MRE T_X
10×6E	14.29%	9.90%
9×6E	13.78%	6.33%
9×4.5E	20.37%	11.46%
9×4.5EP	21.60%	39.07%

The overall differences for both tests were, as expected, low in magnitude. The outlier is the 9×4.5EP propeller, where torque calibration provided abnormally high errors. The results were consistent across multiple tests with this propeller, however.

Plotting mechanical power and thrust (fig. 3.7) yields similar results: the calibration procedure performed is reliable enough to proceed with the experimental part of this work.

For IT2, results are similarly consistent: fig. 3.8(a) suggests a reasonable confidence in resulting coefficients. The same can be said for mechanical power (fig. 3.8(b)).

The same procedure for computing MRE was followed for IT2. The resulting errors are presented in table 3.6

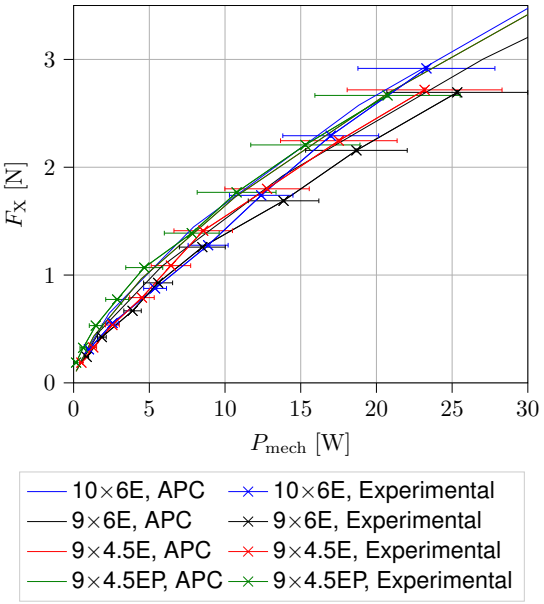

Figure 3.7: Computed thrust as a function of mechanical power (P_{mech}) on IT1. 2D confidence intervals provided are 2σ.

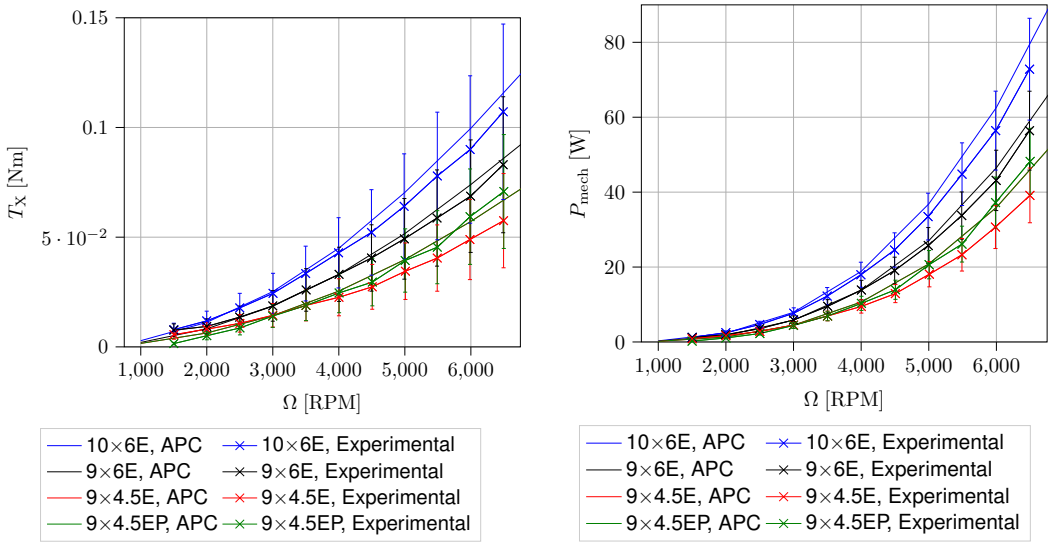

(a) Torque on the rotor T_X, as a function of angular velocity, for IT2.

(b) Mechanical power, as a function of angular velocity, on IT2.

Figure 3.8: Torque and mechanical power as measured by IT2, for calibration verification.

3.2 Experimental Methodology

3.3 Configurations Tested

Seven parameters were explored as to their importance regarding the design of a tandem rotor drone. These variables are:

- Rotation direction;
- Upstream propeller pitch;

Table 3.6: Mean relative error for force and torque calibration on IT2

Propeller	MRE T_{X}
10×6E	6.88%
9×6E	8.06%
9×4.5E	14.83%
9×4.5EP	12.22%

- Downstream propeller pitch;
- Upstream rotor diameter;
- Downstream rotor diameter;
- Rotor-plane distance [H];
- Interaxial distance [d];

Four propellers were chosen from the same family of designs from APC Propellers. These propellers were, as previously mentioned: [10×6E, 9×6E, 9×4.5E, 9×4.5EP]. If possible, the largest propeller was kept as a constant in either rotor, in order to improve the measurements obtained by the ITs. For example, when testing rotation direction, the downstream rotor was the 10×6E, while the upstream rotor varied in rotation direction.

3.3.1 Rotation Direction

Rotation direction is the only set of tests that was done before others. This allows the remaining tests to be greatly reduced in number, since they can be examined only for whichever configuration shows improved efficiency. Coaxial tests showed that equal rotation direction (ER) has a severe negative impact on performance. The same effect implies that, when in tandem, opposite rotation (OR) is more detrimental to performance of the downstream rotor.

Propellers chosen for this test are shown in table 3.7.

Table 3.7: Rotation direction test set

Upstream Rotor	Downstream Rotor
9×4.5E	10×6E
9×4.5EP	10×6E

Theoretical Note on Rotation Direction

The performance of a rotor is proportional to the relative velocity ($\overrightarrow{V_{\mathrm{rel}}}$), defined as the difference between the velocity of the (downstream) rotor ($\overrightarrow{V_{\mathrm{d}}}$) and the velocity of the incoming air (be it from the wake of a rotor upstream, $\overrightarrow{V_{\mathrm{uw}}}$, or quiescent air, in hover).[2]

[2]Since this analysis regards only the variation of rotation direction of the incoming wake relative to the rotor, the implicit assumption is that the downstream-component of $\overrightarrow{V_{\mathrm{uw}}}$ is to be the same.

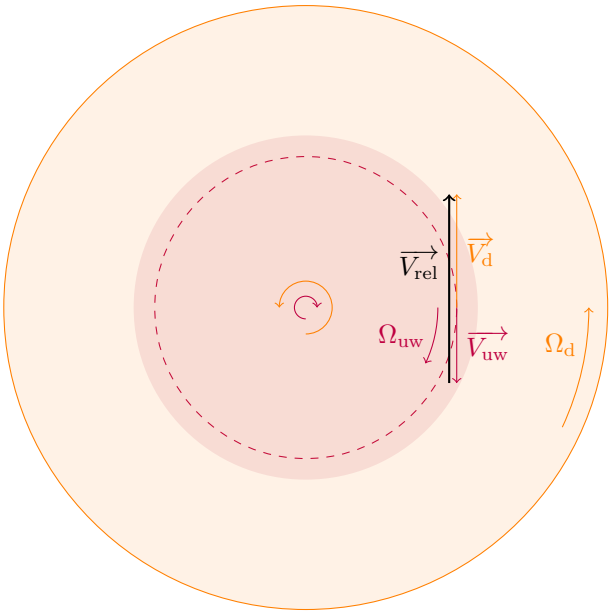

Figure 3.9: Nomenclature conventions and vectorial subtraction for the coaxial relative velocity, at the downstream rotor, for an arbitrary radius (dashed line).

Figure 3.9 shows useful nomenclatures as well as the vectorial subtraction that is relevant for this computation. The shadowed areas represent the areas of influence of each rotor/wake. If the rotation direction were equal (i.e. Ω_{d} is reversed), V_{d} would also be reversed, meaning a lower relative velocity and worse overall performance. The definition of V_{rel} necessarily implies that OR is more performant in the case of coaxial configurations: the relative velocity is of higher magnitude when the non-streamwise components of the incoming air and the downstream rotor are in opposing directions. The concepts of OR and ER cannot be generalised to tandem configurations. However, the observation that, locally, V_{rel} is greater when V_{d} and V_{uw} have opposing directions can.

The same reasoning, applied to the configurations in study, implies that a lower relative velocity is observed when in OR (fig. 3.10). It is important to note that for this line of reasoning to function, the overlap area at the downstream rotor does not include the upstream rotor's axis of rotation (i.e. $d/D_d > \frac{1}{2}$ for equal diameter rotors): when this occurs, the effect is expected to gradually reverse until OR becomes dominant near the coaxial configuration.

3.3.2 Upstream Propeller Pitch

Upstream rotor pitch (p_{u}) variation was tested. The pitch of the upstream rotor is expected to be one of the most important variables since the wake strength is directly related to pitch: a lower pitch propeller produces a weaker wake, as well as less lift; conversely, a higher pitch means a stronger, more disturbing wake and more lift for the same propeller diameter. Two propellers upstream were tested: [9×6E, 9×4.5E]. In these tests the downstream propeller was the 10×6E.

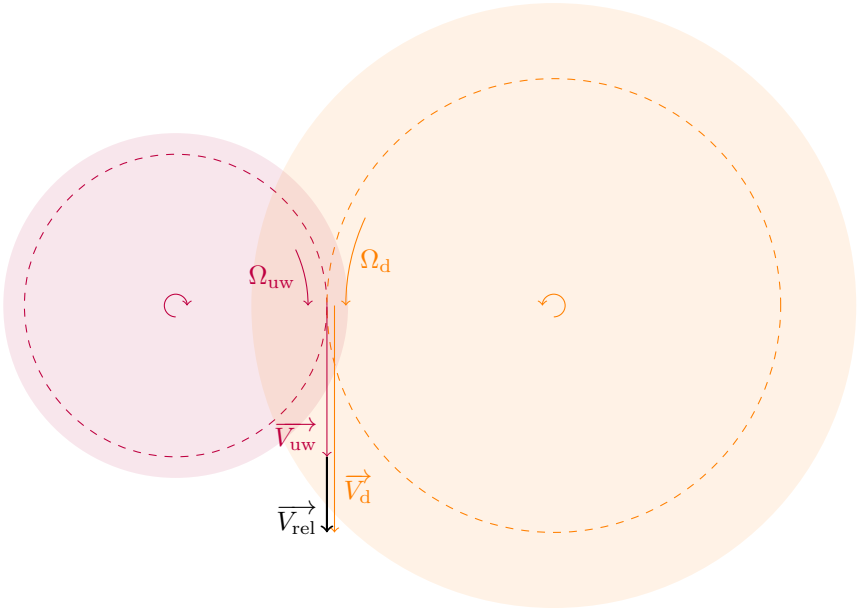

Figure 3.10: Nomenclature conventions and vectorial subtraction for the tandem relative velocity when in OR, at the downstream rotor, for an arbitrary radius (dashed line).

Propellers chosen for this test are shown in table 3.8.

Table 3.8: Upstream pitch test set

Upstream Rotor	Downstream Rotor
9×6E	10×6E
9×4.5E	10×6E

3.3.3 Downstream Propeller Pitch

Downstream rotor pitch (p_d) was also tested. Qualitatively, a lower pitch propeller will produce less lift, but it will probably experience a smaller influence of the upstream-wake than its higher-pitched counterpart. Tested propellers were 9×4.5E and 9×6E in the downstream rotor, with the upstream propeller being the 10×6E.

Propellers chosen for this test are shown in table 3.9.

Table 3.9: Downstream pitch test set

Upstream Rotor	Downstream Rotor
10×6E	9×6E
10×6E	9×4.5E

3.3.4 Upstream Propeller Diameter

The diameter of the downstream rotor was kept constant for the duration of this set of tests, and the upstream diameter (D_{u}) was varied. Though a larger upstream diameter means a larger and stronger wake, the development of the slipstream should mean that this is less impactful for larger rotor-plane distances.

Propellers chosen for this test are shown in table 3.10.

Table 3.10: Upstream diameter test set

Upstream Rotor	Downstream Rotor
9×6E	10×6E
10×6E	10×6E

3.3.5 Downstream Propeller Diameter

The downstream diameter (D_{d}) was varied as upstream diameter was kept constant at 10 inches. Maintaining d constant, a larger downstream diameter theoretically would imply a bigger overall impact. A larger downstream diameter decreases d/D_{d}, implying that the overlap area ratio m' is larger. This, in turn, means that the downstream rotor suffers more interference, thus larger κ_{ov} and lower efficiency. This can be also inferred from fig. 2.4, where an increase in D_{d} implies smaller d/D_{d} and thus larger κ_{ov}.

Propellers chosen for this test are shown in table 3.11.

Table 3.11: Downstream diameter test set

Upstream Rotor	Downstream Rotor
10×6E	9×6E
10×6E	10×6E

3.3.6 Rotor-plane Distance

Rotor-plane distance $[H]$ is measured as the distance between the rotor planes, parallel to the axis of the rotors. 4 distances were tested: $[85, 120, 155, 190]$ mm.

3.3.7 Interaxial Distance

The interaxial distances $[d]$ (i.e. between the axes of rotation of the propellers) were tested for all available propellers and test cases. 3 different distances were tested: in increasing order, $[136, 186, 230]$ mm.

3.3.8 Data Acquisition

With the calibration procedure completed, calibration coefficients obtained and verified to a satisfactory degree, the tandem-configuration rotors can now be tested. The data acquisition software designed for the setup was kept mostly unchanged [10]. The following changes were made:

- The file system was improved, by means of an indexing system and automatic output naming;
- A simple implementation of a proportional speed controller was used to automate the data acquisition process for each distance pair. This was implemented in both single and tandem rotor configurations.

Tested RPM were in the range $[1500,\ 6000]$, in increments of $500\ \mathrm{RPM}$. Higher pitch or diameter propellers (i.e. 9×6E and 10×6E) were not tested above $5000\ \mathrm{RPM}$, since the motors used were somewhat prone to overheating. The nominal upstream and downstream angular velocities are summarised in fig. 3.11. In orange, the full range up to $6000\ \mathrm{RPM}$ is shown.

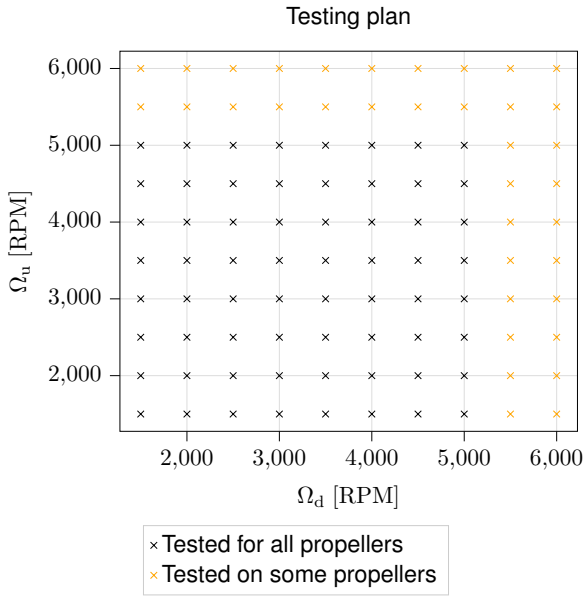

Figure 3.11: Graphical representation of tested nominal upstream and downstream rotor angular velocities.

3.3.9 Data Analysis Methodology

Collected data was stored as pairs of upstream and downstream RPM, which was subsequently treated through a python program. All collected data corresponds to the nominal values in fig. 3.11. To then analyse the performance, the relevant functions (FM as a function of Ω_d and Ω_u for example) are computed at each of the data points. To allow for more versatility in the computation of plots, an intermediate step is introduced: a 2D linear interpolation into a regular, 200×200-point mesh-grid is

constructed. From this, horizontal and vertical sections and isolines (or contour) plots can be generated at will.

A set of tests was designed with the objective of isolating and ascertaining the sensitivity of a tandem rotor system to six variables. Some variables, such as motor K_{v}, were disregarded. Since this work is more concerned with the mechanical behavior of the rotors and mechanical power, motor K_{v} can be safely ignored. This is corroborated with the fact that coaxial tests [10] (where rotor interference is likely much greater) found them to be mostly irrelevant for performance.

Chapter 4

Experimental Results

4.1 Chapter Overview

This chapter is a summary of the data obtained as outlined previously. For brevity, P_{d} and P_{u} refer to the downstream and upstream mechanical power respectively. Subscripts d and u refer to the downstream and upstream property. Rotor diameter is represented by D, rotor pitch is represented by p (e.g. p_{d} is downstream pitch). For each variable examined the general outline of presented data is as follows:

1. An outline of the test performed, expected effects and what specificities are relevant to the test or propellers;
2. Two plots for different distances of thrust as a function of power, with an analysis, for a fixed power on the upstream rotor;
3. A table of quantitative values, with minimum and maximum differences among each configuration;
4. A similar description, table and set of plots for a fixed power on the downstream rotor;
5. Isoline plots for generated thrust downstream as a function of upstream and downstream mechanical power are also shown, to display the increase in consumed downstream power, as upstream power is increased, for the same thrust;
6. An identical analysis to the last three steps for FM and RPM is done, with comparisons to the isolated propeller;
7. Section plots of κ_{ov} at constant angular are analysed;
8. A general conclusions section follows, to summarise the observed effects.

The figure of merit, FM, is a measurement of how efficient the rotor's production of thrust is. Though it is defined in eq. (2.17), the computation was done using mechanical power:

$$FM \approx \frac{P_{\mathrm{ideal}}}{P_{\mathrm{mech}}}$$

Mechanical power was computed as $M_X \times \Omega$, where M_X is the torque required by the motor. Ideal power is computed using (2.11)

The overlap coefficient, κ_{ov}, is a metric of the additional power required in tandem (relative to isolated performance) at an angular velocity pair. It is generally larger than unity. A greater value means that more power is required at an RPM pair, and can be considered less performant. No theoretical predictions are presented for this chapter. This is because the concept of m' loses significance when rotors of different diameters are used. In any case, the theoretically expected value for κ_{ov} is, at most, $\sqrt{2} \approx 1.4142$, and at the least 1. However, as an indicator of overall tandem performance as well as another point of comparison, it is presented here. A value lower than 1 implies that the system performs at a more efficient state, requiring less power for the same conditions.

The isoline plots present at the end of each section provide visual information to evaluate the sensitivity of the downstream propeller to the wake of the upstream one. The closer to vertical a set of lines is, the closer to the isolated performance the specific case is. As the rotors are brought closer, it is expected that the isolines lean clockwise. Isoline plots for the overlap coefficient κ_{ov} turned out to be too confusing and unintelligible, and are omitted for this reason.

These configurations are being tested relative to one another, as well as relative to the isolated case. The focus of most sections is on the downstream propeller, as it is assumed that the upstream propeller is mostly unaffected in tandem operation. Quantitative measurements are computed and presented when relevant for each (d, H) pair, comparing the performances of the better and worse performing pair of rotors:

1. The difference between the thrust (T) of the propellers at the same P_{i} is computed and stored into a vector (Δ);
2. The minimum ($\Delta_{\min}$) and maximum ($\Delta_{\max}$) values of this array are obtained and presented;
3. The (arithmetic) mean of (Δ_i / T_i) is computed, as a metric of mean performance of each case. Results are presented in $\%$, in reference to the more performant configuration.

Quantitative values are only presented when the downstream propeller is the same for a specific test.

4.2 Rotation Direction Sensitivity

In order to reduce the number of single configurations to be tested, a set of propellers was tested in order to determine whether an ER or OR direction is preferable. Tests were done with a 9×4.5E or EP propeller in the upstream position and a 10×6E downstream.

4.2.1 Downstream Thrust Generated as a Function of Mechanical Power

Plotting the downstream rotor's thrust, as a function of input mechanical power (P_{mech}) allows for a simple comparison regarding which rotor configuration is superior. Starting with a fixed power applied

to the upstream rotor, the following plot is obtained:

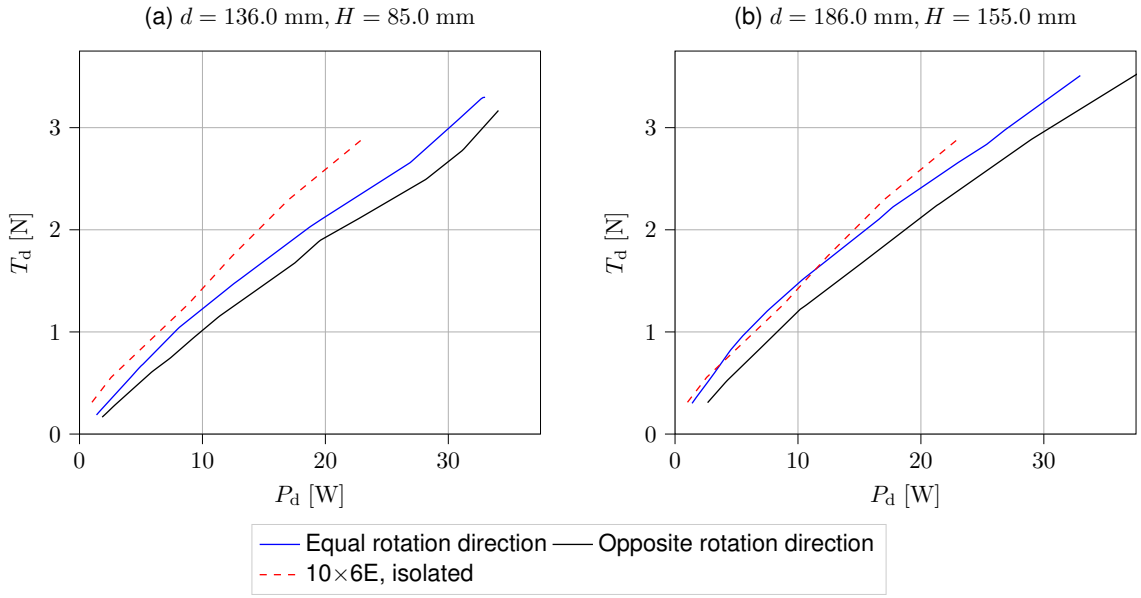

Figure 4.1: Downstream thrust plotted as a function of P_d, for a fixed $P_u = 25$ W, for rotation direction comparison.

Table 4.1: Quantitative information for all tested distances of thrust vs mechanical power differences at fixed $P_u = 25$ W.

d [mm]	H [mm]	$\Delta_{min} \times 10^3$ [N]	$\Delta_{max} \times 10^3$ [N]	Performance difference
136.0	85.0	92.82	335.17	17.3%
136.0	120.0	136.29	331.32	20.2%
136.0	155.0	72.14	284.71	14.3%
136.0	190.0	45.80	303.46	14.0%
186.0	85.0	211.87	345.12	17.5%
186.0	120.0	181.90	347.45	17.8%
186.0	155.0	212.63	327.16	19.8%
186.0	190.0	211.62	295.90	19.5%
230.0	85.0	−4.20	57.66	1.3%
230.0	120.0	72.44	148.84	6.8%
230.0	155.0	63.27	111.46	5.5%
230.0	190.0	24.73	137.34	5.5%

Figure 4.1 shows that, for a fixed input power on the upstream rotor of 25 W, the thrust done by the downstream rotor is higher on the ER case. This is true for all 12 (d, H) pairs tested. The ER case is also much closer to the isolated case even being an improvement over the isolated case in certain conditions.

Fig. 4.2 displays the thrust reduction that is seen when more power is applied to the upstream rotor. The performance declines significantly faster at low power, but stabilises for more distanced upstream-downstream rotors.

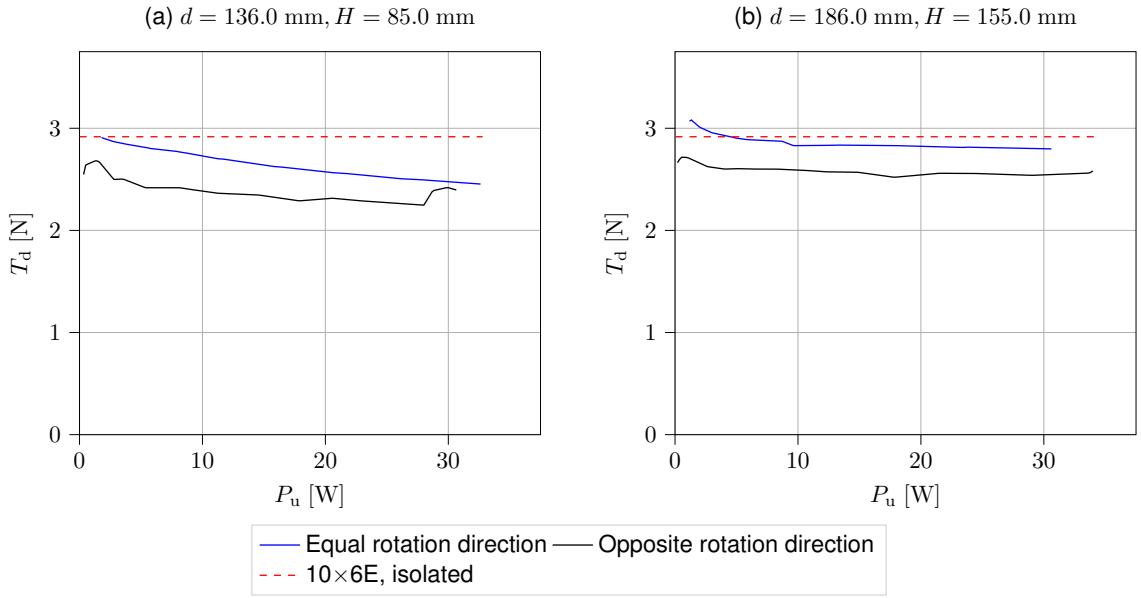

Figure 4.2: Downstream thrust plotted as a function of P_u, for a fixed $P_\mathrm{d} = 25$ W, for rotation direction comparison.

Varying the applied mechanical power in either rotor independently and plotting the resulting isolines, fig. 4.3 is obtained. It synthesises the experimental observation that for all $(P_\mathrm{d}, P_\mathrm{u})$ pairs tested, the ER configuration displays better performance. The negative impact on performance can be observed since, for an increase in P_u, the isolines for thrust lean towards positive P_d.

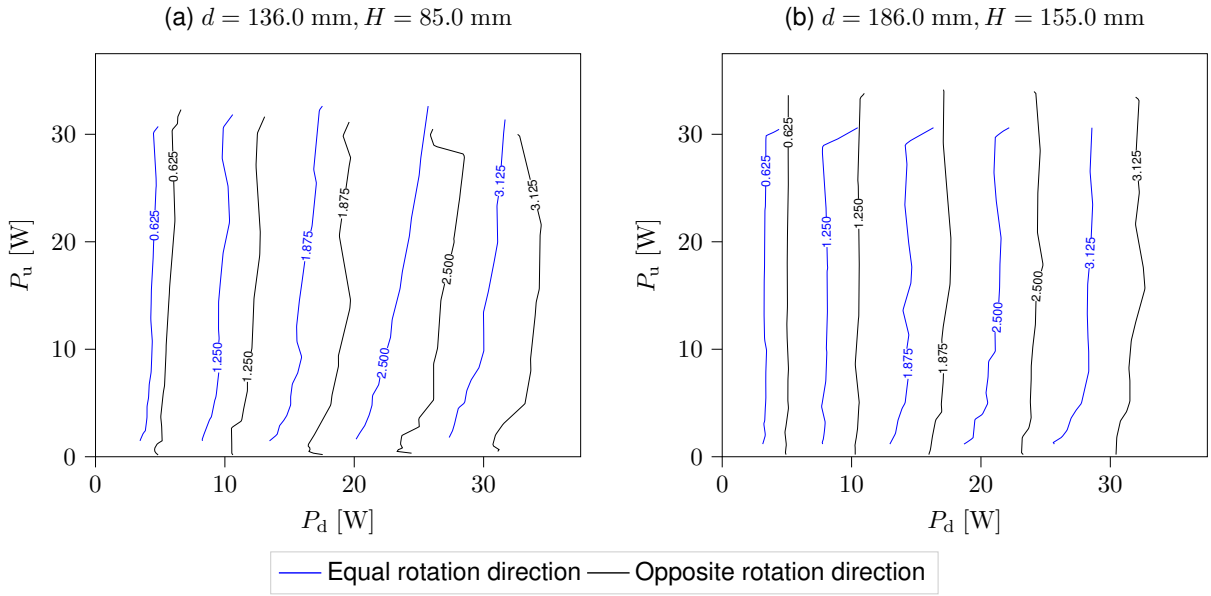

Figure 4.3: Downstream thrust isoline plots for comparison of rotation direction.

Table 4.2: Quantitative information for all tested distances of thrust vs mechanical power differences at fixed $P_{\mathrm{d}} = 25$ W.

d [mm]	H [mm]	$\Delta_{\min} \times 10^3$ [N]	$\Delta_{\max} \times 10^3$ [N]	Performance difference
136.0	85.0	64.20	389.58	12.2%
136.0	120.0	242.60	353.89	12.9%
136.0	155.0	164.90	262.44	9.2%
136.0	190.0	222.67	329.50	11.4%
186.0	85.0	214.19	387.86	12.1%
186.0	120.0	191.06	362.66	11.4%
186.0	155.0	240.58	369.19	10.8%
186.0	190.0	249.63	365.06	10.9%
230.0	85.0	−24.12	52.34	0.9%
230.0	120.0	51.70	159.25	4.3%
230.0	155.0	83.65	131.97	3.6%
230.0	190.0	54.19	153.14	4.3%

4.2.2 Figure of Merit as a Function of Angular Velocity

From the point of view of the Figure of Merit, the results are similarly positive for the ER case. Starting with a fixed $\Omega_{\mathrm{u}} = 4500\mathrm{RPM}$, the resulting plots for the FM are shown in fig. 4.4.

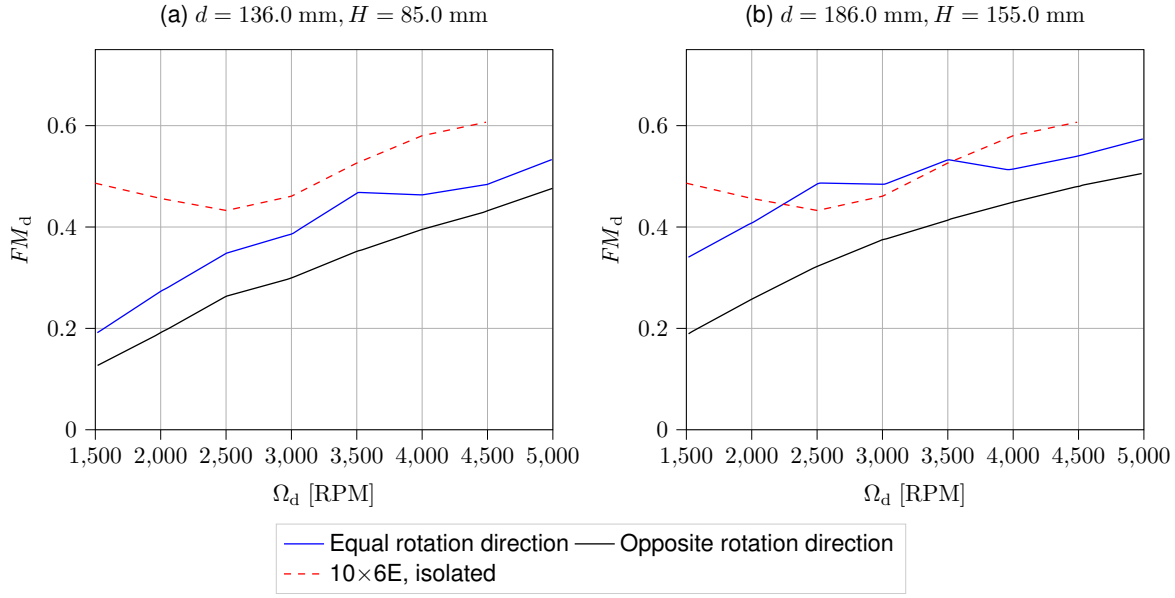

Figure 4.4: Downstream FM plotted as a function of angular velocity, for a fixed $\Omega_{\mathrm{u}} = 4500$ RPM, for rotation direction comparison.

Repeating the same process, but with $\Omega_{\mathrm{d}} = 4500\mathrm{RPM}$ as the fixed independent variable, the negative effect of the upstream rotor on the downstream rotor is evident: with an increase in Ω_{u}, a steady decrease in rotor efficiency is observed (fig. 4.5). As Ω_{u} increases, so does the strength of the generated wake, which negatively impacts performance.

Similar to the analysis for thrust and power, a contour plot can be generated as both rotor angular velocities Ω are independently varied. Fig. 4.6 includes this information, for two (d, H) pairs.

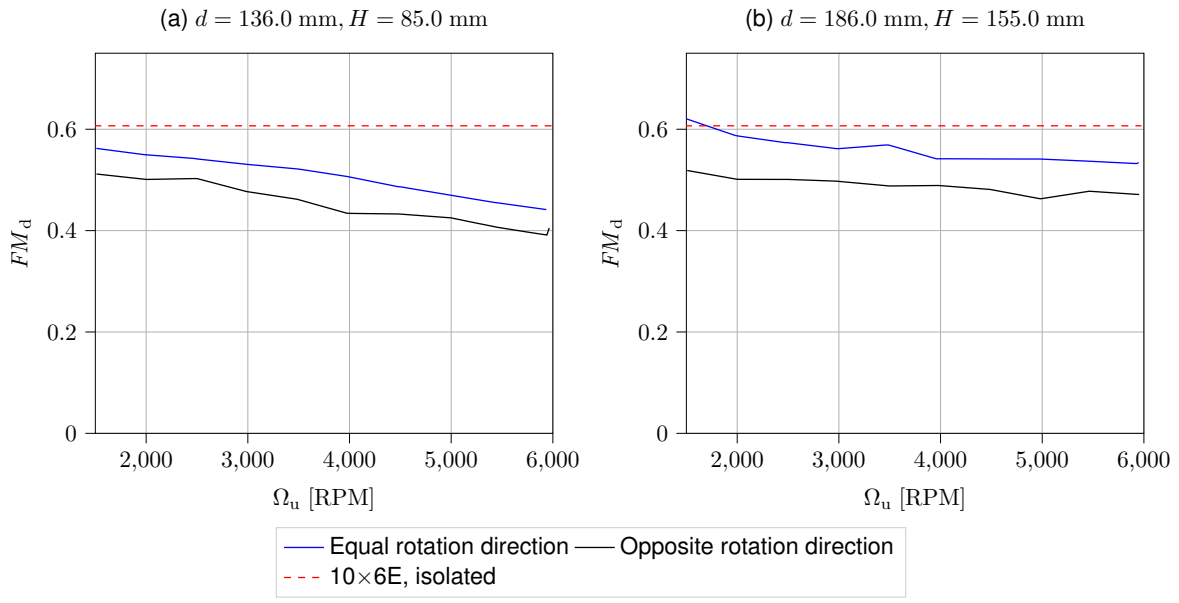

Figure 4.5: Downstream FM plotted as a function of angular velocity, for a fixed $\Omega_\mathrm{d} = 4500$ RPM, for rotation direction comparison.

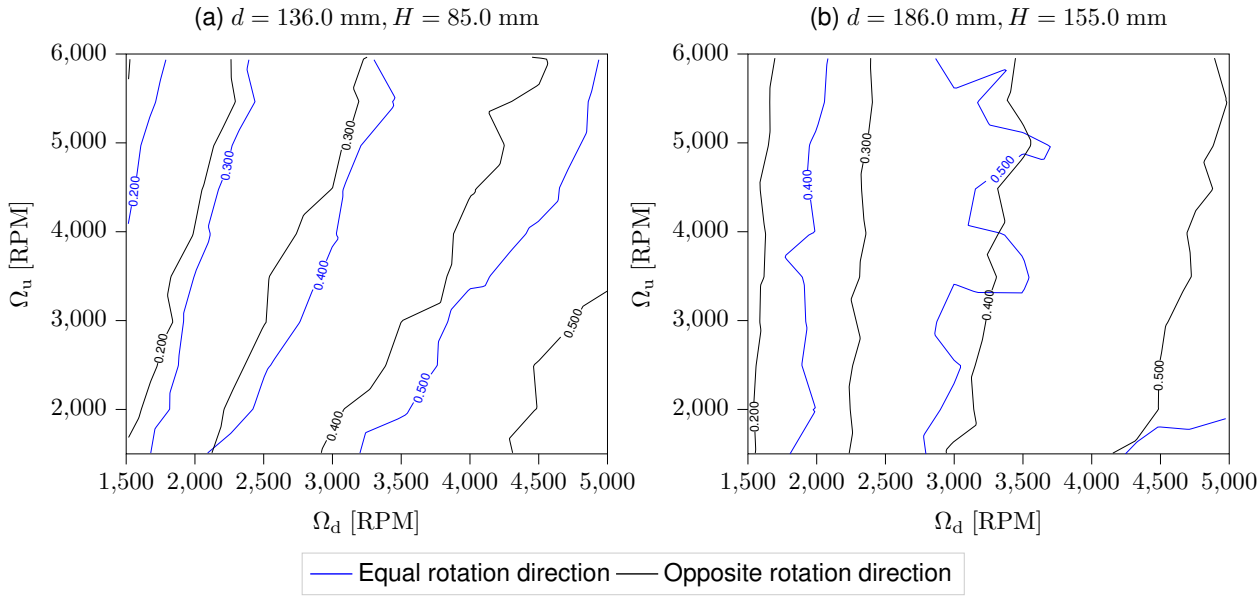

Figure 4.6: Downstream FM isoline plots for comparison of rotation direction.

4.2.3 Overlap Coefficient as a Function of Angular Velocity

At constant $\Omega_\mathrm{u} = 4500$ RPM, the ER case is mostly less performant than the OR one. As distance is increased, ER becomes more performant again. From the point of view of power consumption at an angular velocity, OR is more performant.

For a fixed $\Omega_\mathrm{d} = 4500$ RPM, OR is, again, generally better for smaller distances. As distance is increased, κ_ov becomes higher for the OR case and lower for the ER case while there is interference. It is also of note that there is even a slight improvement in performance between 2500 to 3000 RPM, when

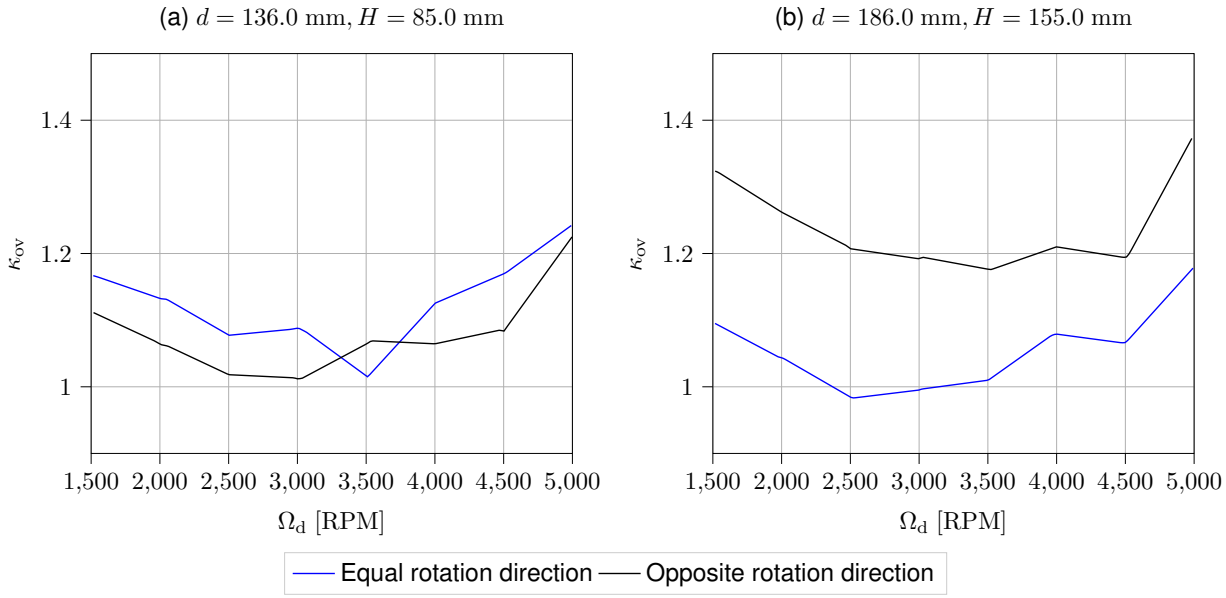

Figure 4.7: Overlap coefficient as a function of Ω_d, for fixed $\Omega_u = 4500$ RPM, for rotation direction comparison.

larger distances are used. Figure 4.8 shows this distinction between larger and smaller distances.

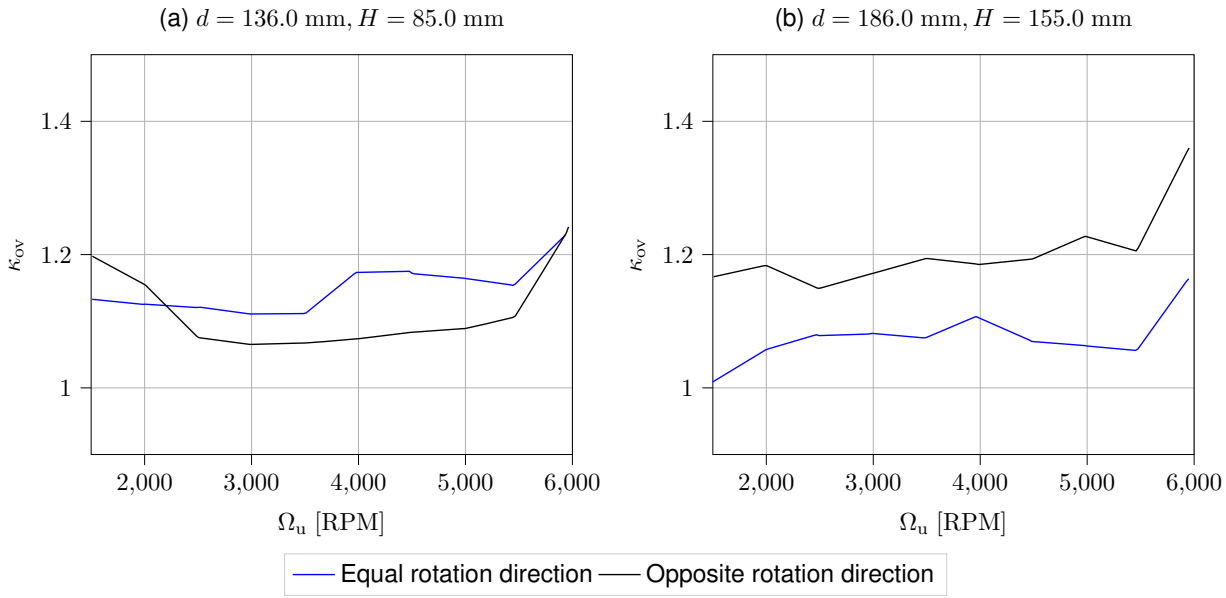

Figure 4.8: Overlap coefficient as a function of Ω_u, for fixed $\Omega_d = 4500$ RPM, for rotation direction comparison.

4.2.4 Conclusions Regarding Rotation Direction and Performance

From the point of view of power consumption for some RPM pair, it appears that OR is better for smaller distances. However, the efficiency of the downstream rotor (both from FM and thrust produced per unit of mechanical power) show a distinct perspective. In fact, in any of the analysed cases, the

downstream rotor is much more performant when under the influence of a similarly rotating propeller. On the other hand, it can be the case that the upstream rotor is also impacted and this can be the reason for the different results observed. The difference in performance between either rotation direction and the isolated propeller can be split into a function of Ω or P_{mech}, and a constant offset (independent of either). This offset appears to be dependent of d or H. Differences among the rotation directions are mostly of offset and not dependent on Ω or P_{mech}.

4.3 Upstream Pitch Sensitivity

Upstream pitch sensitivity was evaluated with a 10×6E propeller downstream and altering upstream pitch using either a 9×4.5E or 9×6E upstream. It is expected that this variable is fairly important: the larger the pitch, the stronger the wake generated by the propeller; a stronger wake, in turn, implies a larger impact in performance.

4.3.1 Downstream Thrust Generated as a Function of Mechanical Power

As expected, a higher pitch on the upstream rotor (p_{u}) yields a clear performance loss over a smaller pitch. However, it appears that, for higher P_{u} this effect becomes less important. Some of this impact can be attributed to the wake for the 9×6E propeller developing slightly faster.

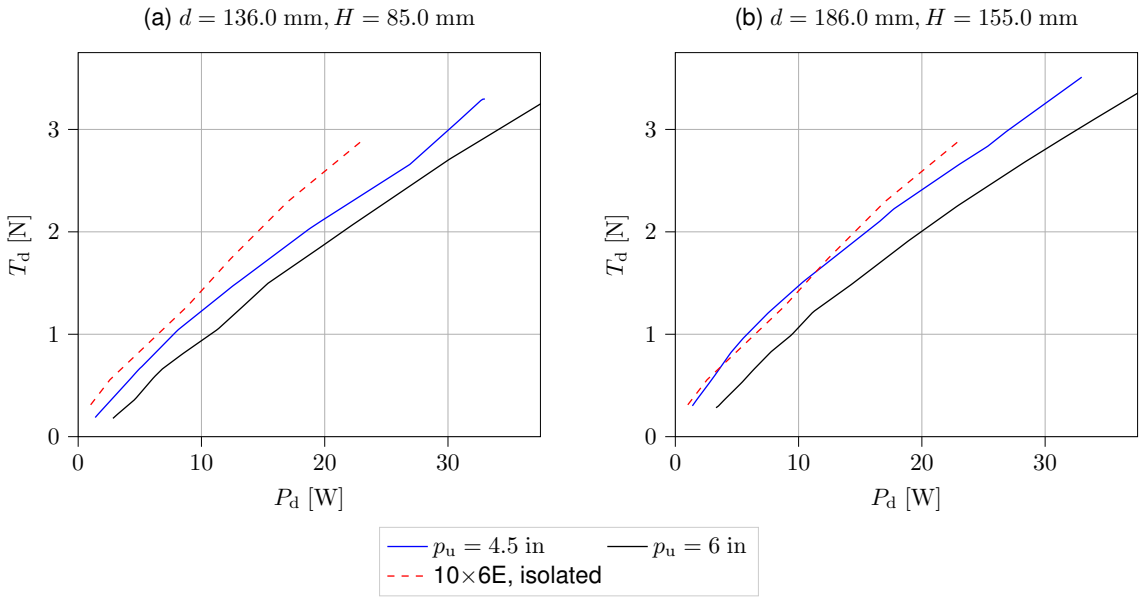

Figure 4.9: Downstream thrust plotted as a function of P_{d}, for a fixed $P_{\text{u}} = 25$ W, for upstream pitch comparison.

Figure 4.9 displays how a smaller pitch on the upstream rotor impacts the downstream rotor. In particular, upstream pitch seems to have a somewhat constant effect on the thrust of the downstream

rotor, for the same mechanical power. Table 4.3 shows quantitative information for a fixed downstream power and variable distances. The results for (d, H) pairs with $d = 230$ mm and $H > 85.0$ mm are likely spurious: it is expected that such high distances have much lower performance differences if any.

Table 4.3: Quantitative information for all tested distances of thrust vs mechanical power differences at fixed $P_{\mathrm{u}} = 25$ W.

d [mm]	H [mm]	$\Delta_{\min} \times 10^3$ [N]	$\Delta_{\max} \times 10^3$ [N]	Performance difference
136.0	85.0	210.52	387.80	22.6%
136.0	120.0	258.08	376.23	27.0%
136.0	155.0	224.22	360.93	25.2%
136.0	190.0	218.62	438.43	29.0%
186.0	85.0	279.84	468.29	24.6%
186.0	120.0	295.78	485.44	28.3%
186.0	155.0	360.11	483.99	30.8%
186.0	190.0	296.14	438.28	28.7%
230.0	85.0	160.08	312.35	15.3%
230.0	120.0	385.63	637.36	40.3%
230.0	155.0	341.64	623.74	37.9%
230.0	190.0	347.94	589.96	35.1%

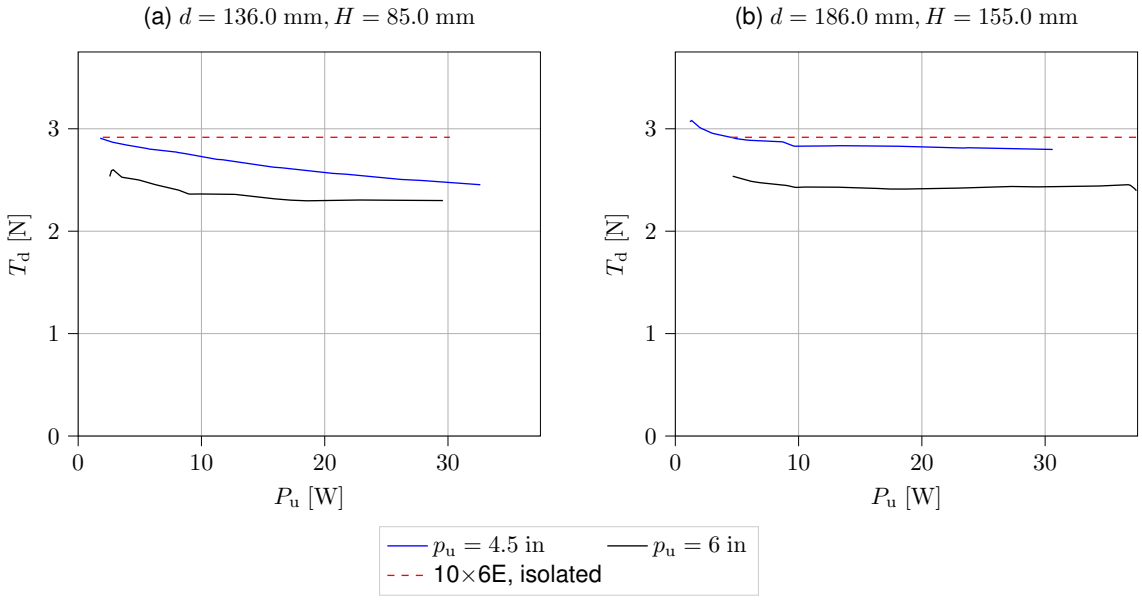

Figure 4.10: Downstream thrust plotted as a function of P_{u}, for a fixed $P_{\mathrm{d}} = 25$ W, for upstream pitch comparison.

It is clear from figure 4.10 that, though they appear approach the same value as P_{u} increases, a larger P_{u} means that the downstream rotor's thrust stabilises faster on this asymptotic value.

Table 4.4 includes quantitative information, computed for constant downstream power. Again, the same apparently spurious results can be observed at the same distance pairs.

Fig. 4.11 synthesises these observations: a larger upstream pitch stabilises on the asymptotic loss

Table 4.4: Quantitative information for all tested distances of thrust vs mechanical power differences at fixed $P_{\mathrm{d}} = 25$ W.

d [mm]	H [mm]	$\Delta_{\min} \times 10^3$ [N]	$\Delta_{\max} \times 10^3$ [N]	Performance difference
136.0	85.0	181.02	386.27	12.2%
136.0	120.0	264.41	372.69	12.4%
136.0	155.0	185.86	354.08	11.0%
136.0	190.0	286.93	457.13	14.9%
186.0	85.0	299.86	460.72	16.0%
186.0	120.0	364.49	442.60	16.8%
186.0	155.0	364.93	419.42	16.3%
186.0	190.0	316.72	447.24	15.6%
230.0	85.0	197.80	302.46	9.6%
230.0	120.0	534.60	621.25	26.3%
230.0	155.0	544.63	600.76	26.2%
230.0	190.0	477.18	596.17	25.1%

in performance, whereas the downstream pitch proves to be superior for low-power applications. In fact, the 9×4.5E propeller has shown a better thrust/power ratio than the 9×6E in isolation. This suggests that, in the upstream position, a lower pitch propeller is likely more performant.

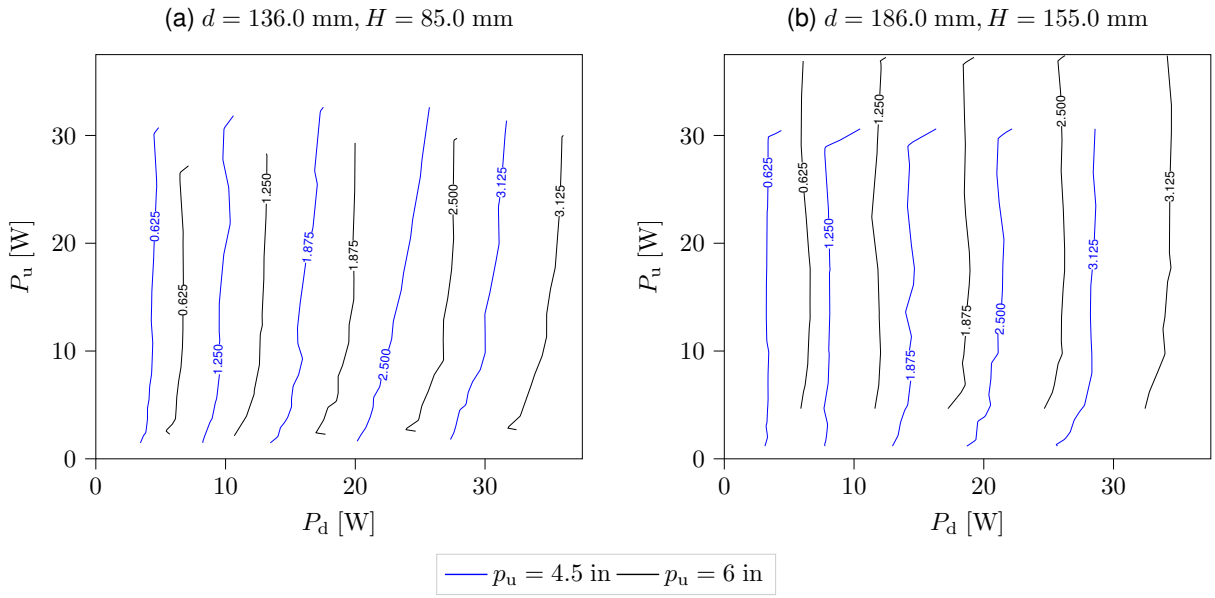

Figure 4.11: Downstream thrust isoline plots for comparison of downstream pitch.

4.3.2 Figure of Merit as a Function of Angular Velocity

Figure 4.12 shows the impact in performance between the isolated and tandem cases. When compared regarding upstream pitch, a lower pitch performs 10 to 12% better. In some cases, the downstream rotor performs slightly better than the isolated case, though the performance gain is, at most, 5%. This performance gain, though small, warrants further investigation; it is, however, consistent with previous observations on larger scale by Dingeldein [2].

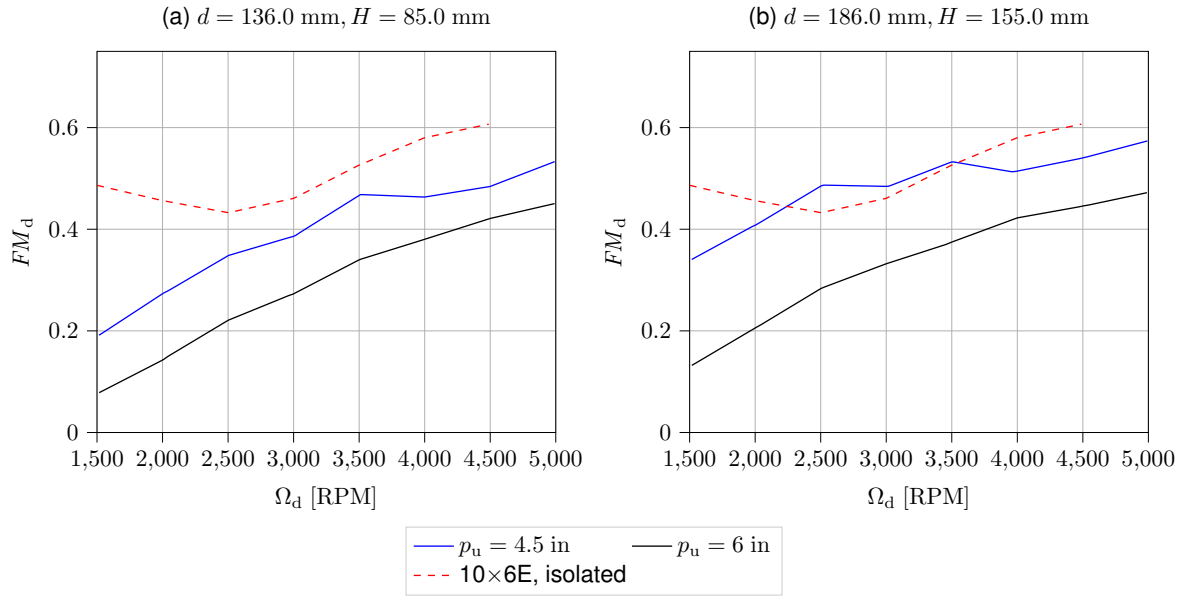

Figure 4.12: Downstream FM plotted as a function of angular velocity, for a fixed $\Omega_\mathrm{u} = 4500$ RPM, for upstream pitch comparison.

With a fixed 4500 RPM on the downstream rotor, the performance loss and subsequent asymptotic behavior is, again, observed: a larger pitch in the upstream propeller stabilises more rapidly than the lower-pitched counterpart. In either case, the FM is close to 10 % better in terms of performance. This effect can be seen in figure 4.13, where an isolated computation for Figure of Merit is also presented.

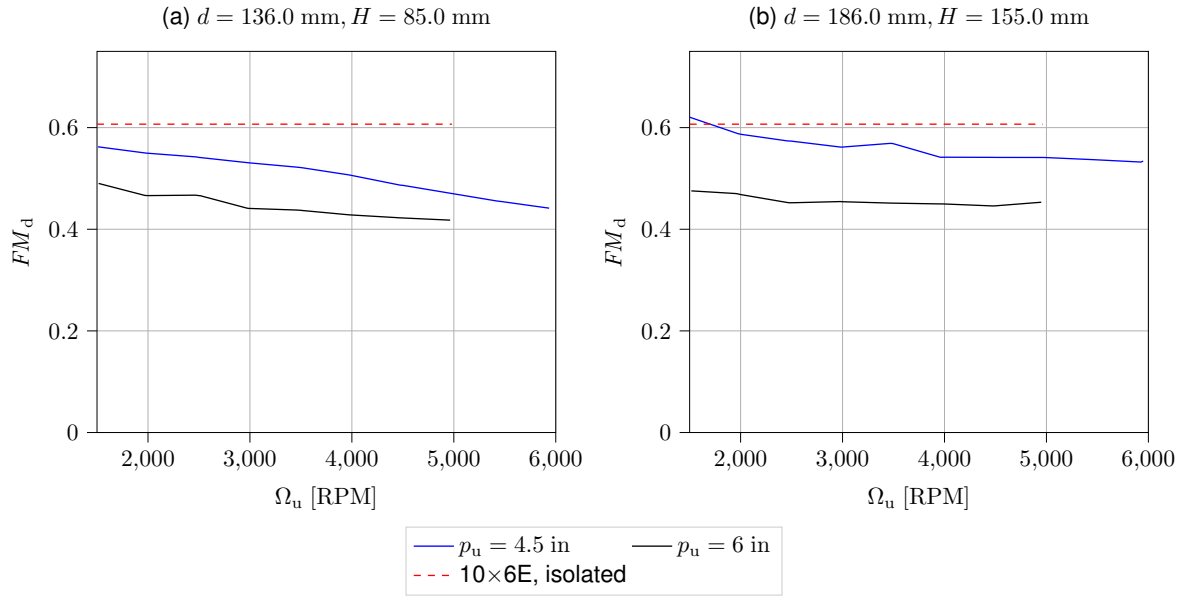

Figure 4.13: Downstream FM plotted as a function of angular velocity, for a fixed $\Omega_\mathrm{d} = 4500$ RPM, for upstream pitch comparison.

Finally, the general effect on performance is synthesised by fig. 4.14. An extremely inclined set of lines, as is the case for the lower distances, shows a deeper interference of the upstream rotor on the

downstream one.

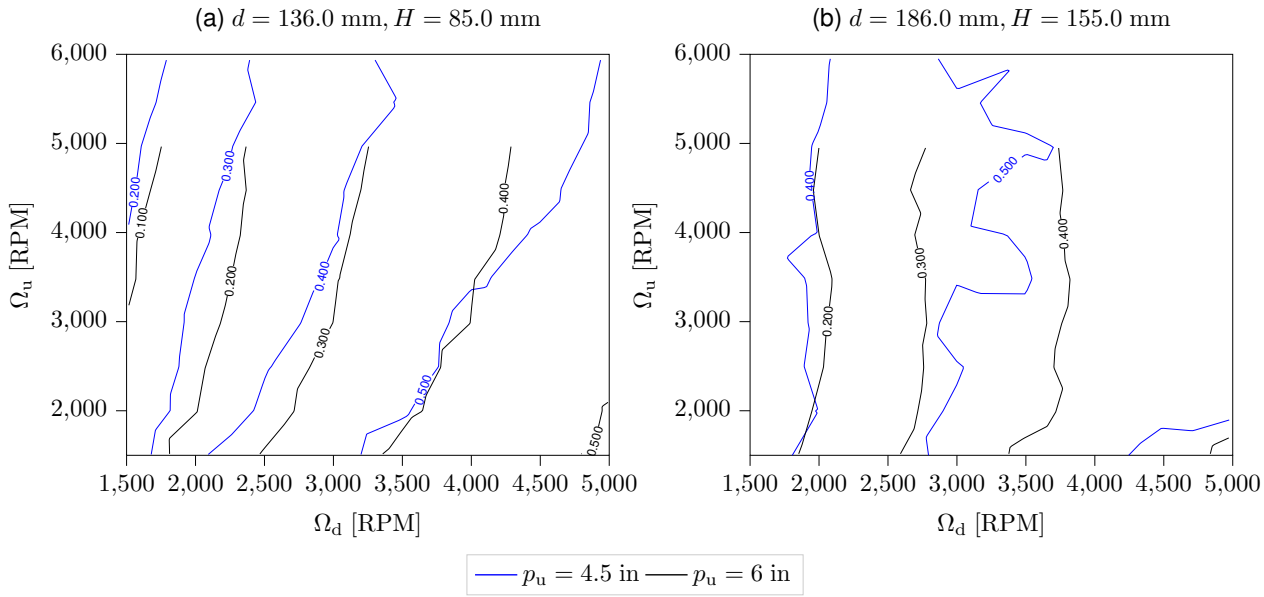

Figure 4.14: Downstream FM isoline plots for comparison of upstream pitch.

4.3.3 Overlap Coefficient as a Function of Angular Velocity

An analysis of the overlap coefficient as a function of Ω yields results that have similar disparity to what was observed earlier. As expected, the larger upstream pitch has a more severe impact. However, it has a surprisingly strong impact on power consumption. For the larger upstream pitch, a larger distance again showed a larger power consumption when compared to isolated rotors. Figure 4.15 summarises these findings.

Similar results are observed when fixing Ω_d: a larger upstream pitch yields much larger κ_{ov}, and this difference increases in magnitude when increasing distance. Fig. 4.16 also shows that the smaller upstream pitch impacts the downstream rotor much less severely, with κ_{ov} being much closer to unity.

4.3.4 Conclusions Regarding Upstream Pitch Influence on Overall Performance

The downstream propeller consumes less power when a lower-pitched upstream propeller is used. Conversely, it produces less thrust, less efficiently for a larger upstream pitch. Results for κ_{ov} also reflect this observation.

4.4 Downstream Pitch Sensitivity

To determine how the downstream propeller's performance is impacted by its own pitch is more difficult to evaluate a priori. On the one hand, a higher pitch accelerates the incoming air more forcefully,

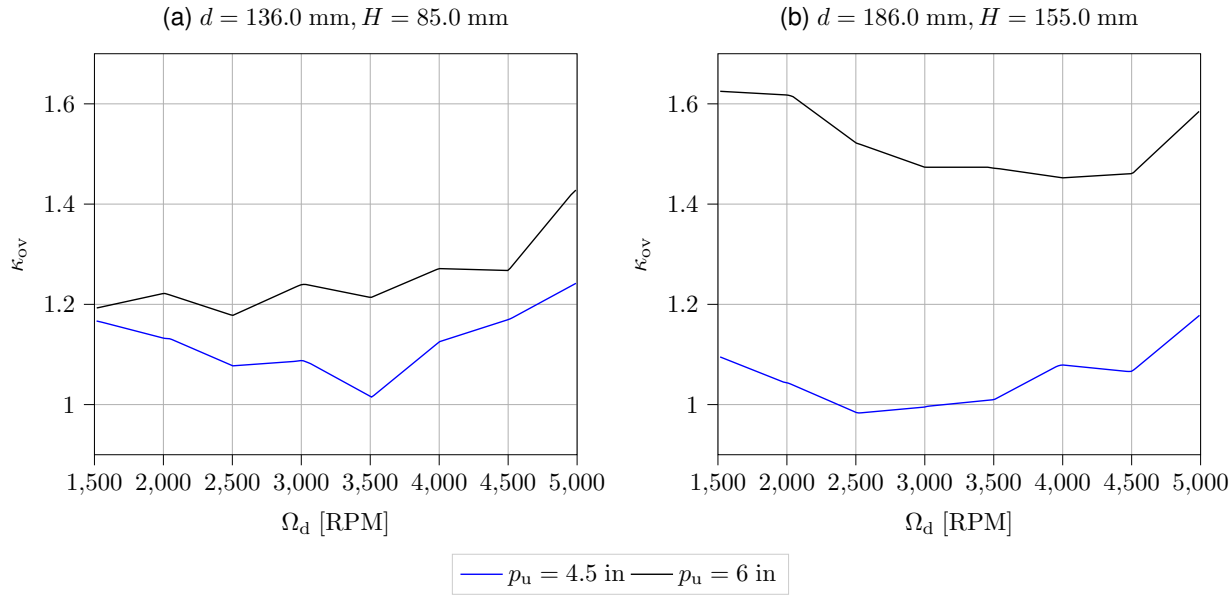

Figure 4.15: Overlap coefficient as a function of Ω_d, for fixed $\Omega_u = 4500$ RPM, for upstream pitch comparison.

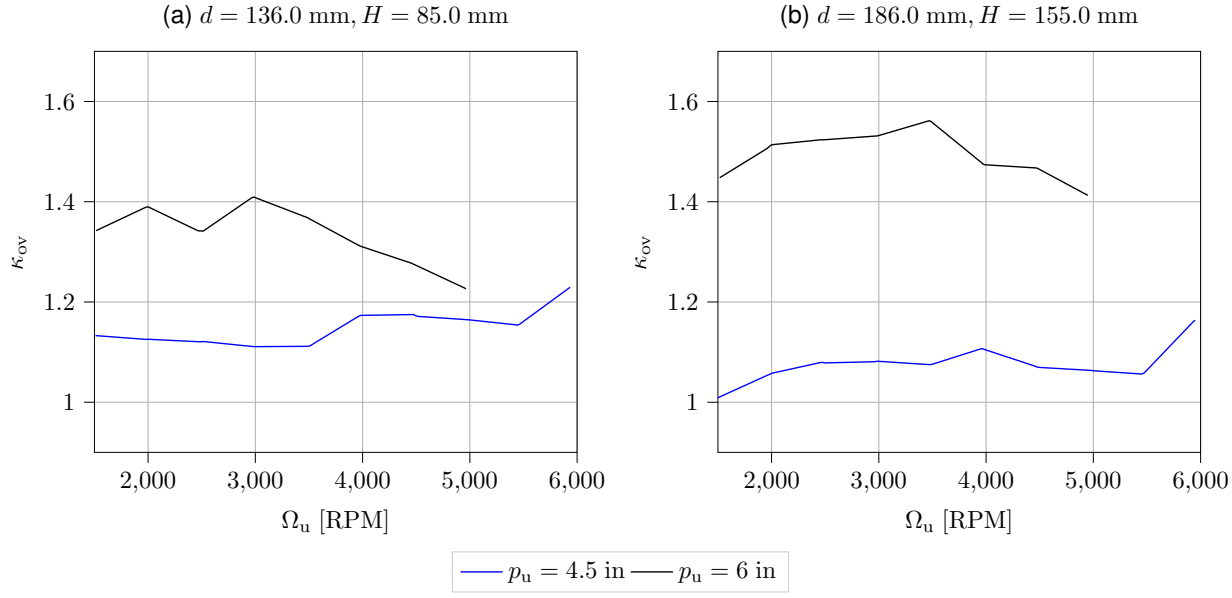

Figure 4.16: Overlap coefficient as a function of Ω_u, for fixed $\Omega_d = 4500$ RPM, for upstream pitch comparison.

and thus generates more thrust; on the other hand, this reasoning also implies that a higher pitched propeller should have a higher power consumption.

To evaluate the influence that downstream pitch has on overall performance, the upstream propeller was the 10×6E, with downstream propellers being the 9×4.5E and 9×6E, similar to what was done for upstream pitch.

4.4.1 Downstream Thrust Generated as a Function of Mechanical Power

By analysing fig. 4.17, it is clear that a downstream pitch that is lower in magnitude generates more thrust for the same power. It also appears that this effect increases in magnitude as P_d increases. The improved performance of a smaller downstream pitch is also confirmed in fig. 4.18, in which a fixed downstream power is applied: the increase of upstream power is met by a clear decrease in generated thrust, and the gap between the downstream propellers gradually reduces as P_u is increased.

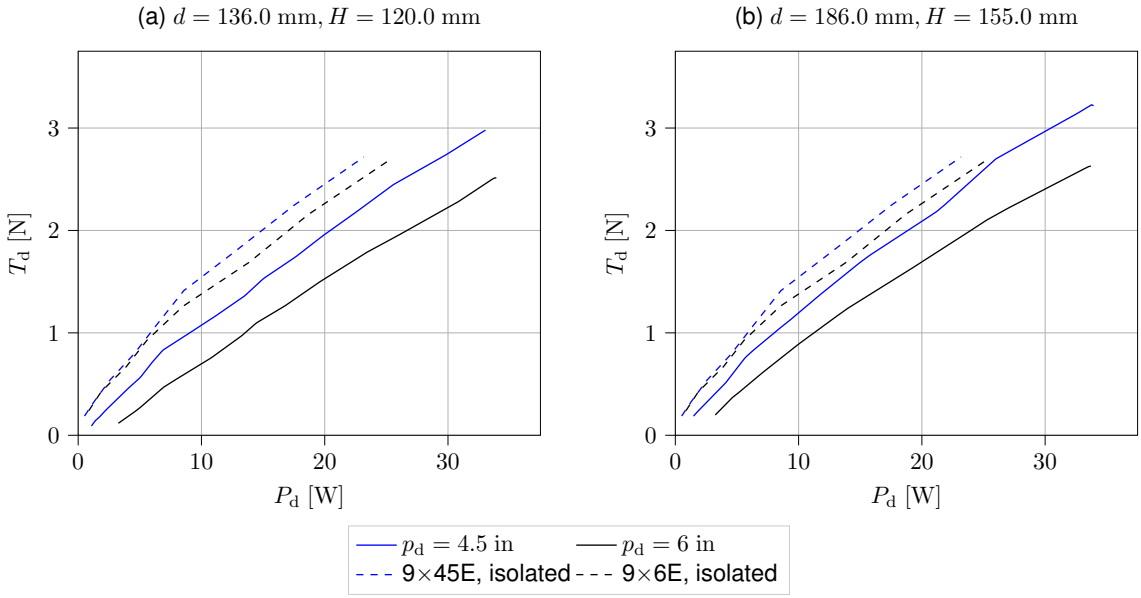

Figure 4.17: Downstream thrust plotted as a function of P_d, for a fixed $P_\mathrm{u} = 25$ W, for downstream pitch comparison.

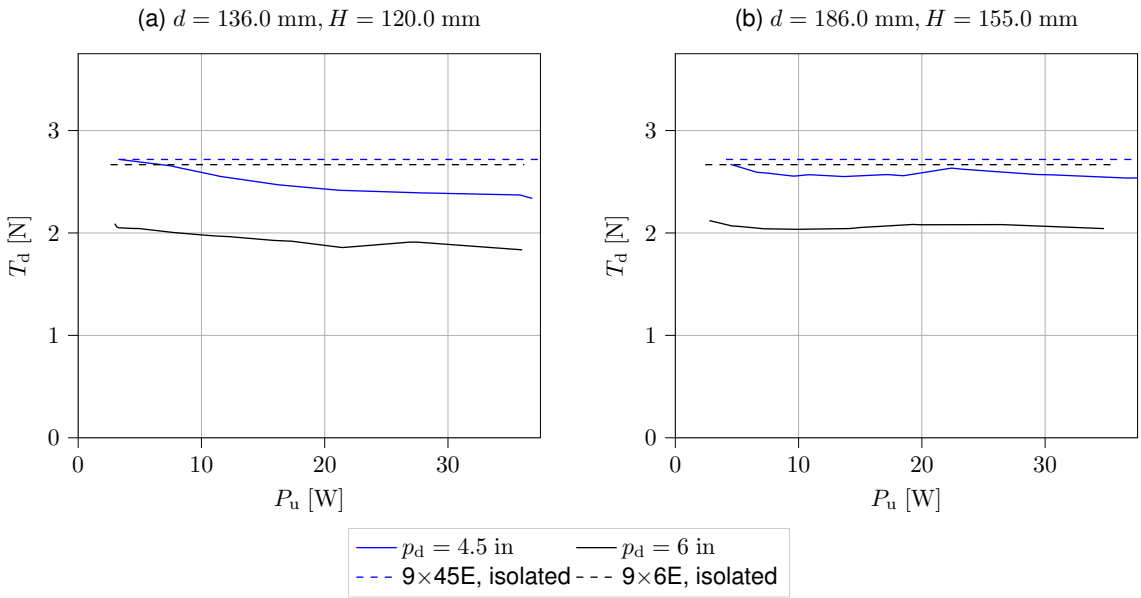

Figure 4.18: Downstream thrust plotted as a function of P_u, for a fixed $P_\mathrm{d} = 25$ W, for downstream pitch comparison.

Qualitative values are not presented for this or the following sections, as the propellers in isolation would already generate different thrusts for different powers. As such, it is unreasonable to compare the behaviors of two different propellers to one another in this case. The effect of downstream pitch can still be qualitatively analysed: a larger pitch in the downstream position appears to be less sensitive to the wake generated by another propeller.

To corroborate the observation that a lower pitch is more sensitive to the wake of another propeller, the isoline plot in figure 4.19 is useful. The isolines lean much more significantly in the 9×4.5E case than in the 9×6E configuration. In any case, this is not offset by the significant difference in lift observed, suggesting that a lower downstream pitch is strongly preferred.

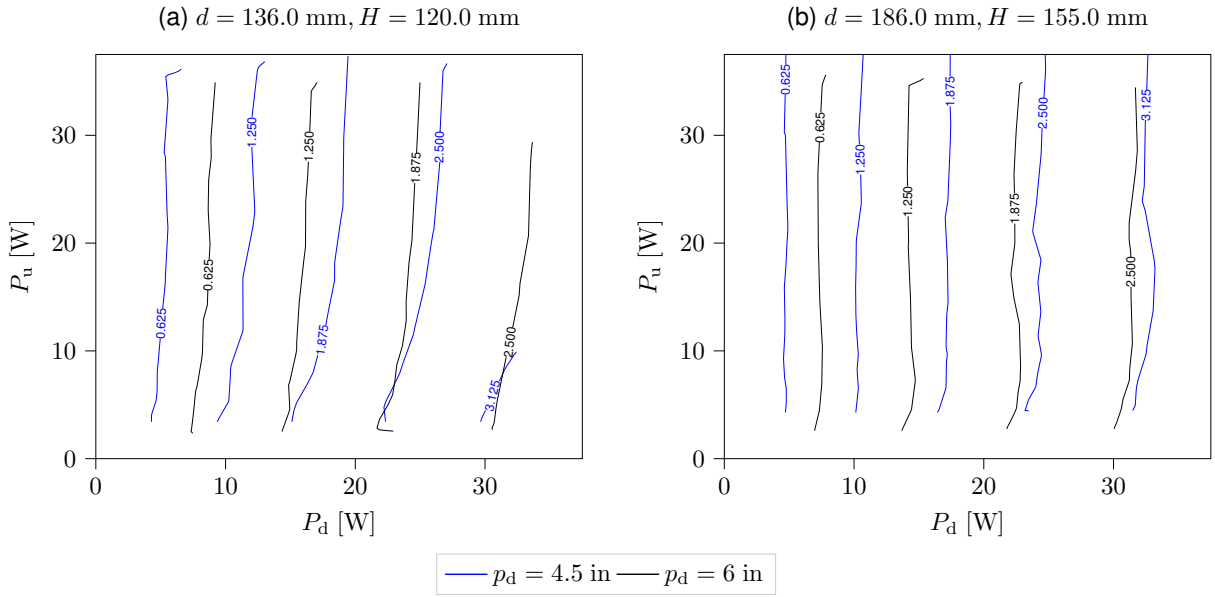

Figure 4.19: Downstream thrust isoline plots for comparison of upstream pitch.

4.4.2 Figure of Merit as a Function of Angular Velocity

The analysis of FM yielded similar results. At a fixed $\Omega_u = 4500$ RPM, a clear difference in efficiency can be observed (see figure 4.20). This difference becomes more severe as Ω_d is increased. As the distance between propellers is increased, it can be seen that low-speed efficiency is also slightly higher. This is also seen through fig. 4.21, where $\Omega_d = 4500$ RPM. Indeed, an increase in Ω_u steadily decreases FM.

Regarding constant FM isolines, the conclusions are mostly similar: though a larger downstream pitch is less affected by an increase in upstream power, the lower pitched propeller has a better performance in the tested ranges.

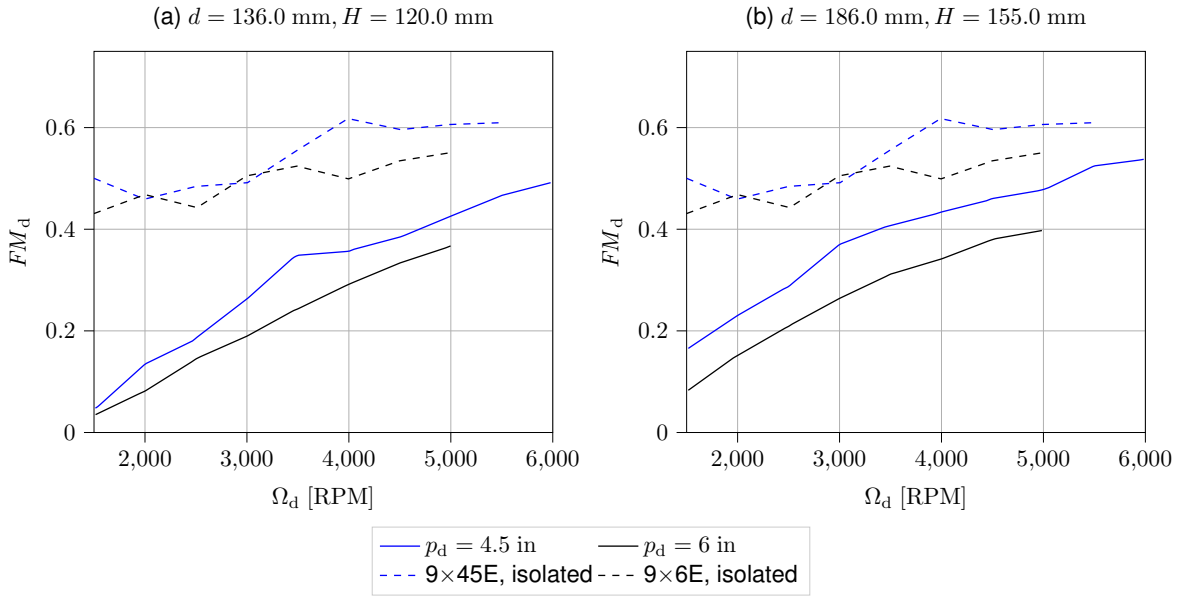

Figure 4.20: Downstream FM plotted as a function of angular velocity, for a fixed $\Omega_\mathrm{u} = 4500$ RPM, for downstream pitch comparison.

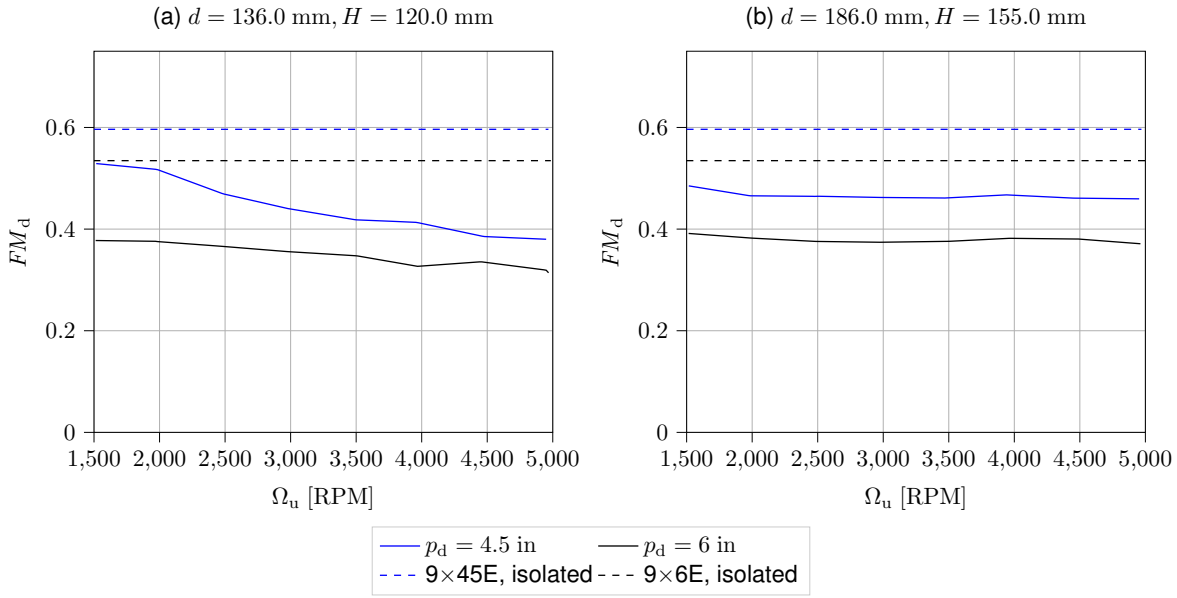

Figure 4.21: Downstream FM plotted as a function of angular velocity, for a fixed $\Omega_\mathrm{d} = 4500$ RPM.

4.4.3 Overlap Coefficient as a Function of Angular Velocity

The performance of both rotors in tandem appears to be much less affected when the downstream pitch is altered. In fact, κ_ov is fairly close across the ranges tested for a fixed upstream angular velocity. Distancing the rotors also plays a fairly large part in the performance of the system: while the smaller pitch performs better in smaller distances, it appears that as distance is increased the larger pitch is less power intensive. As can be seen in figure 4.23, these differences are in the order of close to 10% at most. The same observation is clear for figure 4.24: it appears that as distance is increased, the

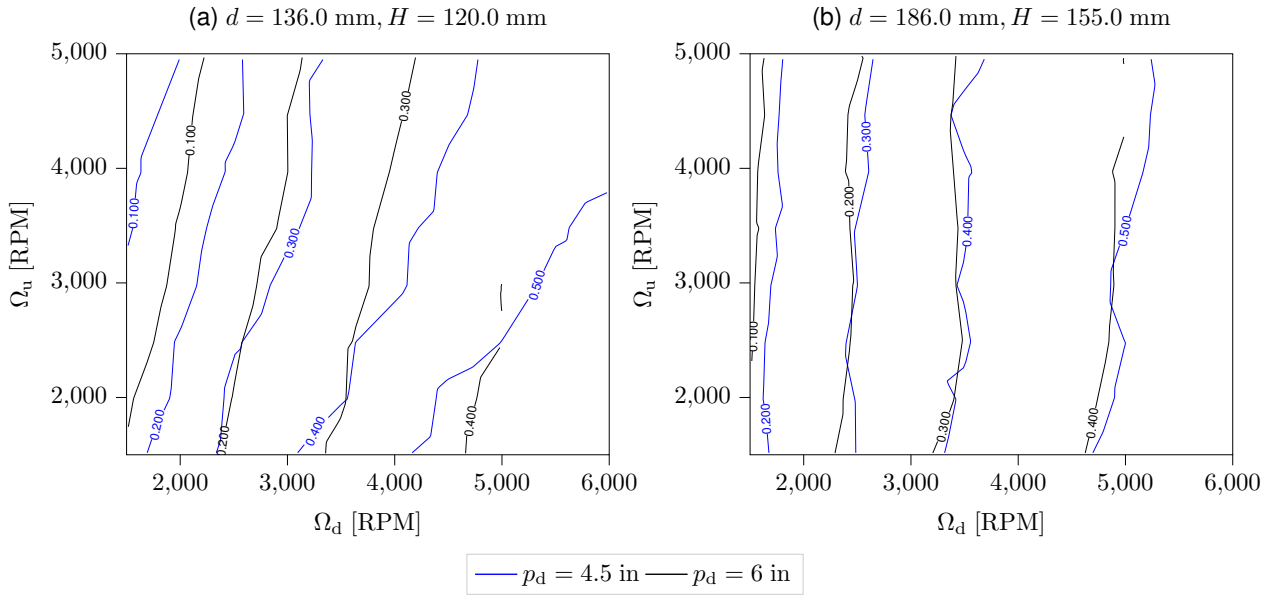

Figure 4.22: Downstream FM isoline plots for comparison of downstream pitch.

lower-pitched propeller consumes more power than a higher-pitched one.

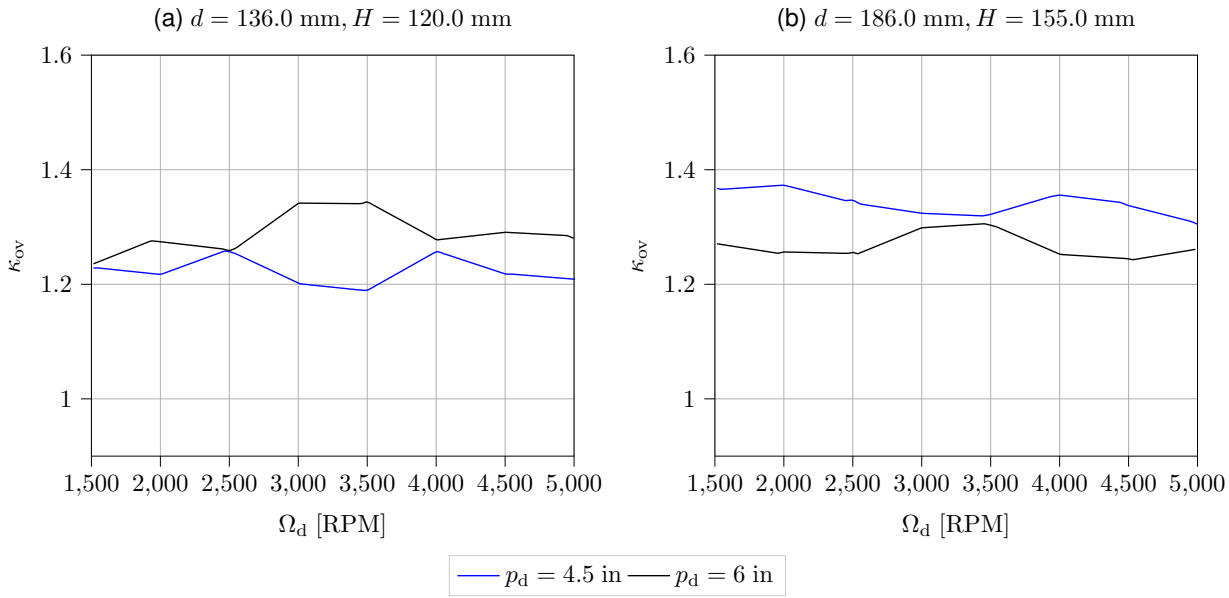

Figure 4.23: Overlap coefficient as a function of Ω_d, for fixed $\Omega_u = 4500$ RPM, for downstream pitch comparison.

4.4.4 Conclusions Regarding Downstream Pitch Influence on Overall Performance

A lower pitched propeller provides a better performance over its higher pitched counterpart, when in the downstream position. This performance difference is similar to what was observed in isolation: a 5

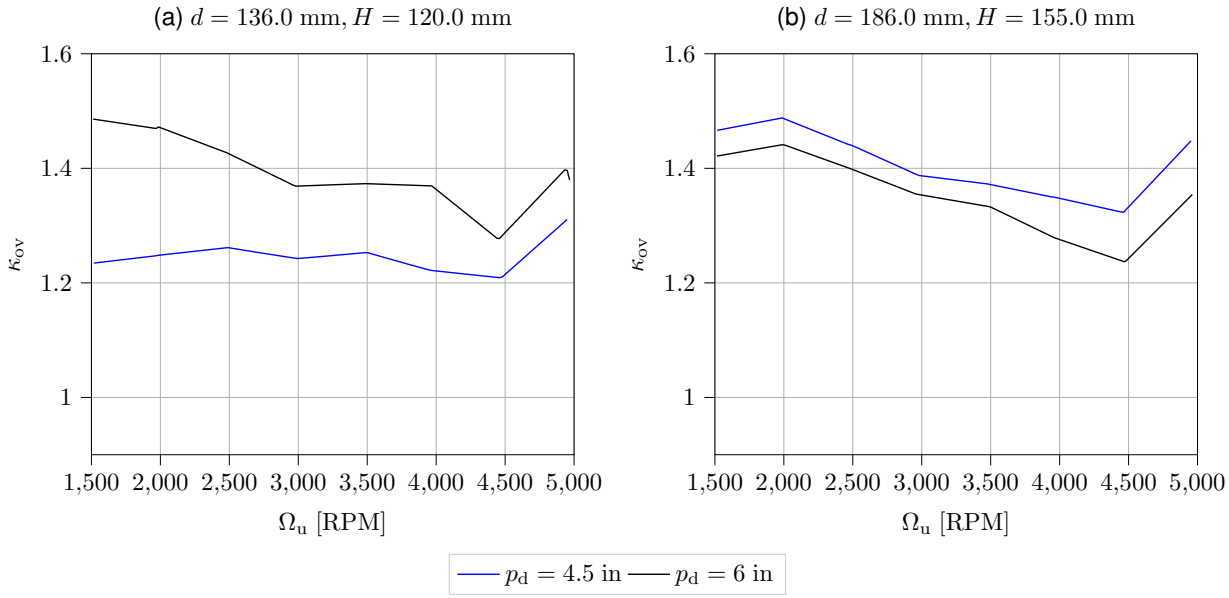

Figure 4.24: Overlap coefficient as a function of Ω_u, for fixed $\Omega_d = 4500$ RPM, for downstream pitch comparison.

to 10% difference between the propellers' FM. However, it is possible that, for higher angular velocities than those tested, there is a crossover where the higher pitched propeller becomes more efficient again.

Regarding κ_{ov}, an increase in distance means that the system with a lower pitch in the downstream position performs worse. Because the lower pitched propeller produces more thrust with less interference (as seen in 4.4.1), it consumes more power relative to the higher pitched propeller.

4.5 Upstream Propeller Diameter Sensitivity

Upstream diameter was tested using an 10×6E or 9×6E propeller in the upstream position, as previously explained. The propeller downstream was a 10×6E. It is expected that the difference on the downstream propeller is somewhat minimal, especially as the wake develops. Quantitative values were omitted here, since they were of a very small magnitude (at most $1 - 3\%$).

4.5.1 Downstream Thrust Generated as a Function of Mechanical Power

The difference between the upstream propeller's diameter is extremely small, as can be seen in fig. 4.25. In fact, at a fixed downstream power, the same minute difference is observed, as is seen in fig. 4.26. The decreasing thrust as upstream power is increased is clear, but not a very significant efficiency difference was observed.

The isoline plot in fig. 4.27 shows that the sensitivity of the 10×6E propeller downstream to upstream diameter increases as distance increases (isolines are further apart). It is also true that, for the same distance, the isolines are further apart the more P_d is increased. This suggests an increase in performance

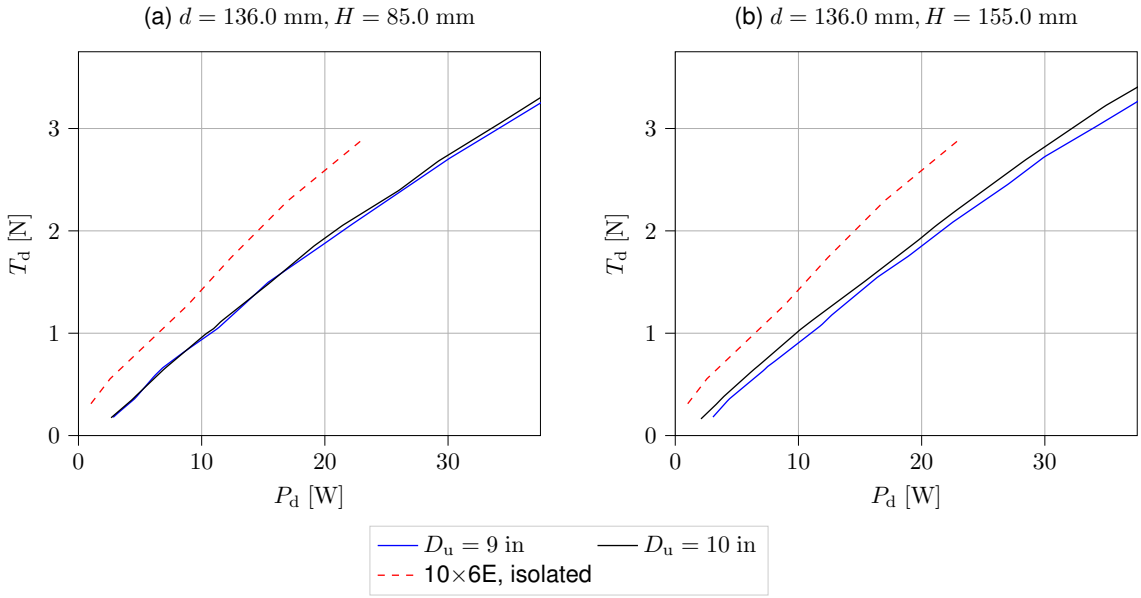

Figure 4.25: Downstream thrust plotted as a function of P_d, for a fixed $P_\mathrm{u} = 25$ W, for upstream diameter comparison.

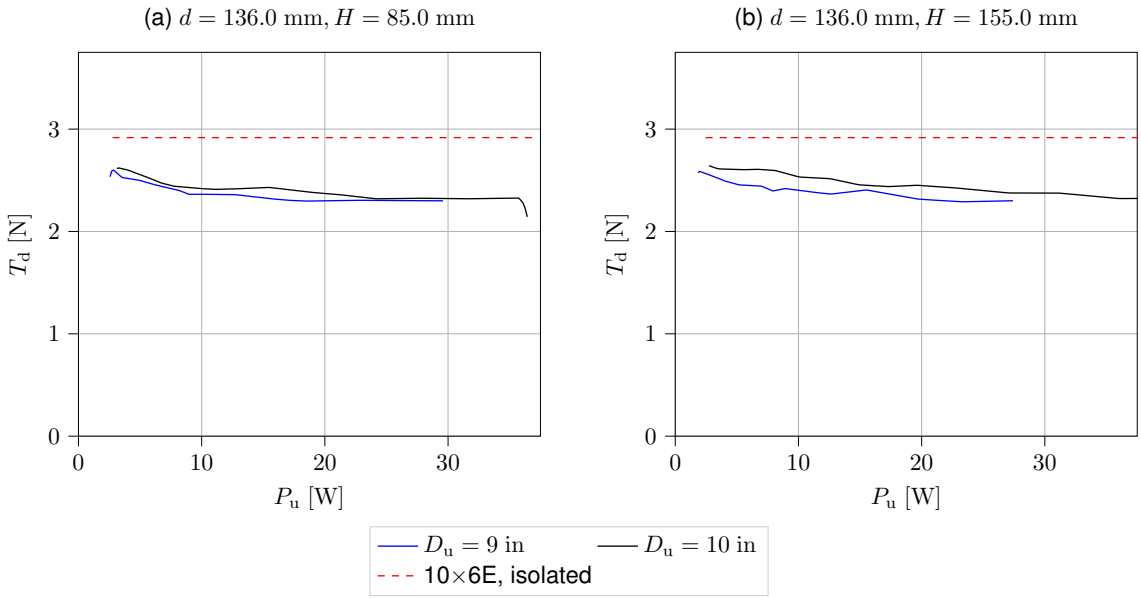

Figure 4.26: Downstream thrust plotted as a function of P_u, for a fixed $P_\mathrm{d} = 25$ W, for upstream diameter comparison.

differences, which is seen in figs. 4.25 and 4.26.

4.5.2 Figure of Merit as a Function of Angular Velocity

The same conclusions can be drawn from the efficiency point of view. Both at a fixed 4500 RPM on the upstream or downstream rotor, the effect of upstream diameter was generally minor, as can be seen in figs. 4.28 and 4.29.

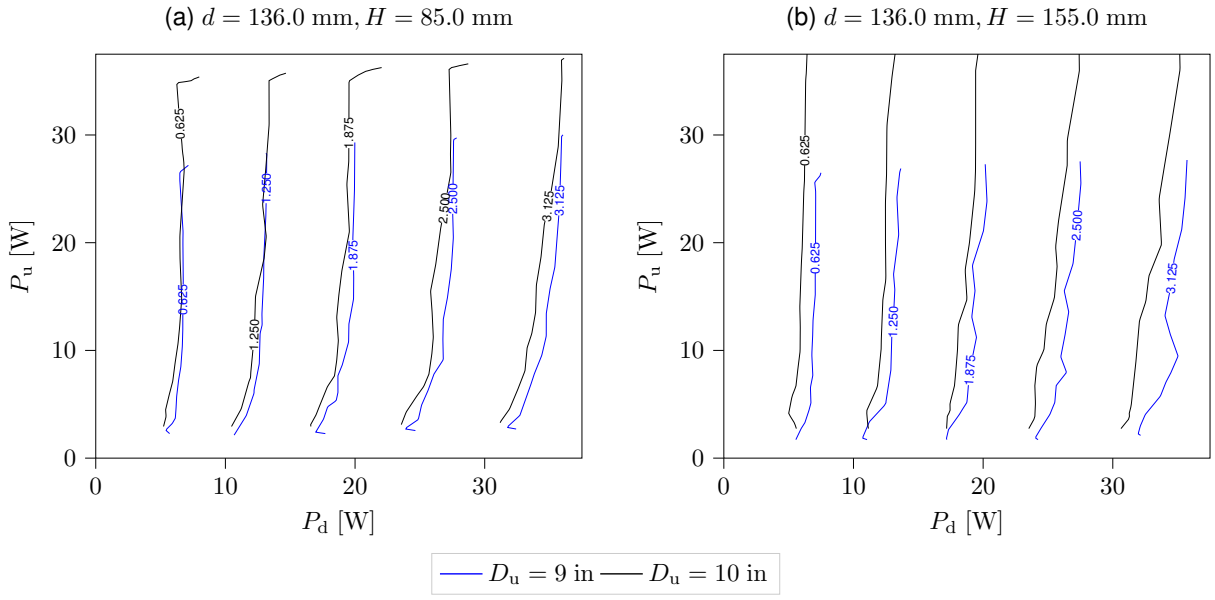

Figure 4.27: Downstream thrust isoline plots for comparison of upstream diameter.

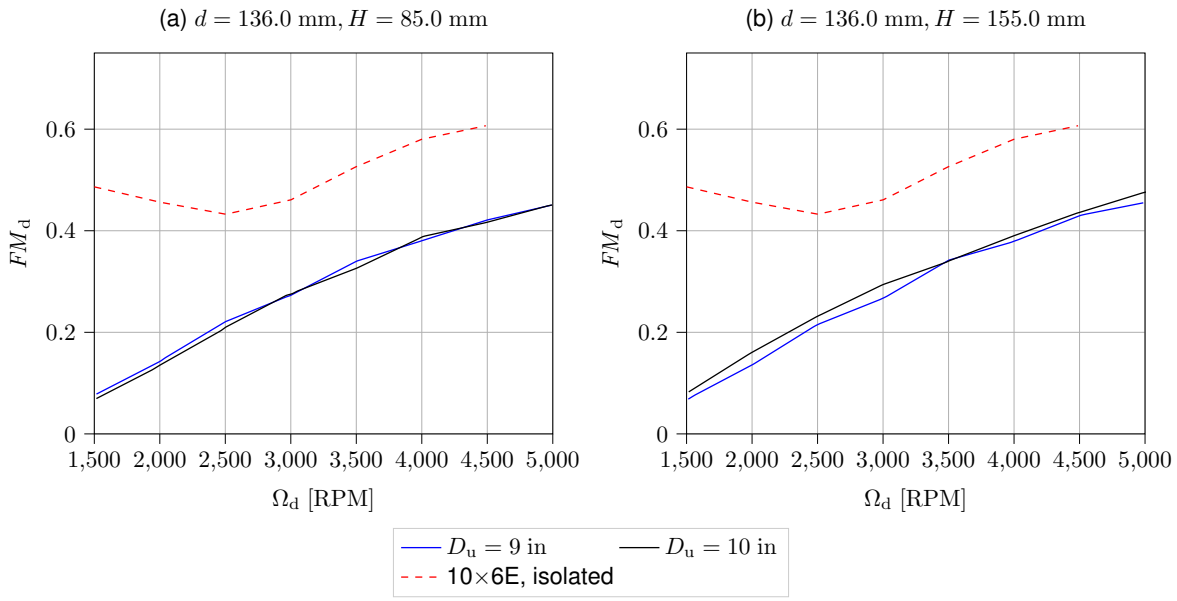

Figure 4.28: Downstream FM plotted as a function of angular velocity, for a fixed $\Omega_u = 4500$ RPM, for upstream diameter comparison.

Again, it is quite clear that the rotor stabilised on some performance loss quite quickly, with linear decay thereafter. In any case, neither appears to be significantly detrimental to Figure of Merit, or unexpectedly decrease a rotor's performance. It appears, however, that a slightly larger upstream diameter can, in fact, improve the rotors' performance slightly.

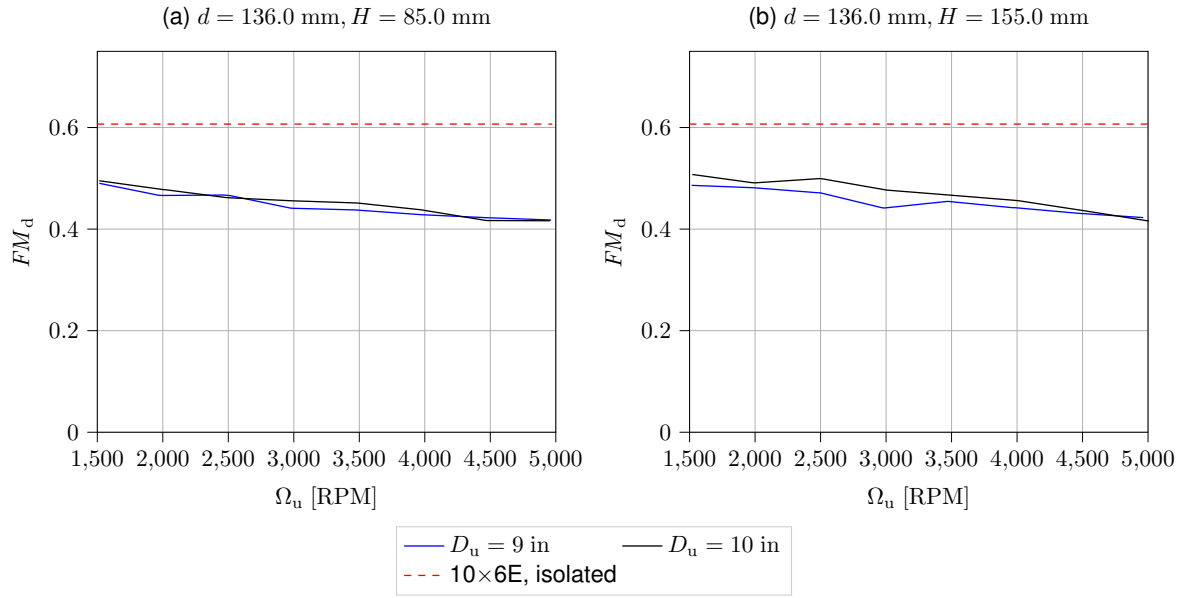

Figure 4.29: Downstream FM plotted as a function of angular velocity, for a fixed $\Omega_d = 4500$ RPM, for upstream diameter comparison.

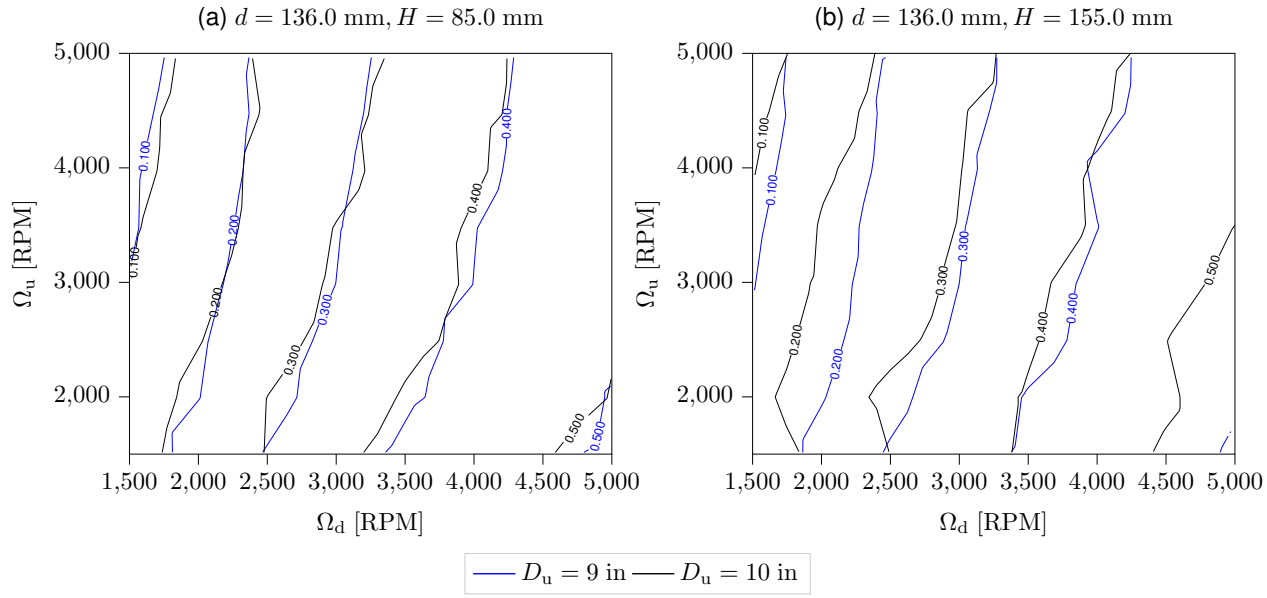

Figure 4.30: Downstream FM isoline plots for comparison of upstream diameter.

4.5.3 Overlap Coefficient as a Function of Angular Velocity

The behavior of the overlap coefficient is very similar to what was previously observed, though slightly more oscillatory than the previously analysed metrics. No clear improvement in κ_{ov} is seen, when upstream diameter is varied. If anything, figures 4.31 and 4.32 show that for most angular velocities tested, a larger upstream diameter is somewhat preferred.

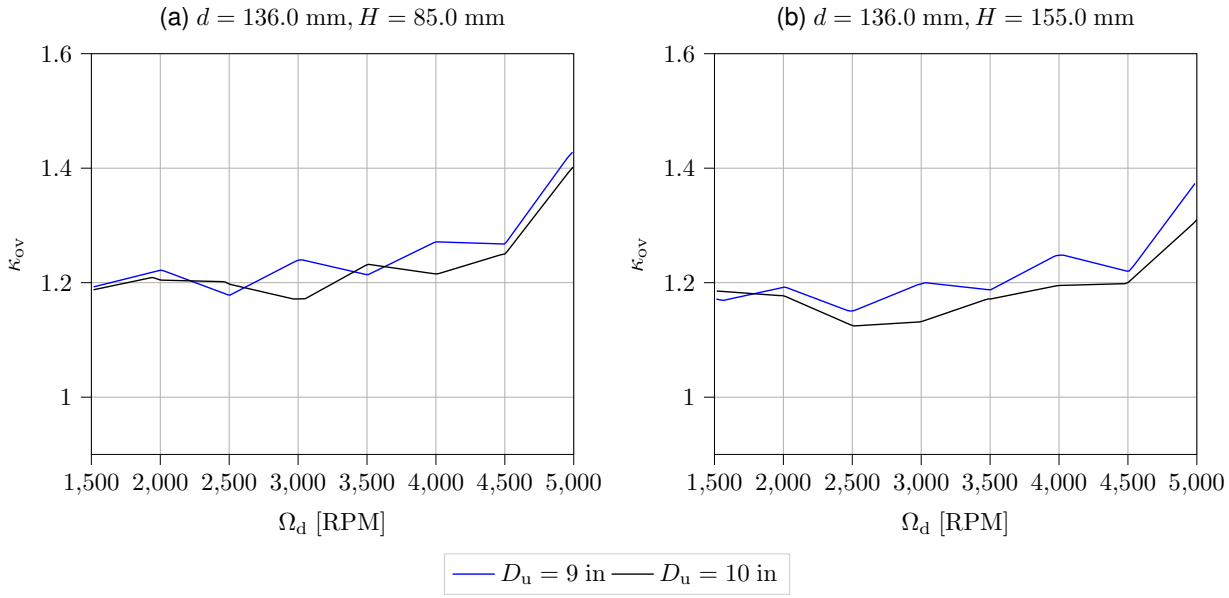

Figure 4.31: Overlap coefficient as a function of Ω_d, for fixed $\Omega_u = 4500$ RPM, for upstream diameter comparison.

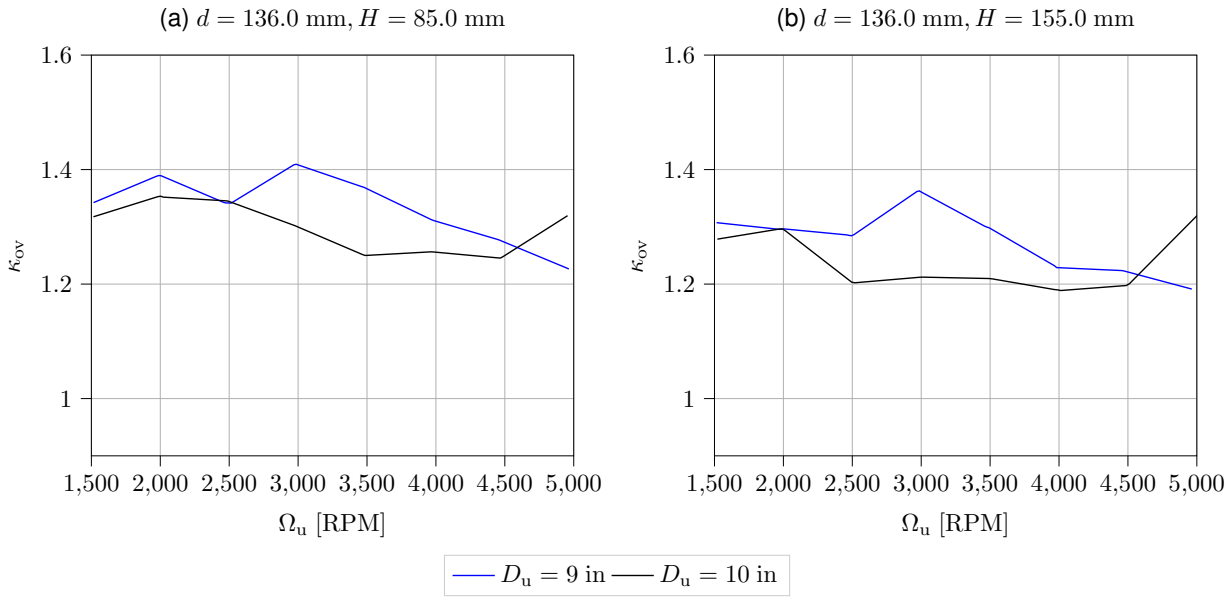

Figure 4.32: Overlap coefficient as a function of Ω_u, for fixed $\Omega_d = 4500$ RPM, for upstream diameter comparison.

4.5.4 Conclusions Regarding Upstream Diameter and Influence on Overall Performance

It appears that a higher diameter on the upstream position makes little difference on the overall performance of the system. As such, a higher diameter generates more thrust in the upstream position, and thus more total thrust. The possibility that a larger diameter in the upstream position implies a slightly better performance, though not unseen in research, is something that requires further study. In any

case, the efficiency improvements seen are in the range of around $1 - 3\%$. Though slightly larger (at most 14%), the improvements in κ_{ov} are not consistent across a large range of Ω.

4.6 Downstream Propeller Diameter Sensitivity

Downstream diameter sensitivity was tested using an 10×6E or 9×6E propeller in the downstream position and a 10×6E upstream. It is expected that the downstream propeller is somewhat influenced, and that a larger diameter is more impacted by the upstream propeller.

4.6.1 Downstream Thrust Generated as a Function of Mechanical Power

It is seen in fig. 4.33 that the impact of the upstream propeller on the one downstream is, somewhat unexpectedly, stronger on the 9×6E propeller. In fact, at the lower end of power, the isolated behavior is similar, but there is a clear difference in the tandem propellers. At a fixed downstream power of 25 W, a fairly constant impact is observed as upstream power is increased. Fig. 4.34, at $P_{\text{d}} = 25$ W shows that the isolated differences in thrust produced are amplified as upstream power is increased.

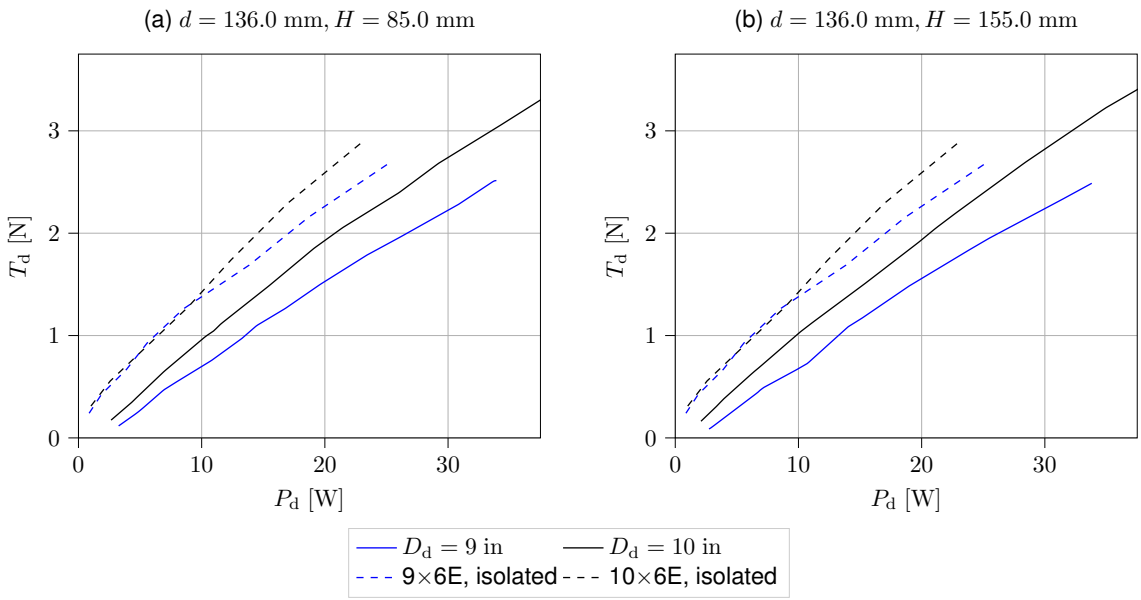

Figure 4.33: Downstream thrust plotted as a function of P_{d}, for a fixed $P_{\text{u}} = 25$ W, for downstream diameter comparison.

Analysing isolines in fig. 4.35, it appears that the overall impact on performance is not increasing with power: the lines remain parallel and mostly consistent across a wide range of powers.

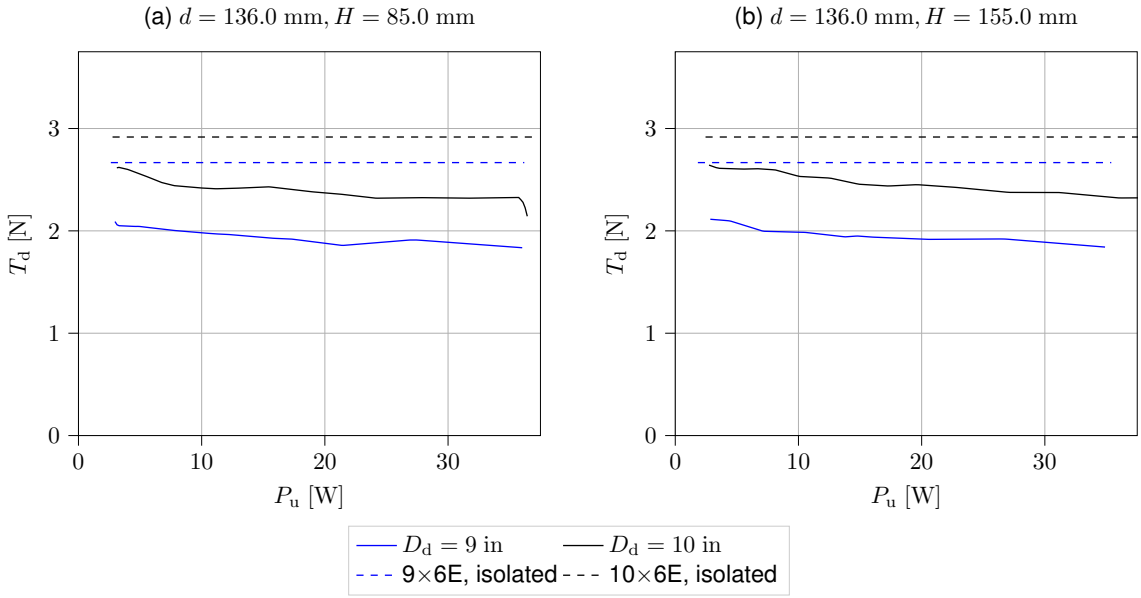

Figure 4.34: Downstream thrust plotted as a function of P_u, for a fixed $P_\mathrm{d} = 25$ W, for downstream diameter comparison.

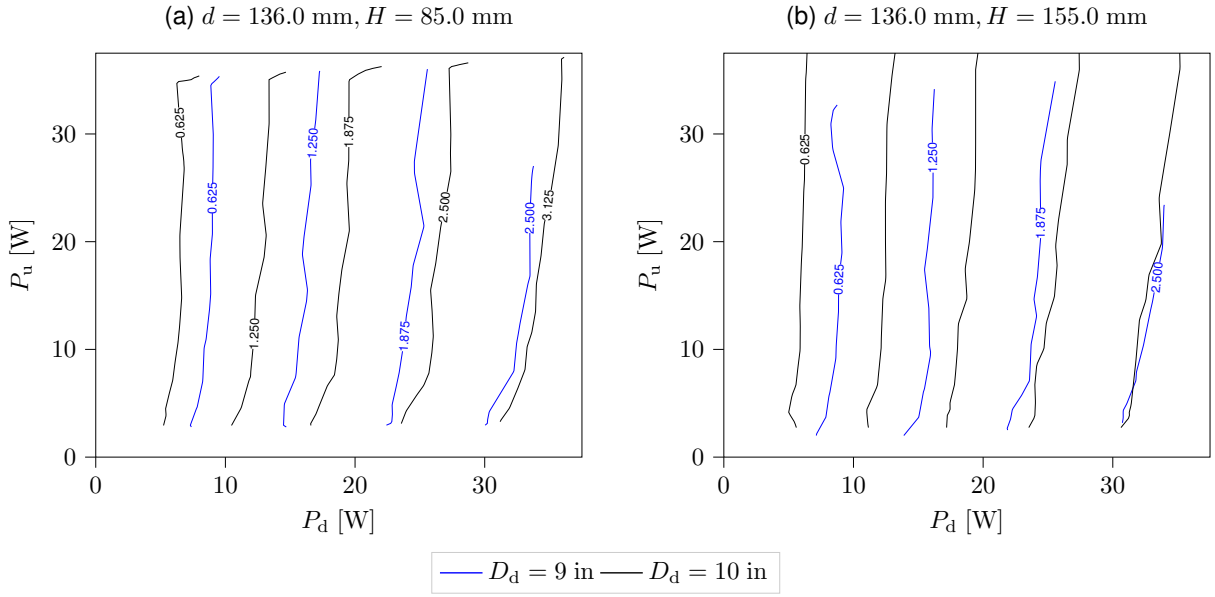

Figure 4.35: Downstream thrust isoline plots for comparison of downstream diameter.

4.6.2 Figure of Merit as a function of Angular Velocity

From the efficiency point of view, at 4500 RPM on the upstream or downstream rotor, the effect observed on the downstream rotor was mostly constant. As Ω_d increases, this impact increases (as seen by the increased difference between lines in fig. 4.36). The difference, however, appears to be constant: fig. 4.37 shows that, as upstream angular velocity increases (for constant Ω_d), the performances of the different diameters remain mostly constant among each other.

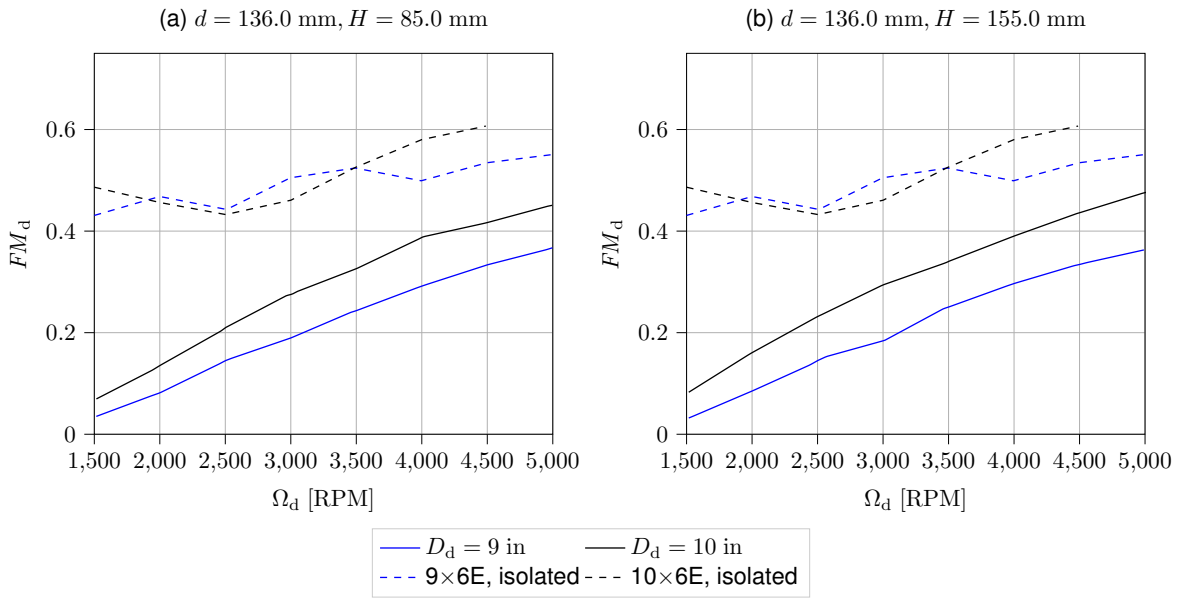

Figure 4.36: Downstream FM plotted as a function of angular velocity, for a fixed $\Omega_u = 4500$ RPM, for downstream diameter comparison.

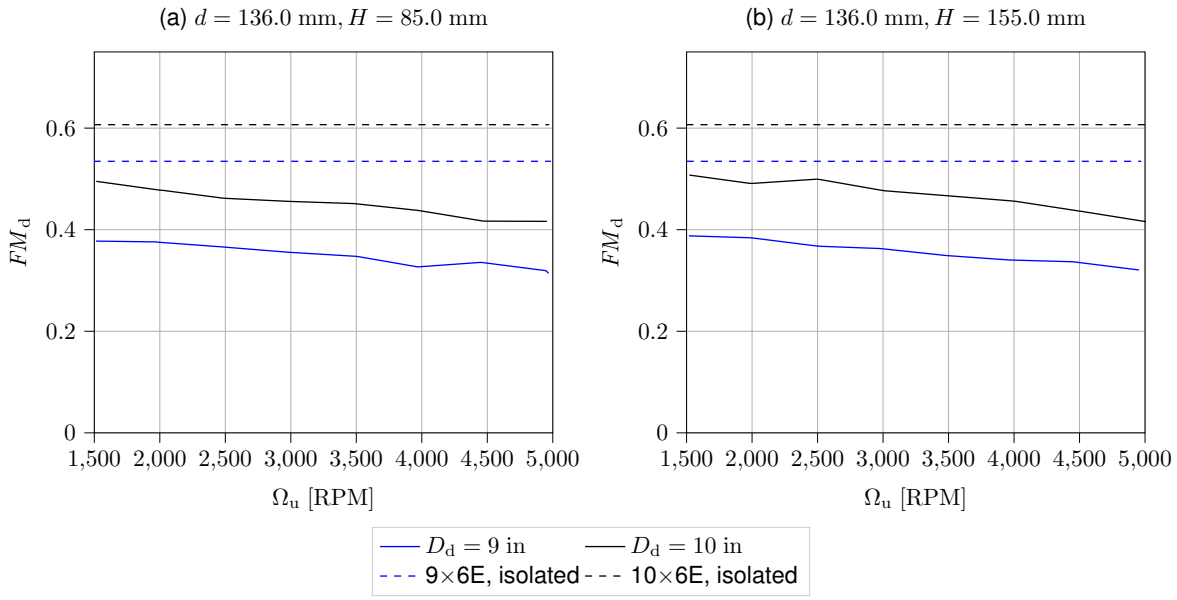

Figure 4.37: Downstream FM plotted as a function of angular velocity, for a fixed $\Omega_d = 4500$ RPM, for downstream diameter comparison.

Isolines in fig. 4.38 are significantly more inclined. This suggests a much higher impact on the downstream rotor. Neither rotor has a clear difference, though the larger diameter rotor is, again, much more performant both in isolation and in tandem.

4.6.3 Overlap Coefficient as a function of Angular Velocity

The overlap coefficient is mostly constant across angular velocity. Figures 4.39 and 4.40 confirm earlier observations that the power consumption for a pair of RPM is generally larger for the smaller

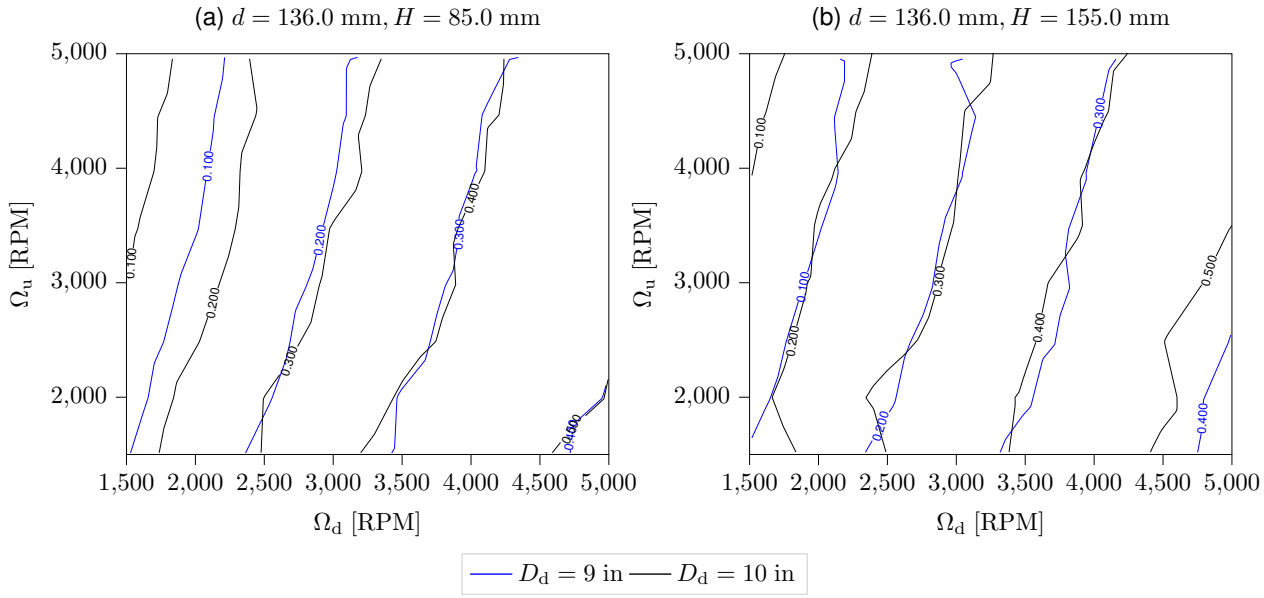

Figure 4.38: Downstream FM isoline plots for comparison of downstream diameter.

diameter downstream rotor.

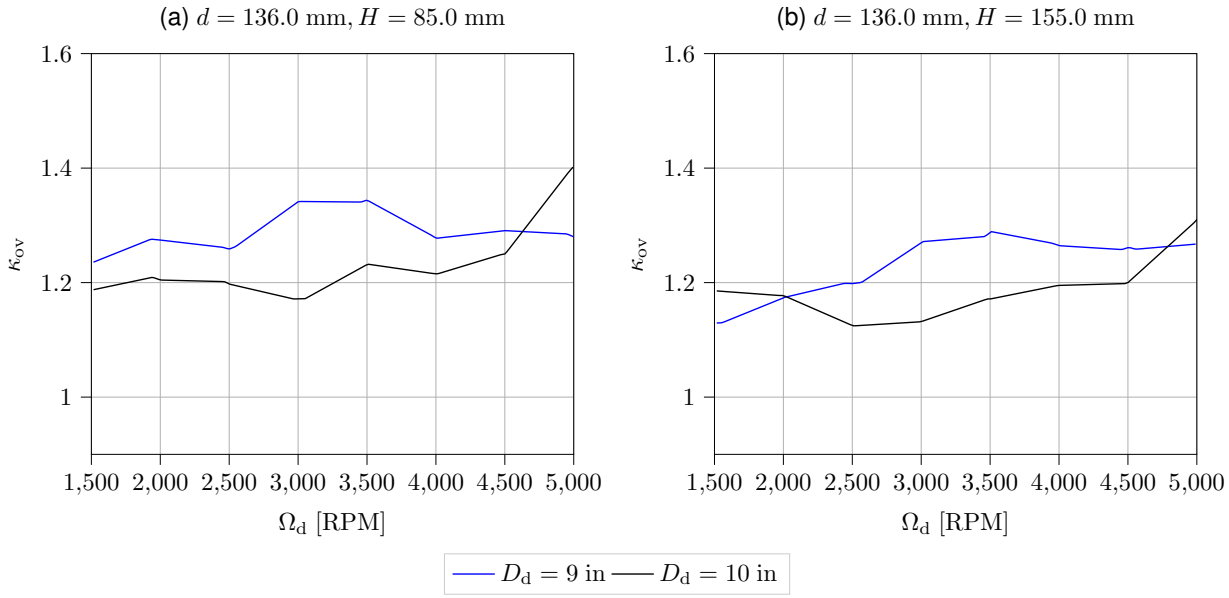

Figure 4.39: Overlap coefficient as a function of Ω_d, for fixed $\Omega_u = 4500$ RPM, for downstream diameter comparison.

4.6.4 Conclusions Regarding Downstream Diameter and Influence on Overall Performance

A relatively small difference in isolated performances was seen in the propellers tested. However, a comparatively large difference was seen in tandem. Because the interrotor and interaxial distances

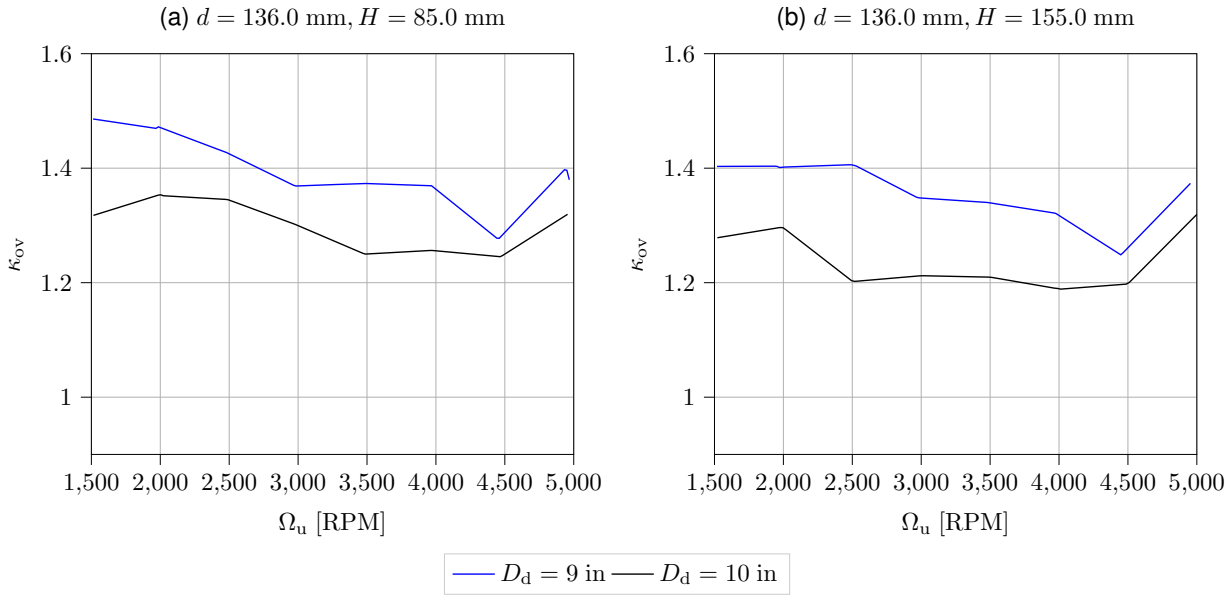

Figure 4.40: Overlap coefficient as a function of Ω_u, for fixed $\Omega_d = 4500$ RPM, for downstream diameter comparison.

observed were constant (i.e. (d, H) pairs were the same for each tandem set), the relative area of overlap for the smaller diameter rotor is larger. Thus, the impact on the smaller rotor is stronger. Although the larger rotor has a larger area, the total area of influence must be larger. It appears that this is not large enough (for the distances tested) to give the smaller diameter propeller an advantage in overlap coefficient.

Similar conclusions can be drawn from thrust and FM evaluations: the impact of downstream diameter is such that performance of the downstream propeller is decreased as the diameter decreases as well. Figure of Merit appears to suffer a stronger impact, even at larger distances.

4.7 Rotor-plane Distance Sensitivity

In order to evaluate rotor-plane distance sensitivity regarding performance, the set of propellers was the 9×4.5E in the upstream position and the 10×6E downstream. A similar approach, of analysing the performances with regards to thrust produced as a function of applied power was used, as well as FM and angular velocity. It is, of course, expected that an increase in rotor-plane distance implies an improved performance, as less interference is observed. However, because the velocity within the wake of the upstream rotor increases, the effect could be reversed at some point.

4.7.1 Downstream Thrust Generated as a Function of Mechanical Power

The following plots (see fig. 4.41) display the impact of H over the performance of the downstream propeller, for a fixed upstream power on 4.41(a) and a fixed downstream power on 4.41(b). The decrease

in thrust is mostly small, though noticeable. It is, at most a 0.1 N difference for the same power in either case. A 15.2% performance decrease was observed relative to the isolated rotor case.

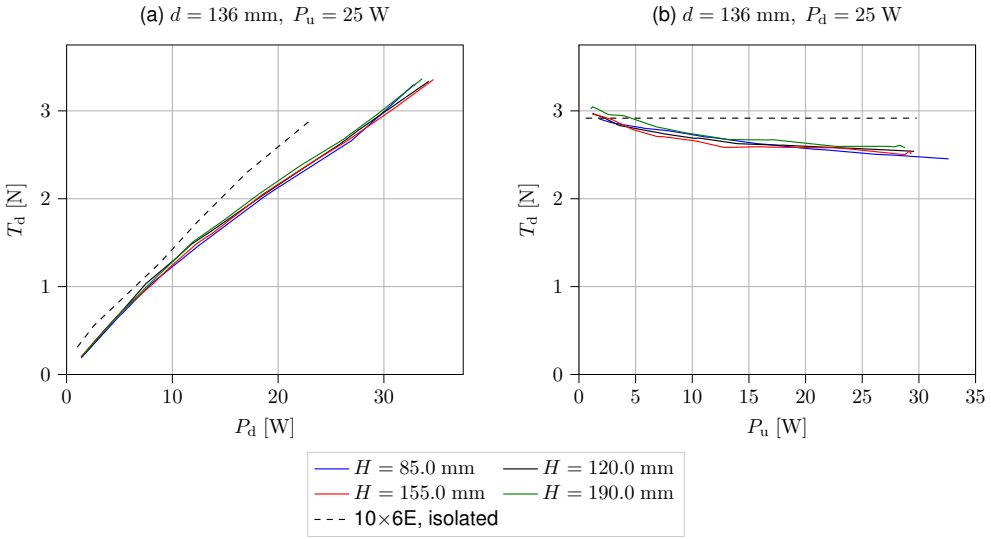

Figure 4.41: Downstream thrust plotted as a function of mechanical power, for a fixed $P_i = 25$ W, for interrotor distance comparison.

Regarding isoline plots, two distances are shown: $d = 136$ mm and 186 mm. At $d = 230$ mm, isolines are mostly vertical, and were omitted for that reason. Fig. 4.41 shows how, for smaller H and a given thrust, more power at the downstream rotor is required to produce it.

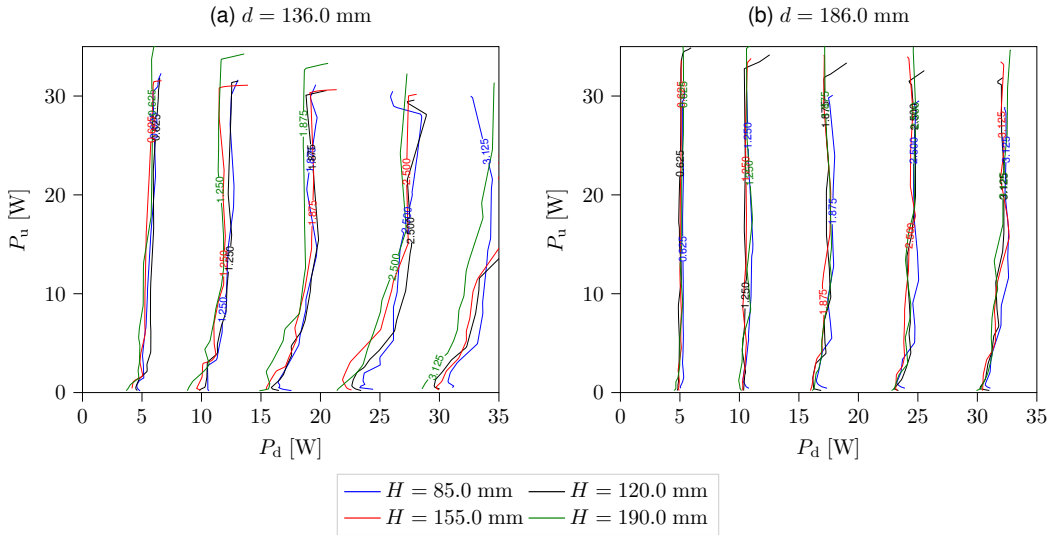

Figure 4.42: Downstream thrust isoline plots comparing the effect of altering interrotor distance H.

4.7.2 Figure of Merit as a Function of Angular Velocity

Evaluating Figure of Merit as done previously yields fairly similar results: at a fixed $\Omega_u = 4500$ RPM (fig. 4.43(a)) shows no appreciable difference, though a slightly greater difference can be seen for the plot

on fig. 4.43(b). Figure 4.44 shows how the Figure of Merit is influenced by upstream and downstream rotor angular velocity. It is clear that, though a smaller H is less efficient, this difference is not of great importance.

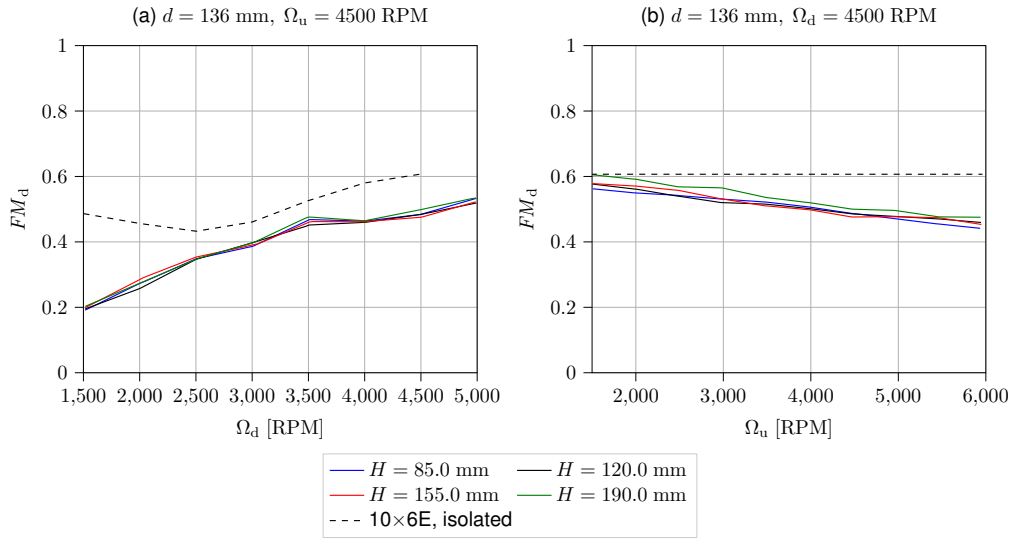

Figure 4.43: Downstream FM plotted as a function of angular velocity, for a fixed $\Omega_i = 4500$ RPM, for interrotor distance comparison.

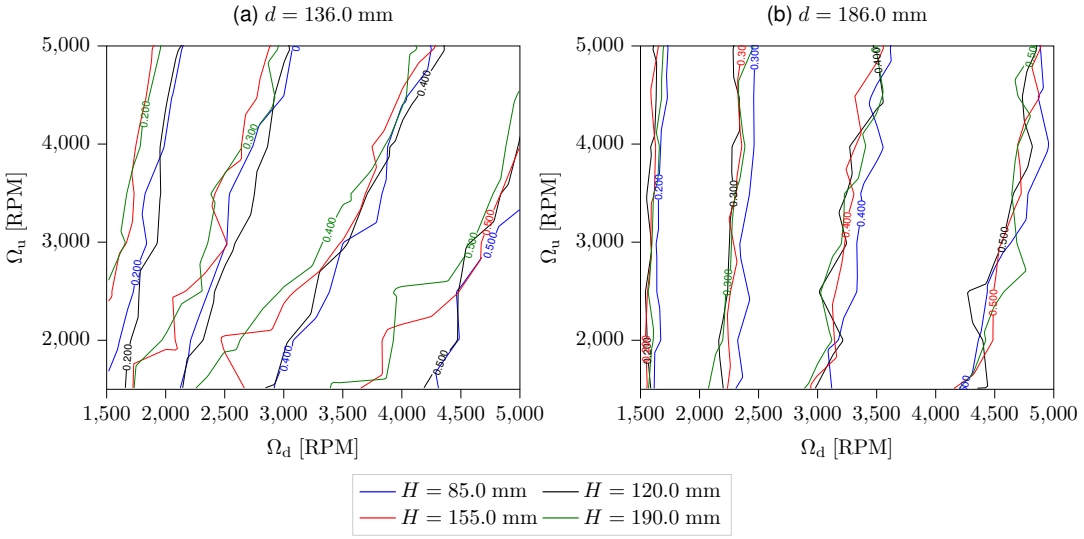

Figure 4.44: Downstream FM isoline plots comparing the effect of altering interrotor distance H.

4.7.3 Overlap Coefficient as a Function of Angular Velocity

As expected, the decrease of H has a small but noticeable effect on κ_{ov}. Though its magnitude is small, two points of relatively lower overlap coefficient can be identified. Some angular velocities appear to have less sensitivity in regards to the overlap coefficient, as can be seen at $\Omega_{u,d} = (4500, 3500)$ RPM.

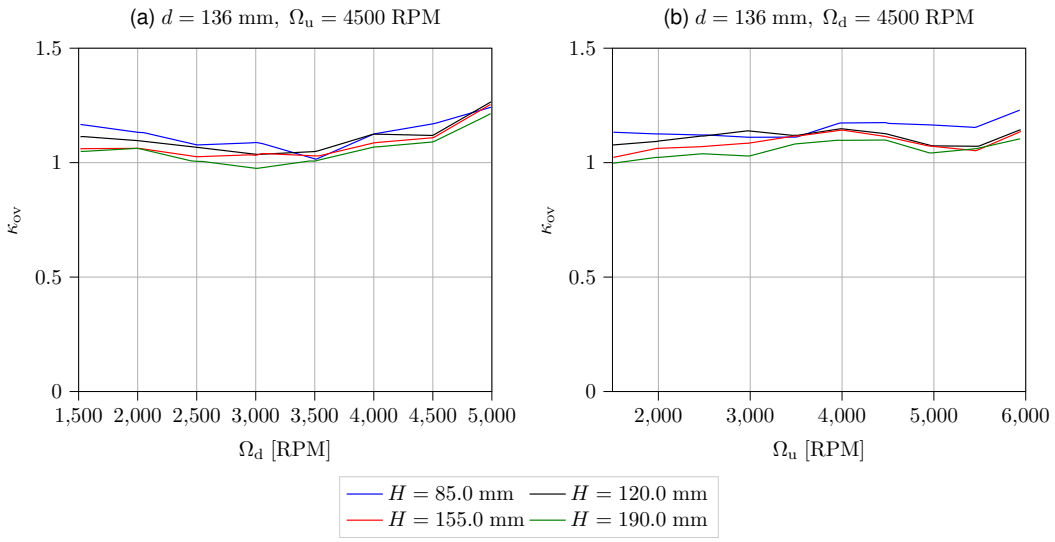

Figure 4.45: Overlap coefficient as a function of angular velocity, for fixed $\Omega_i = 4500$ RPM, for interaxial distance comparison.

4.7.4 Conclusions Regarding Rotorplane Distance

It is clear that rotor plane distance, though significant, does not have as much of a severe impact on downstream-rotor performance as was initially expected. This is possibly due to the wake of the upstream rotor developing faster than expected. The properties of a fully developed wake are such that velocity is mostly constant (and so is its area). The hypothesis that the wake develops quite quickly is corroborated by the observation that the variations in κ_{ov} are small.

4.8 Interaxial Distance Sensitivity

Interaxial distance (the distance between the rotors' axes), d, is expected to be more significant than H. Similar to what was done for H, fixed-variable plots are presented for the smallest distance tested. Isoline plots are also displayed, though for all examined distances in this case.

4.8.1 Downstream Thrust Generated as a Function of Mechanical Power

It is expected that an increase in d means an improvement in performance. However, the intermediate distance ($d = 186$ mm) showed a slightly higher thrust for the same power. Figure 4.46(a) shows that, for a small range of P_d, there is an increase in thrust even when comparing to an isolated propeller. For either fixed P_d (fig. 4.46(a)) or P_u (fig. 4.46(b)), the asymptotic behavior of the thrust curve is similar for $d = 186$ or 230 mm.

Four isoline plots, one for each examined H were obtained. A much clearer impact on performance is seen over the decrease in d. At larger interaxial distances (see fig. 4.47), the effects of interference

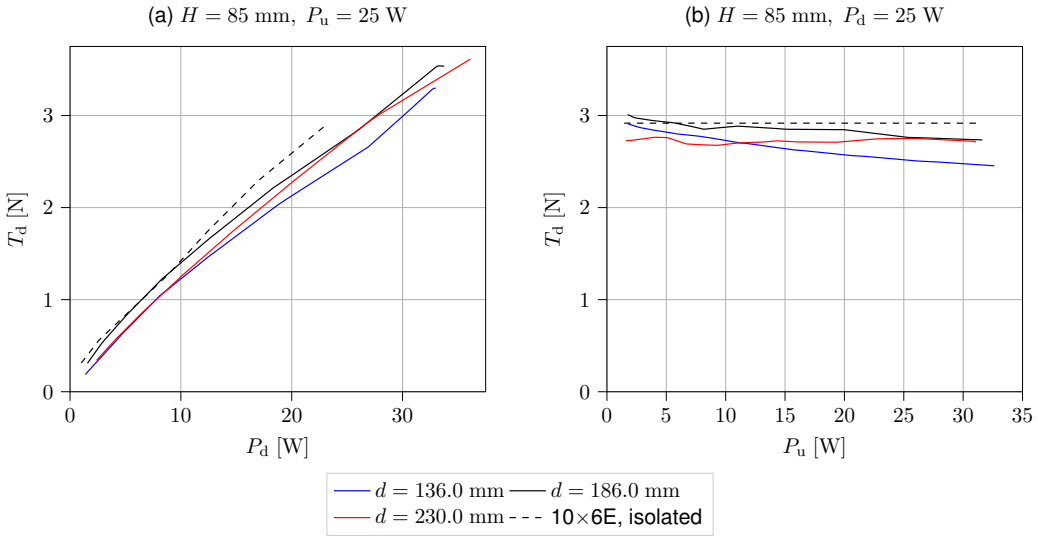

Figure 4.46: Downstream thrust plotted as a function of mechanical power, for a fixed $P_i = 25$ W, for interaxial distance comparison.

become, as expected, less and less pronounced. This variation is not constant, but is dependent on P_u and H. Increasing power on the upstream rotor makes the downstream rotor perform worse. Conversely, increasing H makes this effect less noticeable, i.e. increasing H decreases the negative effect that P_u has on performance.

4.8.2 Figure of Merit as a Function of Angular Velocity

Regarding FM, an increase in d is expected to imply an improvement in performance. However, $d = 186$ mm outperforms other interaxial distances. In fact, for specific ranges of Ω, this interaxial distance performs slightly better than an isolated propeller. Fig. 4.48 shows how performance is affected for fixed Ω.

Finally, examining fig. 4.49 shows the isolines for FM and how the rotors interfere with one another. As interaxial distance is increased, the isolines become more and more vertical, so that interference is minimal. At low Ω_u, a smaller interaxial distance is more efficient. This effect reverses around some Ω_u, where larger distances are more eficient. As H is increased, this threshold changes from < 2000 RPM in 4.49(a) up to 2500 RPM in 4.49(c,d).

One observation that is key from fig. 4.49: as H is increased, the threshold for smaller d being more performant increases as well. This can be explained by the fact that, as H increases, the downstream rotor experiences a larger relative velocity. As d is decreased for the same H, the edge of the downstream rotor experiences a larger magnitude relative velocity.

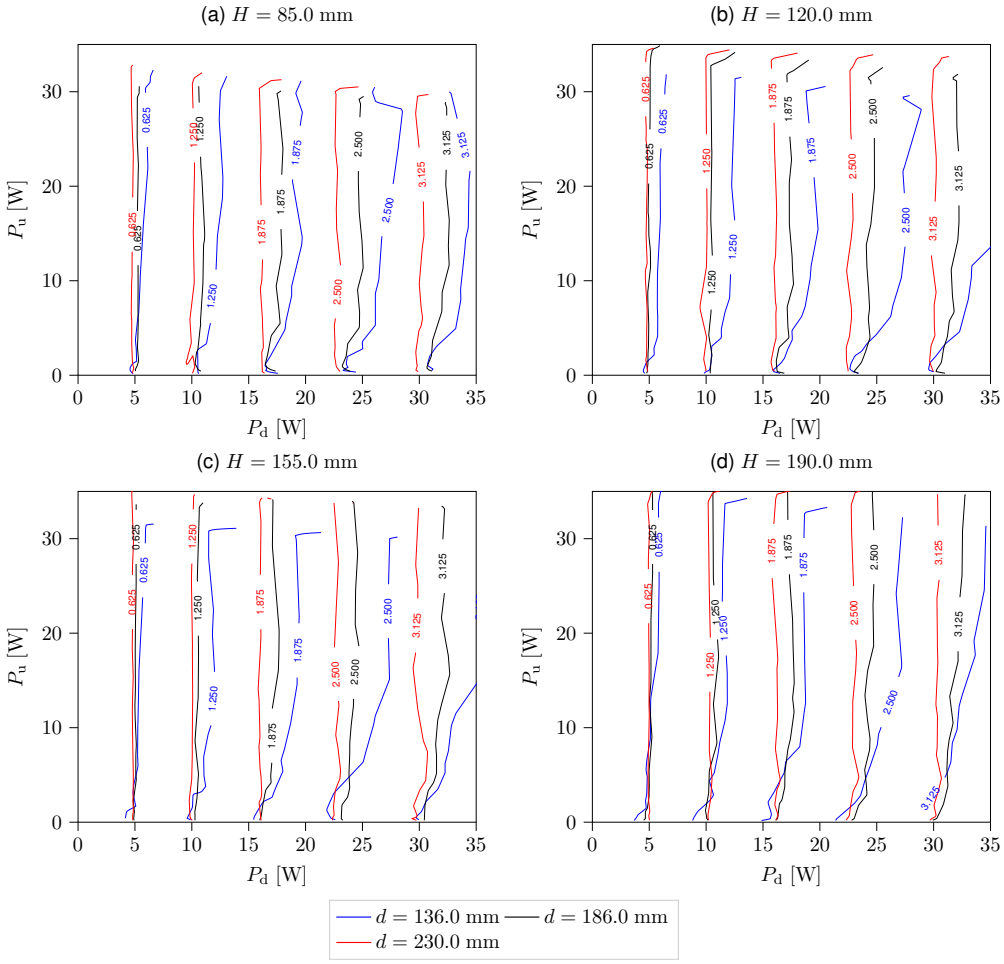

Figure 4.47: Downstream thrust isoline plots comparing the effect of altering interaxial distance d.

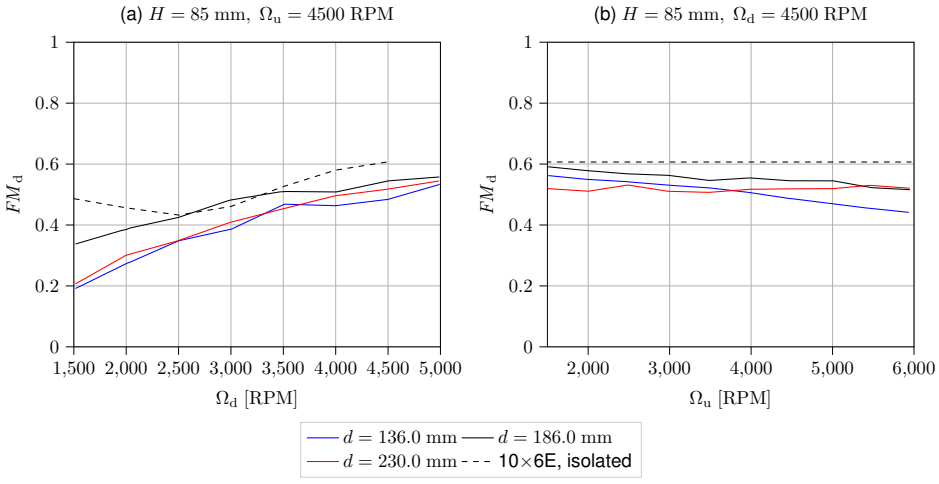

Figure 4.48: Downstream FM plotted as a function of angular velocity, for a fixed $\Omega_i = 4500$ RPM, for interaxial distance comparison.

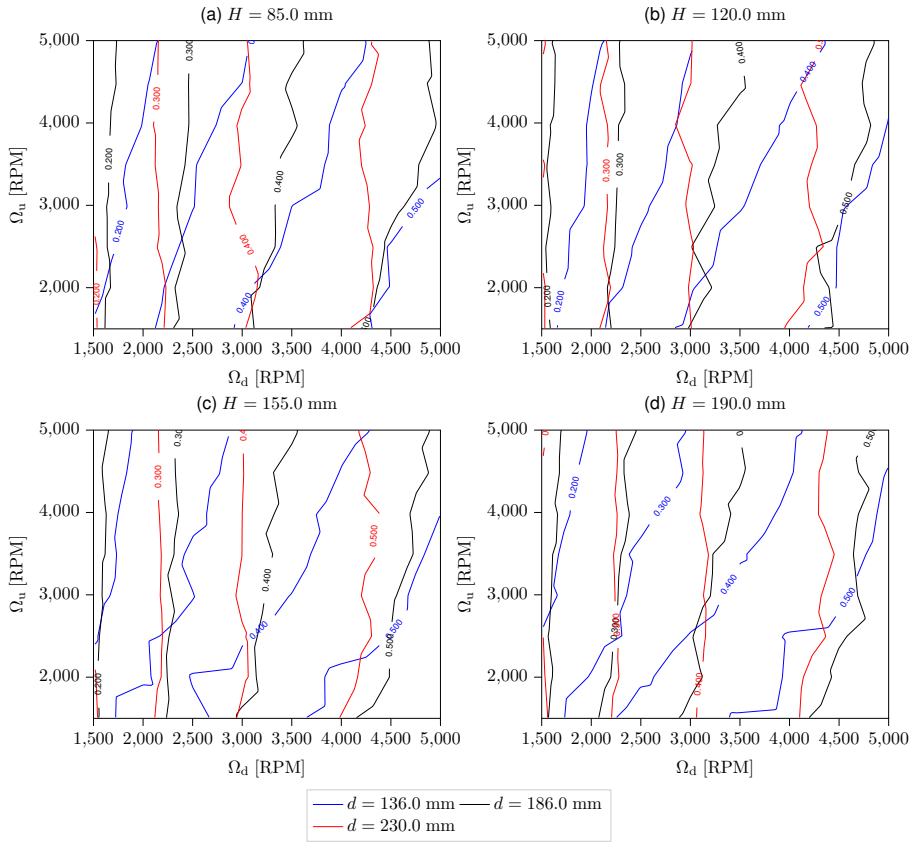

Figure 4.49: Downstream FM isoline plots comparing the effect of altering interaxial distance d.

4.8.3 Overlap Coefficient as a Function of Angular Velocity

Fixing $\Omega = 4500$ RPM for either the upstream or downstream rotor and computing the overlap coefficient results in fig. 4.50. For small H, increasing d appears to increase the overlap coefficient slightly. This is unexpected, since for larger d/D_d it is expected that the total power consumption (and thus κ_{ov}) decreases. For larger H, this effect becomes insignificant.

4.8.4 Conclusions Regarding Interaxial Distance

An increase of interaxial distance d is significantly more effective at reducing overall negative effects on performance than an equivalent increase in H. More research is needed to understand whether the increase in performance observed in this section is reproducible and in what conditions.

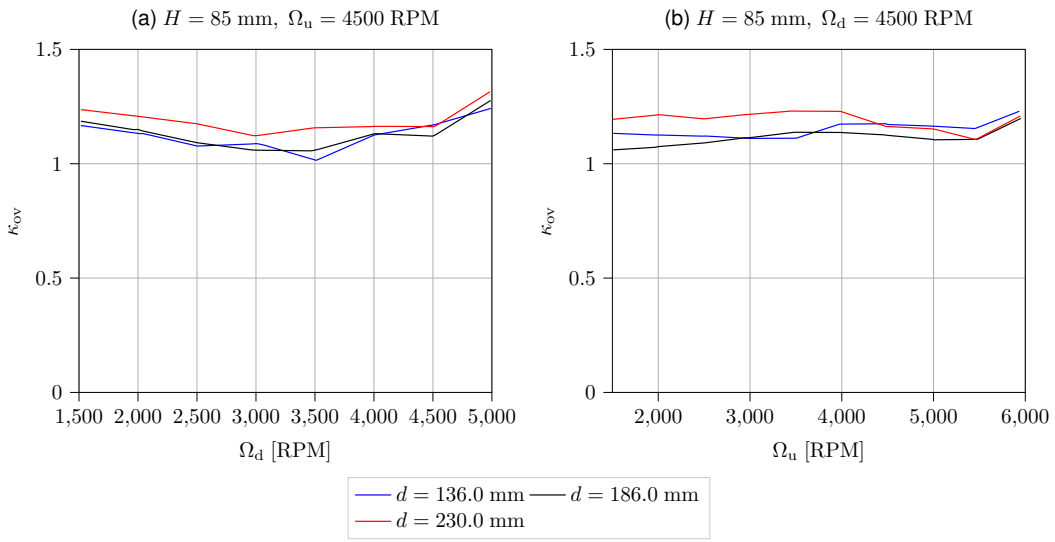

Figure 4.50: Overlap coefficient as a function of angular velocity, for fixed $\Omega_i = 4500$ RPM, for interaxial distance comparison.

Chapter 5

Conclusions

5.1 Conclusions on Experimental Results

Regarding each of the parameters and variables tested, the following conclusions could be extracted:

1. Rotation Direction:

   (a) **Rotation direction** had a clear impact on performance. ER direction performed close to 10% better than OR in close proximity ($d/D_{\mathrm{d}} < 0.732$, $H/D_{\mathrm{d}} = 0.334$ to 0.748).

   (b) In these conditions, not only was ER superior to OR, but the downstream propeller outperformed the isolated rotor when moderate RPM are used. More analysis is required to identify the exact conditions of these points.

   (c) The system as a whole performed slightly better when in OR from the point of view of the overlap coefficient when $d/D_{\mathrm{d}} = 0.732$. In the same conditions, the OR rotor downstream produced more thrust for the same power.

2. Upstream Pitch:

   (a) **Upstream pitch** was found to have a moderate effect on performance of the downstream rotor. A larger upstream pitch settled more quickly on some asymptotic behavior, regardless of interrotor or interaxial distance.

   (b) The smaller upstream pitch showed a more linear behavior for lift when $d/D_{\mathrm{d}} = 0.535$. At $d/D_{\mathrm{d}} = 0.732$, the smaller upstream pitch showed almost no effect, for $P_{\mathrm{u}} > 10\ \mathrm{W}$. A very similar effect can be observed for FM_{d}.

   (c) Total power consumption for the system was significantly higher when $d/D_{\mathrm{d}} = 0.535$, averaging $\kappa_{\mathrm{ov}} \approx 1.48$. This suggests that, while the downstream rotor behaves more efficiently for smaller upstream pitch, the overall system consumes significantly more power than an equivalent planar system.

3. Downstream Pitch:

(a) **Downstream pitch** showed large differences in downstream thrust. Smaller p_d showed improved performance over larger ones. While the differences for the isolated propellers were small, the registered differences were significantly higher when in tandem.

(b) Moderate differences in FM on the downstream rotors were also observed, with smaller p_d performing better. With either rotor having a constant Ω, the differences in FM between the downstream rotors tend to remain mostly constant for $d/D_\mathrm{d} > 0.814$.

(c) Power consumption over the planar configuration was somewhat variable with d/D_d: a smaller downstream pitch was more effective regarding κ_ov when $d/D_\mathrm{d} = 0.595$, but used more power when $d/D_\mathrm{d} > 0.814$, compared to a larger downstream pitch.

4. Upstream Diameter:

(a) **Upstream diameter** showed essentially no differences in downstream thrust or FM, when compared to one another. Differences in κ_ov were generally small, though the smaller upstream diameter showed slightly greater results (and thus power consumption).

5. Downstream Diameter:

(a) **Downstream diameter** had a stronger effect on downstream performance. At constant power or RPM on the downstream rotor, the magnitude of the differences between the downstream rotors increased if D_d was varied. In general, smaller D_d performed worse than larger ones.

6. Interrotor Distance:

(a) **Interrotor distance** had almost no noticeable effect on thrust for the same power on the downstream rotor.

(b) Isolines for FM_d for $d/D_\mathrm{d} = 0.535$ indicate that, for $H/D_\mathrm{d} \geq 0.610$ the downstream rotor was more impacted by the upstream rotor, as isolines had more inclination. $H/D_\mathrm{d} = 0.472$ to 0.335 showed no difference in either FM or thrust.

(c) Changes in H/D_d showed no noticeable impact for $d/D_\mathrm{d} \geq 0.732$.

7. Interaxial Distance:

(a) **Interaxial distance** had a fairly significant impact on the performance of the system. At $d/D_\mathrm{d} = 0.535$, the lowest thrust to power ratio and lowest FM were observed. Regarding κ_ov, performance was similar for $d/D_\mathrm{d} = 0.535$ and $d/D_\mathrm{d} = 0.732$.

(b) The best performance of the downstream rotor was achieved at $d/D_\mathrm{d} = 0.732$, for both thrust and FM.

(c) For small RPM on the upstream rotor ($\Omega_\mathrm{u} \leq 2500\ \mathrm{RPM}$), $d/D_\mathrm{d} = 0.535$ performed better than a larger d/D_d. More research should be conducted to identify whether these results can be expanded to include a larger range of operation.

5.2 Achievements

This work aimed to find the most critical parameters in a tandem rotor system. In particular, rotation direction, upstream rotor pitch and downstream rotor diameter had the largest effects on overall and downstream performance. Interaxial distance had varying effects, and in some cases had a positive effect on downstream performance if combined with other rotor parameters.

To perform the necessary tests, an experimental test bench designed by Amado [10] was modified. The test bench was adapted to allow for movement in both horizontal axes, and the software that controls the setup was also adapted and improved to reflect these changes. Calibration and verification of the strain gauges was performed, using reference data from the manufacturer of the propellers. For the tests, four off-the-shelf propellers were used, acquired from *APC Propellers*: [9×4.5E, 9×4.5EP, 9×6E, 10×6E].

Data was collected with flexibility in post processing in mind, to computing performance parameters and generate the plots for further analysis. These plots allow for easier identification of where and in which conditions each configuration is more performant.

5.3 Future Work

The effects of the downstream rotor on the performance of the upstream rotor, though disregarded in this work, is lacking in research. Another area that warrants more investigation is regarding tandem configurations where the centerline of a rotor intersects the other rotor disk. In addition, the trade-off between OR being more performant (near-coaxial) and ER (far-tandem) remains unstudied. Identifying where this transition occurs is of some importance as well. Finally, the introduction of a third rotor to more accurately mimic the behavior of a 8-rotor tandem drone, where the rotors are in 2 separate planes is the most natural follow-up to this work.

In tandem, some parameters influence the downstream rotor positively, improving the overall efficiency of the system. In specific conditions, the downstream rotor's performance was improved by the presence of the upstream rotor (e.g. fig. 4.48(a), where $(H/D_\mathrm{d}, d/D_\mathrm{d}) = (0.334, 0.732)$ showed a small improvement in performance for particular RPM pairs). More research should be conducted on the specific conditions and flow regarding these improvements.

Finally, only hovering rotors were studied; an analysis of a tandem rotor drone in upward, downward or forward movement and their impact on alternative configurations is of interest for their effective design.

Bibliography

[1] C. P. Coleman. A survey of theoretical and experimental coaxial rotor aerodynamic research. Technical report, NASA Ames Research Center Moffett Field, CA United States, 1997.

[2] R. C. Dingeldein. *Wind-Tunnel Studies of the Performance of Multirotor Configurations*. National Advisory Committee for Aeronautics, Aug 1954.

[3] R. J. Huston. Wind-tunnel measurements of performance, blade motions, and blade air loads for tandem-rotor configurations with and without overlap. *NASA Technical Note*, 1963.

[4] W. Z. Stepniewski and C. N. Keys. *Rotary-Wing Aerodynamics*. Dover Books on Aeronautical Engineering. Dover Publications, reprint edition, 1984. ISBN 0-486-64647-5,978-0-486-64647-3.

[5] A. Bagai and J. G. Leishman. Free-wake analysis of tandem, tilt-rotor and coaxial rotor configurations. *Journal of the American Helicopter Society*, 41(3):196–207, 1996.

[6] J. G. Leishman, M. J. Bhagwat, and A. Bagai. Free-vortex filament methods for the analysis of helicopter rotor wakes. *Journal of aircraft*, 39(5):759–775, 2002.

[7] B. Theys, G. Dimitriadis, P. Hendrick, and J. D. Schutter. Influence of propeller configuration on propulsion system efficiency of multi-rotor unmanned aerial vehicles. In *International Conference on Unmanned Aircraft Systems (ICUAS)*, pages 195–201, 2016.

[8] M. Ramasamy. Measurements comparing hover performance of single, coaxial, tandem, and tilt-rotor configurations. In *AHS 69th Annual Forum*, volume 31, page 32, 2013.

[9] M. Brazinskas, S. D. Prior, and J. P. Scanlan. An empirical study of overlapping rotor interference for a small unmanned aircraft propulsion system. *Aerospace*, 3(4):32, 2016.

[10] I. Amado. Experimental comparison of planar and coaxial rotor configurations in multi-rotors. Master's thesis, Instituto Superior Tecnico, Sep 2017.

[11] J. G. Leishman. *Principles of Helicopter Aerodynamics*. Cambridge aerospace series, 12. Cambridge University Press, 2nd ed edition, 2006. ISBN 0521660602,9780521660600.

[12] F. D. Harris. Twin rotor hover performance. *Journal of the American helicopter society*, 44(1):34–37, 1999.

[13] J. C. for Guides in Metrology. Evaluation of measurement data-guide to the expression of uncertainty in measurement. *JCGM*, 100(2008):1–116, 2008.

[14] Performance data. URL https://www.apcprop.com/technical-information/performance-data/. Accessed 2021-03-05.